
Some studies on Minimal and Non-minimal Universal Extra Dimension

by

Ujjal Kumar Dey

Enrolment Number : PHYS08200605001

Harish-Chandra Research Institute, Allahabad

A Thesis submitted to the
Board of Studies in Physical Science Discipline
in partial fulfillment of the requirements
for the degree of

DOCTOR OF PHILOSOPHY
of
Homi Bhabha National Institute



October, 2014

Statement by author

This dissertation has been submitted in partial fulfillment of requirements for an advanced degree at Homi Bhaba National Institute (HBNI) and is deposited in the Library to be made available to borrowers under rules of the HBNI.

Brief quotation from this dissertation are allowable without special permission, provided that accurate acknowledgement of source is made. Requests for permission for extended quotation from or reproduction of this manuscript in whole or in part may be granted by the Competent Authority of HBNI when in his or her judgment the proposed use of the material is in the interests of scholarship. In all other instances, however, permission must be obtained from the author.

Date:

Ujjal Kumar Dey
(Ph. D. Candidate)

Declaration

I, hereby declare that the investigation presented in the thesis has been carried out by me. The work is original and has not been submitted earlier as a whole or in part for a degree/diploma at this or any other Institution/University.

Date:

Ujjal Kumar Dey
(Ph. D. Candidate)

Certificate

This is to certify that the Ph.D. thesis entitled **Some studies on Minimal and Non-minimal Universal Extra Dimension** submitted by **Ujjal Kumar Dey** for the award of the degree of Doctor of Philosophy is a record of bona fide research work done under my supervision. It is further certified that the thesis represents the independent work done by the candidate and collaboration was necessitated by the nature and scope of the problems dealt with.

Biswarup Mukhopadhyaya

(Thesis Supervisor)

Date:

List of publications arising from the thesis

Journals

1. "Boundary localized terms in universal extra-dimensional models through a dark matter perspective",
A. Datta, **U. K. Dey**, A. Raychaudhuri and A. Shaw,
Phys. Rev. D **88**, 016011 (2013).
2. "Constraining minimal and nonminimal universal extra dimension models with Higgs couplings",
U. K. Dey and T. S. Ray,
Phys. Rev. D **88**, 056016 (2013).
3. "KK-number violating decays: Signal of $n = 2$ excitations of Extra-Dimensional Models at the LHC",
U. K. Dey and A. Raychaudhuri,
arXiv:1410.1463 [hep-ph],
Nucl. Phys. B **893**, (2015) 408-419

Conferences

1. "Universal Extra-Dimensional models with boundary terms: Probing at the LHC",
A. Datta, **U. K. Dey**, A. Raychaudhuri and A. Shaw,
Nucl. Phys. Proc. Suppl. **251-252**, (2014) 39-44.
2. "Universal extra dimensions : life with BLKs",
A. Datta, **U. K. Dey**, A. Raychaudhuri and A. Shaw,
J. Phys. Conf. Ser. **481**, (2014) 012006.

Ujjal Kumar Dey
(Ph. D. Candidate)

**To
My Mother**

Acknowledgments

I would like to thank Prof. Biswarup Mukhopadhyaya for supervising my thesis work. I have learned a lot from him. His guidance and help at various stages played a pivotal role in the completion of my thesis work.

I would like to express my profound gratitude to my collaborator and mentor Prof. Amitava Raychaudhuri for his guidance and continuous support throughout my Ph. D. life. His immense patience, deep knowledge, encouragement to think and work independently catalyze my transition from a student to a researcher.

I am grateful to my collaborator Prof. Anindya Datta, from whom I learned various aspects of extra dimensions. I would like to thank Avirup Shaw for his diligence and sincerity during our collaboration. I enjoyed working with Tirthada (Tirtha Sankar Ray). He has this brilliant capability of coming up with a solution to any problem. I would like to acknowledge the wonderful experience that I have working with my friend Dipankar and brother-like junior Landau (Nabarun).

I am thankful to the past and present members of the particle physics phenomenology group at the Harish-Chandra Research Institute (HRI), Prof. Raj Gandhi, Prof. Aresh K. Datta, Prof. V. Ravindran, Prof. Sandhya Choubey, Dr. Santosh Rai, Dr. Andreas Nyffeler from whom I learned many aspects of high energy physics. The physics discussion sessions at the Pheno-Lunch was an exciting way to remain updated on the recent developments of the subject.

I am deeply indebted to the faculty members of HRI for creating an excellent environment for learning through various course works and projects. I take this opportunity to thank Prof. Ashoke Sen, Prof. Rajesh Gopakumar, Prof. L. Sriramkumar, Prof. Satchidananda Naik, Prof. Dileep Jatkar, Prof. Pinaki Majumdar, Prof. Sudhakar Panda, Prof. Tapas K. Das and Prof. J. S. Bagla. I would also like to acknowledge Anirbanda (Dr. Anirban Basu) for his candid friendship with all of us students. I am also thankful to the faculty members of University of Calcutta where a large part of my thesis work has been done. Especially I am grateful to Prof. Anindya Datta and Prof. Anirban Kundu.

The administration at HRI has always been very helpful and efficient. I would like to express my gratitude to all the non-academic members of this institute for their help and support at every stage. The workers and staffs are also acknowledged for always being ready at their services.

A very special thanks to my batch-mates at HRI. The life at HRI would not have been the same without them. Thank you Bhuruda (Sourav Mitra), Thikaa (Saurabh Niyogi), Manojda, Rambha (Saurabh Pradhan), Arunabhada, Taratda and Vikas for all the happy moments that we shared together throughout our journey in the Ph. D. life. I will always cherish those memories.

I am very grateful to my seniors at HRI. At each step their help and support take me through many difficult situations. Arjunda, Shubhoda, Shamikda, Soumyada, Kaka (Kirtimanda), Joydeepda, Sanjoyda, Dhirajda, Satyada, Atrida, Arijitda, Arindamda, Arghyada, Ambreshji, Kenji – thank you all. I am deeply indebted my other friends – Shankha, Tanumoyda and Animeshda. The void created by the leaving of the seniors are beautifully filled up by the set of juniors and in no time they became close friends. Thanks Aritra, Dibya, Rana, Taushif, Titas, Soumyarup, Arijit, Tamoghna, Sauri, Swapnamay, Masud, Avijit, Avishek, Nyaya for keeping a vibrant and lively campus life. I will miss the late night long refreshing tea sessions at the guest house where *all possible* topics of the Universe were discussed among the friends with ardent zeal. I am also thankful to Paromitadi, Anushreedi and Ushoshi. As I have spent a considerable part of my Ph. D. life at the University of Calcutta, I would like to thank all of my friends there. Special thanks to T. K. Bose, Kartick, Khaleque, Swarupda and Shirshenduda for making the otherwise mundane stay at Kolkata a very lively one. I am deeply grateful to Kalida (Kalipada Das) for providing me shelter whenever I had to stay at Kolkata.

Evidently for the remaining of my life I can safely presume that I would be able to say that "...those were the best days of my life".

Finally, I am indebted beyond measure to all my family members for their love and constant support. Special thanks to Chunilal Das, Shankar Chandra Dey and Arun Kumar Pan for shaping me from the very beginning of my academic life and being constant source of inspiration.

Thank you all...

Contents

Synopsis	iii
List of tables	vii
List of figures	ix
1 Universal Extra Dimension	1
1.1 Introduction	1
1.2 Standard Model and beyond	1
1.2.1 Particle content and interactions	3
1.2.2 Brout-Englert-Higgs mechanism	5
1.2.3 A few shortcomings of SM	8
1.3 Extra Dimension	10
1.3.1 Large Extra Dimension	11
1.3.2 Warped Extra Dimension	12
1.4 Universal Extra Dimension	12
1.4.1 Basic features	13
1.4.2 KK parity	17
1.4.3 Standard Model in 5D	17
1.4.4 Particle content and interactions	19
1.5 Structure of this thesis	21
2 Minimal and Non-minimal Universal Extra Dimension	23
2.1 Minimal Universal Extra Dimension	23
2.1.1 Radiative corrections	23
2.1.2 Mass spectrum	26
2.2 Non-minimal Universal Extra Dimension	27

2.2.1	Model description	28
3	Dark Matter & Non-minimal Universal Extra Dimension	35
3.1	Dark Matter	35
3.1.1	Evidences	35
3.1.2	Basic properties	37
3.1.3	A few candidates	38
3.2	Relic density	40
3.2.1	Standard calculation of relic density	40
3.2.2	Coannihilation	43
3.3	Relic density in mUED and nmUED	44
3.3.1	mUED	44
3.3.2	nmUED	46
3.4	Direct Dark Matter Detection in mUED and nmUED	53
3.4.1	mUED	55
3.4.2	nmUED	56
3.5	Summary and Conclusions	60
4	Non-minimal Universal Extra Dimension Confronting Higgs Data	65
4.1	Loop-induced Higgs couplings	66
4.2	mUED results	67
4.3	nmUED results	69
4.4	Conclusion	73
5	Signal of Second Level Kaluza-Klein Particles	75
5.1	Coupling of the $2n$ -level top quark to zero mode states	76
5.2	Decays of a $2n$ -level top quark	79
5.3	Detection prospect of the $n = 2$ top quark	80
5.4	Conclusion	83
6	Summary and conclusions	85

SYNOPSIS

The Standard Model (SM) is by far the most successful model of particle physics. Very recently the discovery of the Higgs particle and other observations at LHC augment this fact. Even after the immense success of SM the reticence of it to provide us with the answer to some aesthetic (Gauge coupling unification, hierarchy problem etc.) and compelling questions (massive neutrinos, baryon asymmetry, dark matter (DM) etc.) leads us to think beyond SM (BSM). Supersymmetry (SUSY) and Extra Dimensional (ED) theories are two strong proponents to solve some of these problems. A particular variant of ED models is Universal Extra Dimensional (UED) models where all the Standard Model (SM) fields can access one or more extra spatial dimensions. The simplest case can be of one extra dimension. The extra spatial dimension must be compactified at a scale $1/R \sim \mathcal{O}(\text{TeV})$, where R is the compactification radius. To get chiral fermions, orbifold compactification is needed. Although orbifolding breaks 5D translational invariance there remains a residual symmetry, called KK-parity, responsible for the stability of the lightest Kaluza-Klein particle (LKP). In the effective four dimensional theory there will be towers of heavy Kaluza-Klein (KK) modes for each SM field. The masses of these heavy modes depend on the compactification scale. For a specific level the mass spectrum is thus almost degenerate. But radiative corrections lift this degeneracy. Without violating the 4D symmetries of SM, additional interaction terms between the KK modes can be written at the fixed points of the orbifold. Such terms can also creep in as counterterms to compensate for radiative effects of the 5D theory. In minimal UED (mUED) these terms are chosen in such a way that the 5D loop contributions are exactly compensated at the cut-off scale. Being a 5D quantum field theory, mUED is non-renormalisable and should be considered as an effective field theory and valid up to some high energy scale. This is why one should not discard *a priori* any operator that is allowed by 4D Lorentz invariance and SM gauge invariance. Boundary localised terms (BLTs) are such operators. The scenario with arbitrary non-vanishing BLTs is termed as non-minimal UED (nmUED).

Even after conclusive evidence of existence of DM, the actual identity of DM is still unknown. In the context of mUED, the first KK level photon $\gamma^{(1)}$, being the LKP and thus having the required stability governed by the conservation of KK parity, can be a good candidate for DM. In nmUED the mass spectrum is determined by the BLT parameters

and thus depending on them the identity of LKP can be changed. The existence of stable LKP in nmUED is possible only when there are equal strength BLTs at two boundaries. In the first study, we considered the possibility of various possible LKPs. In each case we calculated the relic density following the standard procedure of solving Boltzmann equation with appropriate assumptions. Co-annihilation, which is a necessary consideration for near degenerate mass spectra, has also been taken into account. We have derived all the necessary cross sections analytically, using CalcHEP. We used direct detection data from XENON100 to constrain the parameter space. We found for specific choice of parameters, not only $\gamma^{(1)}$ can be a good DM candidate but also the narrow bounds on compactification scale from similar studies in mUED can be evaded. We also found that the first level Z -boson, with mass at TeV range, can not be a single component DM candidate as it does not meet the criteria for appropriate relic density.

The *tour de force* of LHC is the discovery of Higgs particle, till date. Apart from measuring its mass, LHC data finds a few discrepancies in the Higgs couplings. For example, global analysis of ATLAS and CMS data showed that there is slight excess in $H \rightarrow \gamma\gamma$ (which is actually a loop-induced process) decay rate from the SM prediction. However, these deviations sustained even after the refined analysis of available data. It is possible that this excess is due to some new physics. The heavier new particles can leave their footprints in loop-induced processes where they can come as virtual intermediate particles. In this way, heavier KK modes can alter various loop-induced decay processes of Higgs and we can compare between this alteration and observed data. In this spirit, in the second work we showed that the present data disfavors new physics scale below 1.3 TeV with 95% confidence level for the mUED. However, we showed that a more general scenario in nmUED can accommodate scales as low as 0.4 TeV.

In the simplest UED models KK parity distinguishes the states with odd and even KK-number. As has already been mentioned, the KK-excitations of all SM particles at any KK-level n are degenerate in mass which is lifted by mUED radiative corrections. In the third work, in preparation, we focused our attention on the KK-parity conserving coupling of a $2n$ -level KK top quark to the $n = 0$ top quark and an $n = 0$ Higgs boson. Since mUED interactions are KK-number conserving this coupling will be loop induced. We compare the decay mediated by this coupling with the KK-number conserving decay to two n -level states which proceeds through tree-level couplings. The latter process is phase space suppressed and becomes allowed only after mUED corrections are incorporated. As an application of this result we have examined the prospect of pair producing $n = 2$ level KK top-antitop quarks at the LHC with $\sqrt{s} = 13$ TeV and 33 TeV and examine

the prospects of the detection of both of them in the above mentioned decay mode.

List of Tables

3.1	The $B^{(1)}$ annihilation and relevant $B^{(1)}$ -lepton scattering process that are important for the relic density calculation of $B^{(1)}$	49
3.2	The $\nu^{(1)}$ and $\ell^{(1)}$ annihilation and scattering processes which contribute to the relic density calculation.	49
3.3	The $\nu^{(1)}$ - $\ell^{(1)}$ scattering processes which contribute to the relic density calculation.	50
3.4	Upper bound on R^{-1} from overclosure of the universe ($\Omega h^2 = 0.48$). The masses of the LKP for the limiting R^{-1} are also presented. For the $W_3^{(1)}$ LKP case only the process $W_3^{(1)} W_3^{(1)} \rightarrow W^+ W^-$ is taken into account. Including coannihilation will further enhance the upper bound in this case.	52

List of Figures

1.1	Particle content of the SM.	4
1.2	The Higgs potential in the SM (taken from [19]).	7
1.3	Pictorial description of orbifolding.	15
2.1	An example of a loop winding around the extra dimension.	24
2.2	(From [58]). Particle spectrum for the first level KK particles at tree level (left) and after one loop correction (right). Assuming Higgs mass $m_H = 120$ GeV, $1/R = 500$ GeV and $\Lambda R = 20$	27
2.3	Variation of $M^{(1)} = m_1 R$ with BLT strength $R_{\text{BLT}} = r/R$. Larger R_{BLT} yields a smaller mass. This result applies to any type of fields when their corresponding BLTs are symmetric.	32
3.1	The observed rotation curve of the dwarf spiral galaxy M33. The dashed line is predicted purely on the basis of luminous stellar disc. The observed curve is flatter than the predicted one. This suggests the presence of a halo of dark matter, extending to large galactic radii. (From [77]).	36
3.2	Relic density of LKP (i) $\gamma^{(1)}$ (left) and (ii) $Z^{(1)}$ (right) as a function of LKP mass. The green band gives 2σ allowed region from WMAP 5yr data [130], $\Omega_{\text{CDM}} h^2 \in (0.1037, 0.1161)$ and the vertical cyan band excludes the mass of LKP from precision data. Here KK singlet and doublet quarks are assumed to be degenerate and the mass of the level one quarks are varied by hand, such that $\Delta_{q_1} = 0.01, 0.02, 0.05, 0.1$ and 0.5 . Also $Z^{(1)}$ and $W^{(1)\pm}$ are taken to be degenerate. The red dotted line gives the result of full mUED calculation including all coannihilation processes. Adapted from [117].	46

LIST OF FIGURES

3.3	Variation of Ωh^2 with relic particle mass, $m_{B^{(1)}}$. Curves for different choices of the fermion BLKT parameter R_f are shown and the corresponding Δ_f indicated. The narrow horizontal blue band corresponds to the 1σ allowed range of relic particle density from Planck data [74]. The allowed $1/R$ (or $m_{B^{(1)}}$) can be read off from the intersections of the curves with the allowed band. The three panels are for different choices of R_B , the BLKT parameter for B	51
3.4	Allowed region in the $m_{f^{(1)}} - m_{B^{(1)}}$ plane that satisfies the observed Ωh^2 limits. The three panels are for different choices of R_B . Only the narrow strip <i>between</i> the two curves is allowed from the relic density constraints. . .	52
3.5	Variation of the relic density with $m_{W_3^{(1)}}$ in the case of $W_3^{(1)}$ LKP. The current observed value (~ 0.12) disfavors this alternative.	53
3.6	Schematic presentation of DM interaction (taken from [131]).	54
3.7	Spin dependent and scalar LKP-nucleon cross section as a function of $B^{(1)}$ mass for $\Delta_{q^{(1)}} = 5, 10, 15\%$ and $m_H = 120$ GeV. Adapted from [109].	56
3.8	The Feynman diagrams for $B^{(1)}$ and quark scattering.	58
3.9	Variation of the scalar $B^{(1)}$ -nucleon cross section with relic particle mass for Xenon. The three panels are for three values of R_B . The shaded (blue) region represents the cross section for a continuous variation of R_q within the range bounded by the two curves.	59
3.10	Variation of the spin dependent $B^{(1)}$ -nucleon cross section with relic particle mass for Xenon. The three panels are for three values of R_B . The shaded (blue) region shows the cross section for a continuous variation of R_q within the range bounded by the two curves.	59
4.1	The ratios of the Higgs couplings in UED scenario to their SM values are plotted as functions of the inverse radius of compactification of the extra dimension ($1/R$). The blue (shaded) bands represent the 95% confidence level allowed values for these ratios [156], with the red (solid) horizontal lines representing the central values from LHC data. The blue (dashed) lines correspond to the SM points. The black (dark) curves are the UED predictions. We have assumed $m_H = 125$ GeV.	69

4.2	The ratios of the Higgs couplings in the BLKT scenario to their SM values are plotted as functions of the inverse radius of compactification of the extra dimension ($1/R$). The blue (shaded) bands represent the 95% confidence level allowed values for these ratios [156], with the red (light) horizontal lines representing the central values from LHC data. The blue (dashed) lines correspond to the SM points. The black (dark) points represent the BLKT results. We have assumed $m_h = 125$ GeV. The BLKT parameters r_Q and r_Y are varied within the range $[-\pi R/2, \pi R/2]$	72
5.1	The dominant diagrams in the unitary gauge generating an effective $t_L^{(2n)} t_R^{(0)} H^{(0)}$ coupling.	77
5.2	The branching ratio for the process $t^{(2)} \rightarrow t^{(0)} H^{(0)}$ as a function of ΛR . The red solid (blue dot-dashed) curve is for $t_L^{(2)}$ ($t_R^{(2)}$) decay.	80
5.3	The production cross section for a $t^{(2)} \bar{t}^{(2)}$ pair at the LHC. The blue solid (red dashed) curve corresponds to $\sqrt{s} = 13$ TeV (33 TeV).	81
5.4	The cross section for the $(tH)(tH)$ signal at the LHC as a function of the $t^{(0)} H^{(0)}$ invariant mass. The histograms for different choices of $1/R$ (explained in the legend) and the SM background (shown shaded) at the LHC running at $\sqrt{s} = 13$ TeV (left) and 33 TeV (right).	82

Chapter 1

Universal Extra Dimension

1.1 Introduction

In this chapter we will set the notations and conventions required for the later chapters. We will discuss extra-dimensional theories, with a special emphasis on universal extra dimensional model which, along with some variants of it, is the main topic of interest in this thesis. Before delving into the extra dimensions it would not be out of place to recall the most successful theory of elementary particles, the Standard Model (SM). In Sec. 1.2 we revisit the SM and in subsequent Secs. 1.3 and 1.4 we will give a brief introduction to extra dimensions.

1.2 Standard Model and beyond

The Standard Model (SM) of particle physics epitomizes our current understanding of the basic building blocks of the universe. These basic building blocks are elementary particles which are fundamental, in the sense that they are indivisible and have no sub-structure. SM is a theory of three of the four fundamental forces of Nature, namely electromagnetic, weak and strong interactions (gravity is not included in the paradigm of SM) that superintend the dynamics of these particles. The matter of the universe is composed of fermionic fields and the interaction between them is governed by the bosonic fields. In SM we have three types of particles: spin-1/2 fermions, spin-1 gauge bosons and a spin-0 scalar field, Higgs boson. SM is a quantum field theory (QFT) based on various symmetries. Actually QFT is the result of the combination of quantum mechanics and special theory of relativity. SM possesses the following symmetries.

- (i) **Lorentz symmetry** : This is a space-time symmetry. The manifestation of Lorentz

symmetry is that the laws of nature are independent of rotations and boosts. The fields (elementary particles are described by fields in QFT) of SM have definite transformation properties depending on their spins. Lorentz invariance is a symmetry of the Lagrangian describing the theory. If the Lagrangian transforms as a scalar under the Lorentz transformations then the theory is said to be Lorentz invariant. As it stands SM is manifestly Lorentz invariant.

- (ii) **Gauge symmetry** : Gauge transformations are local transformations of the fields. Actually the interactions among matter fields, *i.e.*, the fermionic fields and gauge fields are described by the principle of local gauge invariance. The gauge group of the SM is $SU(3)_c \otimes SU(2)_L \otimes U(1)_Y$ which dictates the three fundamental interactions of Nature. The strong interactions are described by the $SU(3)_c$ gauge group whereas $SU(2)_L \otimes U(1)_Y$ accounts for the electroweak (EW) interactions. This EW symmetry breaks to the electromagnetic symmetry, $U(1)_{em}$ via the Brout-Englert-Higgs (BEH) mechanism with the help of a scalar field which is called Higgs field.
- (iii) **Discrete symmetry** : There are discrete transformations that arise in QFT. Charge conjugation (C), parity transformation (P) and time reversal (T) are examples of such transformations. Among these P and T are just the subset of Lorentz transformations. Actually P and T are discrete Lorentz transformations. The action of P is to reflect the spatial coordinates (*e.g.*, $\vec{x} \rightarrow -\vec{x}$) which ultimately results in a flip in chirality (handedness) of the field. The operation of T is just to flip the direction of time. The effect of C is to interchange the particle to its antiparticle and vice-versa. The electromagnetic interaction is invariant under C , P , and T . The electroweak interaction violates both C and P . Thus, individually none of these are good symmetries of SM. However, the combined operation CPT is always conserved in any standard QFT¹.
- (iv) **Global symmetry** : SM also has two *accidental* global symmetries: baryon number (B) and lepton number (L). However, they can be violated by quantum effects. These type of symmetries which are conserved classically but violated via quantum effects are called *anomalous*. It is worth mentioning that $(B - L)$ is still a good symmetry of SM and is not anomalous.

Apart from these symmetries there are some other important aspects of SM. It is a renormalizable theory, *i.e.*, all the ultra-violet (UV) divergences that can arise from higher

¹See [1] for a proof of CPT -theorem.

order quantum effects can be removed by judicious redefinition of bare fields and parameters of the model. Unitarity, *i.e.*, the conservation of probability in various interaction processes, and the stability of EW vacuum are two other important facets of SM.

1.2.1 Particle content and interactions

We have already mentioned that the matter of the universe is made up of spin-1/2 fermions. Among these there are six types of quarks and six types of leptons (three electrically charged and three neutral). The transformation properties of these fields under SM gauge group are determined by their respective charges under the gauge groups. The quark fields transform as triplets (fundamental representation) of $SU(3)_c$, whereas the leptons are singlet under this gauge group and have no color charge and consequently do not take part in strong interactions. SM being a chiral theory, treats left-handed and right-handed fields differently. The left-handed² fields transform as doublets (fundamental representation) under $SU(2)_L$ while the right-handed fields are singlets under this group. Thus we have for quarks,

$$\begin{aligned} \text{Doublets : } & \begin{pmatrix} u \\ d \end{pmatrix}_L, \begin{pmatrix} c \\ s \end{pmatrix}_L, \begin{pmatrix} t \\ b \end{pmatrix}_L \\ \text{Singlets : } & u_R, d_R, c_R, s_R, t_R, b_R. \end{aligned}$$

For leptons we have,

$$\begin{aligned} \text{Doublets : } & \begin{pmatrix} \nu_e \\ e \end{pmatrix}_L, \begin{pmatrix} \nu_\mu \\ \mu \end{pmatrix}_L, \begin{pmatrix} \nu_\tau \\ \tau \end{pmatrix}_L \\ \text{Singlets : } & e_R, \mu_R, \tau_R. \end{aligned}$$

Note that there is no right-handed neutrino in SM³. The $SU(2)_L$ group has three generators constructed out of the three Pauli matrices, σ^a ($a = 1, 2, 3$). If T_3 be the eigenvalue of the third generator and Q be the electric charge of the field, then the transformation of that field under the $U(1)_Y$ is determined by the quantum number called *hypercharge* which is defined as,

$$Q = T_3 + \frac{Y}{2}. \quad (1.1)$$

²The left-handed projection of a field ψ is defined as $\psi_L = P_L\psi = [(1 - \gamma_5)/2]\psi$ and for the right-handed one, $\psi_R = P_R\psi = [(1 + \gamma_5)/2]\psi$.

³In SM the neutrinos are massless particles. But recent neutrino experiments show that they have tiny masses. Some extensions of SM add right-handed neutrinos to explain the mass of the neutrinos.

With this convention the lepton doublets will have hypercharge (-1) , and for lepton singlets it is (-2) . The quark doublets are of hypercharge $+1/3$ and up-type quark singlets it is $+4/3$ and down-type quark singlets will have hypercharge $(-2/3)$.

With the knowledge of the transformation property of the fields under SM gauge group one can write the gauge invariant Lagrangian of the theory. The kinetic term⁴ for the fermionic fields (ψ) can be written as,

$$\mathcal{L}_{\text{matter}} = i\bar{\psi}\not{D}\psi = i\bar{\psi}\gamma^\mu D_\mu\psi, \quad (1.2)$$

where the most general form of the covariant derivative D_μ is given by,

$$D_\mu = \partial_\mu - ig_1 \frac{Y}{2} B_\mu - ig_2 \frac{\sigma^a}{2} W_\mu^a - ig_3 \frac{\lambda^i}{2} G_\mu^i, \quad (1.3)$$

where g_1 , g_2 and g_3 are the gauge couplings for $U(1)_Y$, $SU(2)_L$ and $SU(3)_c$ groups respectively. It should be noted that if a field transforms as a singlet under a specific gauge group then that specific gauge coupling will be zero for that field. Here B_μ is the gauge field for $U(1)_Y$, W_μ^a ($a = 1, 2, 3$) are for $SU(2)_L$ and G_μ^i ($i = 1, 2, \dots, 8$) for $SU(3)_c$ group. Substituting this form of D_μ in Eq. 1.2 one can obtain the interaction vertices between the fermions and the gauge bosons.

	Fermions			Bosons	
Quarks	u up	c charm	t top	γ photon	Force carriers
	d down	s strange	b bottom	Z Z boson	
Leptons	ν_e electron neutrino	ν_μ muon neutrino	ν_τ tau neutrino	W W boson	
	e electron	μ muon	τ tau	g gluon	
				Higgs boson	

Source: AAAS

Figure 1.1: Particle content of the SM.

The kinetic terms for the gauge fields can be written, in terms of their field strengths, as,

$$\mathcal{L}_{\text{gauge}} = -\frac{1}{4} B_{\mu\nu} B^{\mu\nu} - \frac{1}{4} W_{\mu\nu}^a W^{a\mu\nu} - \frac{1}{4} G_{\mu\nu}^i G^{i\mu\nu}, \quad (1.4)$$

⁴Mass terms will be discussed later.

where the field strength tensors are defined as,

$$B_{\mu\nu} = \partial_\mu B_\nu - \partial_\nu B_\mu, \quad (1.5a)$$

$$W_{\mu\nu}^a = \partial_\mu W_\nu^a - \partial_\nu W_\mu^a + g_2 \epsilon^{abc} W_\mu^b W_\nu^c, \quad (1.5b)$$

$$G_{\mu\nu}^i = \partial_\mu G_\nu^i - \partial_\nu G_\mu^i + g_3 f^{ijk} G_\mu^j G_\nu^k, \quad (1.5c)$$

where ϵ^{abc} and f^{abc} are the structure constants of $SU(2)_L$ and $SU(3)_c$ groups respectively. Thus from the kinetic terms it is evident that for non-Abelian gauge fields there exists triple and quartic self-interaction vertices.

We have talked about the kinetic terms of fermions and gauge bosons. Actually gauge symmetry forbids any kind of mass terms for gauge fields. But it is an established fact that the weak interaction mediator gauge bosons, W^\pm and Z -bosons are massive. Moreover, the incongruity in the transformation properties of the left-handed and right-handed fermions prohibits gauge invariant mass term for fermions also. These facts lead us to think that the electroweak gauge symmetry must be broken. The introduction of the concept of spontaneous symmetry breaking (SSB) [2–10] helps to reconcile these mass related issues. The crux of this SSB is that the Lagrangian of the theory is invariant under the gauge transformations but the vacuum does not respect that symmetry. The electroweak theory, also known as Glashow-Salam-Weinberg model [11–13] incorporates SSB by introducing a spin zero complex scalar field, called Higgs field, which transforms as doublet under $SU(2)_L$ and takes appropriate vacuum expectation value (vev) to break the gauge symmetry spontaneously. As a consequence of this breaking the fermions and the gauge bosons can obtain masses. The SM particle zoo has been shown in Fig. 1.1. It is worth mentioning that the spontaneously broken gauge theory is also renormalizable [14, 15]. In the next subsection we are going to describe the mechanism in a nut shell.

1.2.2 Brout-Englert-Higgs mechanism

We have already mentioned that to explain the masses for the W^\pm and Z bosons and fermions in the SM we have to resort to the spontaneous breaking of electroweak symmetry. The difference between explicit and spontaneous symmetry breaking is that in the latter case the Lagrangian is invariant under the symmetry transformations of the theory but the vacuum, *i.e.*, the ground state is not. It is worth mentioning that spontaneous breaking of global continuous symmetries gives rise to massless bosonic fields, called Goldstone bosons. The previous statement summarizes, what is called Goldstone theo-

rem [4]. In the case of spontaneous breaking of gauge symmetry⁵ the Goldstone boson disappears from the spectrum and the gauge boson becomes massive. This mechanism is called the Brout-Englert-Higgs mechanism.

It has been observed that in the SM the electric charge is conserved and therefore the concerned gauge group of electromagnetism, $U(1)_{em}$ is an exact symmetry of the theory. So, under SSB we should have the following symmetry breaking pattern,

$$SU(2)_L \otimes U(1)_Y \rightarrow U(1)_{em} \quad (1.6)$$

This breaking can be achieved by introducing a spin-0 scalar field, Φ , that transforms as a doublet under the $SU(2)_L$ with $U(1)_Y$ hypercharge +1. This doublet is defined as,

$$\Phi = \begin{pmatrix} \phi^+ \\ \phi^0 \end{pmatrix} = \frac{1}{\sqrt{2}} \begin{pmatrix} \phi_1 + i\phi_2 \\ \phi_3 + i\phi_4 \end{pmatrix}. \quad (1.7)$$

The gauge invariant Lagrangian for this field is given by,

$$\mathcal{L}_\Phi = (D^\mu \Phi)^\dagger D_\mu \Phi - V(\Phi), \quad (1.8)$$

where D_μ is defined in Eq. 1.3 and the potential $V(\Phi)$ is given as,

$$V(\Phi) = \mu^2 \Phi^\dagger \Phi + \lambda (\Phi^\dagger \Phi)^2 \quad (1.9a)$$

$$= \frac{\mu^2}{2} \left(\sum_{k=1}^4 \phi_k^2 \right) + \frac{\lambda}{4} \left(\sum_{k=1}^4 \phi_k^2 \right)^2. \quad (1.9b)$$

Clearly this potential has a global $SO(4)$ symmetry. In Eq. 1.9 we consider $\lambda > 0$. Now using the minimization condition of the potential, $\frac{\partial V}{\partial \Phi} = 0$, one can show that

- for $\mu^2 > 0$, \exists a unique minimum at $\Phi^\dagger \Phi = 0$,
- for $\mu^2 < 0$, the potential develops degenerate minima at $\Phi^\dagger \Phi = \frac{-\mu^2}{2\lambda} \equiv \frac{v^2}{2}$.

The second scenario has been pictorially depicted in Fig. 1.2. Now, utilizing the freedom of $SU(2)_L$ symmetry and without any loss of generality, one can choose the vev of the field Φ entirely on the electrically neutral component of the field ϕ^0 as,

$$\langle \Phi \rangle \equiv \langle 0 | \Phi | 0 \rangle = \begin{pmatrix} 0 \\ \frac{v}{\sqrt{2}} \end{pmatrix}. \quad (1.10)$$

⁵It is interesting to note that spontaneous breaking of gauge symmetry is possible only for space dimensions $d > 2$. This is known as Coleman-Mermin-Wagner-Hohenberg theorem [16–18].

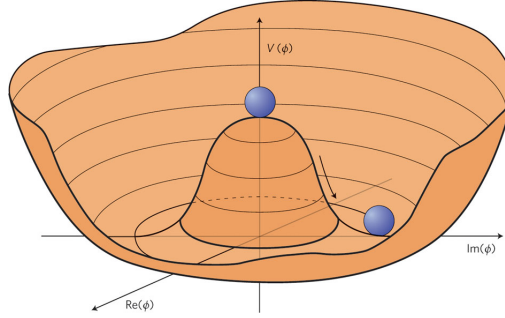


Figure 1.2: The Higgs potential in the SM (taken from [19]).

This vev of the field Φ is responsible for the breaking mentioned in Eq. 1.6. In the *unitary gauge* the field $\Phi(x)$ can be parametrized as,

$$\Phi(x) = \frac{1}{\sqrt{2}} \begin{pmatrix} 0 \\ v + H(x) \end{pmatrix}, \quad (1.11)$$

where, $H(x)$ is a real-valued field with $\langle H(x) \rangle = 0$. The quantum of the field $H(x)$ is called the Higgs boson. Now substituting $\Phi(x)$ in the kinetic term of \mathcal{L}_Φ one can obtain the mass terms for W^\pm and Z -bosons. The W^\pm is defined as,

$$W_\mu^\pm = \frac{1}{\sqrt{2}} (W_\mu^1 \mp iW_\mu^2), \quad (1.12)$$

whereas the Z -boson and photon are the orthogonal combinations of the fields B_μ and W_μ^3 ,

$$Z_\mu = -\sin \theta_W B_\mu + \cos \theta_W W_\mu^3, \quad (1.13a)$$

$$A_\mu = \cos \theta_W B_\mu + \sin \theta_W W_\mu^3. \quad (1.13b)$$

The weak mixing angle θ_W is called Weinberg angle and is defined as,

$$\theta_W \equiv \tan^{-1} \left(\frac{g_1}{g_2} \right). \quad (1.14)$$

The masses of the gauge bosons as obtained from the kinetic term in \mathcal{L}_Φ are,

$$m_A = 0, \quad (1.15a)$$

$$m_W = \frac{1}{2} g_2 v, \quad (1.15b)$$

$$m_Z = \frac{1}{2} v \sqrt{g_1^2 + g_2^2}. \quad (1.15c)$$

Apart from the mass terms of gauge bosons the kinetic term also gives the interaction vertices between the Higgs field $H(x)$ and the gauge bosons W^\pm and Z . Photon has no coupling with $H(x)$. A general rule of thumb, in this context, is worth mentioning; the more massive a particle is, the stronger interaction it has with the Higgs boson. From the potential term of \mathcal{L}_Φ we get the mass ($m_H = 2v^2\lambda$) of Higgs field itself and its cubic and quartic self-couplings.

Apart from giving masses to the gauge fields the field Φ also takes care of the masses of fermions⁶. The gauge invariant interactions between the scalar field and the fermions are given by the Yukawa terms,

$$\mathcal{L}_{\text{Yuk}} = \sum_{i,j=\text{generation}} \left(-Y_{ij}^u \bar{Q}_i \tilde{\Phi} u_j - Y_{ij}^d \bar{Q}_i \Phi d_j - Y_{ij}^l \bar{L}_i \Phi e_j + \text{h.c.} \right), \quad (1.16)$$

where $\tilde{\Phi} = i\sigma_2 \Phi^*$ and Q and L represents the quark and lepton doublets respectively and Y^u , Y^d , Y^l are the Yukawa coupling matrices for the up-quark, down-quark and charged leptons respectively. After the field Φ gets the vev v , the Yukawa Lagrangian takes the form of $m_\psi \bar{\psi}_L \psi_R$ with the mass matrices,

$$m_{ij}^u \propto v Y_{ij}^u, \quad m_{ij}^d \propto v Y_{ij}^d, \quad m_{ij}^l \propto v Y_{ij}^l. \quad (1.17)$$

These mass matrices are in the flavor basis and are to be diagonalized to get the mass basis. These Yukawa couplings are free parameters in the SM and are fixed by the masses of the corresponding fermions. Note that neutrinos do not have any mass terms due to the absence of their right chiral partners.

The SM has undergone decades of experimental scrutiny with ever-increasing accuracy. Various experiments carried out at both high energy colliders like LEP, Tevatron and LHC as well as low energy experiments of flavor physics and electroweak precision measurements put SM on a strong footing. The long elusive Higgs boson has also been discovered in LHC [20,21]. Apart from a few minor discrepancies (*e.g.*, anomalous magnetic moment of muon, the $H \rightarrow \gamma\gamma$ decay width etc.) the SM is the most consistent model of particle physics till date. But there are some observations that lead us to think of something beyond the SM. In the next subsection we discuss some of them.

1.2.3 A few shortcomings of SM

We have seen in the earlier section how SM encompasses almost all of the experimental observations and all the predictions of it have been successfully verified. The latest

⁶Not only gauge symmetry breaking but also chiral symmetry breaking, in the fermionic sector, is induced by Higgs vev.

discovery of Higgs boson provides the last missing block in the particle spectrum of SM.

In spite of its successes there are at least two burning issues on which SM provides no explanation and leaves room for some *new physics* beyond SM. One of them comes from the observed oscillations in neutrinos (see *e.g.*, [22,23] and references therein). This implies non-vanishing masses for neutrinos and we know that there are no mass terms possible in SM. However, postulating the existence of right handed neutrinos can solve the problem. Various proposals are put forward to address the neutrino mass problem via *see-saw* mechanisms which are largely motivated by grand unified theories (GUT).

The second issue originates from various astrophysical/cosmological observations which mandate the existence of *dark matter*. None of the ingredients of SM can fit in properly to explain this. See Sec. 3.1 for an elaborate discussion on this matter. It is also worth mentioning, in this context, the observed matter-antimatter asymmetry in the universe is another issue which can not be explained in the parlance of SM.

Apart from these experimental observations there are some theoretical problems too. One of them arises from the presence of the all-important scalar sector. In the SM the masses of the fermions are protected by inexact chiral symmetry, whereas the masses of gauge bosons are protected by the remnant gauge symmetry after EWSB. But this is not the case for the Higgs field. The mass of the Higgs boson receives radiative corrections that are quadratically sensitive to the cut-off scale which is set by new physics, *e.g.*, gravity. So to keep the Higgs boson mass at electroweak scale one can add a counter-term to cancel the large contribution. But such a huge cancellation would be highly unnatural as it needs large fine-tuning of the parameters. This is called fine-tuning problem or naturalness problem. Sometimes it is also termed as hierarchy problem owing to the fact that the cancellation of such large numbers, of the order of the cut-off scale (usually the Planck scale, $M_{\text{Pl}} = 1.22 \times 10^{19}$ GeV), is required to leave behind a relatively much smaller Higgs mass near the electroweak scale.

There are many free parameters in SM. They are fixed by experiments. There is no explanation as to why they are the values the parameters take. Moreover the reason for large hierarchy between the fermion masses remains unanswered. Lastly, gravity, one of the four fundamental forces of Nature, is not included in SM.

Above, we mentioned some of the criticism of SM. Clearly we need some theory beyond SM (BSM) to address these shortcomings. BSM theories can be constructed in many possible ways. Taking extra space-time symmetries as the guiding principle, theory of *supersymmetry* (SUSY) has been put forward. According to SUSY all the SM particles have their corresponding supersymmetric partner, differing in spin by half. Thus the

quadratically divergent contributions that are coming in the Higgs mass correction from the particles running in the loop are exactly canceled by the contributions coming from their supersymmetric partners. In this way the Higgs mass is stabilized in SUSY theories. Apart from this there are many other virtues of the SUSY theories which we will not discuss here. Also there are models where there are no fundamental scalars (composite Higgs, technicolor type of models) and EWSB takes place dynamically based on some new strong dynamics. Lastly, there are models with extra space-time dimensions. We are going to talk at length about them in the next section.

A word of caution in this context would not be inappropriate. Even though there are a host of BSM theories, as of now, none of them have received any confirmatory signatures from any experiment. The currently operative highest energy collider, LHC has already cornered many of the BSM theories and with more data that will come in future years should be able to judge the remaining models.

1.3 Extra Dimension

The concept of extra space-time dimension is not a new import in theoretical physics. It dates back to 1920s. At that time the only known forces of Nature were gravitation (Einstein's theory) and electromagnetism (discovered by Maxwell). As early as in 1914, Gunnar Nordström [24] used a five-dimensional space-time setting to describe Maxwell's theory of electromagnetism and came up with a electromagnetic vector potential and a scalar field which satisfies his own scalar theory of gravity. Later Theodore Kaluza [25] and Oskar Klein [26] advanced this idea of extra space dimension to give a unified theory of gravitation and electromagnetism. According to their idea, the extra spatial dimension is compactified on a circle and thus the presence of this extra dimension can be *felt* only if the experiments have a resolution higher than the radius of the circle of compactification. However with new discoveries in the field of particle physics the original idea of Kaluza-Klein (KK) has been discarded owing to many objections (see *e.g.*, [27] for an account of viability of KK theory in the context of SM).

In the modern parlance, extra dimensions revived with renewed interests in the late 70's and 80's, thanks to the developments in supergravity and string theory. For the internal consistency of string theory one needs a total of 26 space-time dimensions if one considers bosonic theory only; superstring theory takes fermions also into account and it needs 10 space-time dimensions. The extra-dimensions considered in these theories are extremely small ($\mathcal{O}(M_{\text{Pl}}^{-1})$) and are beyond the reach of any experiment possible in near

future.

Very recently the ideas of extra dimension much larger than the Planck length have been put forward:

- TeV-scale extra dimensions, related to the SUSY-breaking, were first introduced by Antoniadis [28].
- The possibility that large extra dimensions (LED) can solve the hierarchy problem was considered by Arkani-Hamed, Dimopoulos and Dvali [29].
- The warped extra dimensional model proposed by Randall and Sundrum [30, 31] is an interesting alternative to the large extra dimension scenario which solves the hierarchy problem.
- Also there is universal extra dimensional model [32] which we will elaborate in Sec. 1.4.

Below we will briefly mention the primary features of LED and the Randall-Sundrum (RS) model.

1.3.1 Large Extra Dimension

We know that there is a large hierarchy between the electroweak scale ($\sim 10^{2-3}$ GeV) and the Planck scale ($M_{\text{Pl}} = 10^{19}$ GeV). To put it another way gravitational interaction is extremely weak compared to the other interactions in SM. To address this question Arkani-Hamed, Dimopoulos and Dvali [29] came up with the idea that there are *flat* extra spatial⁷ dimensions which are compactified. Only gravity can propagate in the *bulk* of the extra dimensions but the SM fields can not. Actually SM fields are localized on a 3-brane⁸. The weakness of the gravitational interactions can be explained by the large volume suppression of the zero-mode (any extra dimension theory gives rise to a tower of KK excitations and the zeroth level of these excitations are identified with the SM fields) graviton⁹ interactions with the 3-brane localized SM fields.

In this model the number of extra spatial dimension, $\delta \geq 2$ is only allowed. Earlier it was assumed that the size of the extra dimension (assuming $\delta = 2$) is $\mathcal{O}(1 \text{ mm})$ but recent

⁷Extra temporal dimensions are problematic, in the sense that they can give rise to tachyonic states also there can exist closed time-like loops which might violate causality. For a detailed discussion see the Introduction section of [33].

⁸In the context of string theory, D -branes are a class of extended objects with spatial dimensionality D .

⁹Gravitons are spin-2 particles which are assumed to be the force carrier of gravitational interaction.

experimental observations put bounds on the size to be less than $30\mu\text{m}$ [34]. However, no significant bound is obtained for $\delta > 3$.

1.3.2 Warped Extra Dimension

The assumption of *flat* extra dimension is valid as long as one assumes that the background metric remains unaffected by the gravity itself. However, the effect of this *back-reaction* of gravity on the branes leads to warped extra dimension. This has important cosmological implications [35,36]. It was shown by Randall and Sundrum [30,31] warped extra dimensional models can also solve the hierarchy problem in an elegant way. In the original RS set-up two 3-branes (called TeV or IR brane and Planck or UV brane) are present. Actually the bulk is a slice of 5D anti-de Sitter (AdS_5) space which is bounded by the two 3-branes. In the minimal version of the RS model only gravity can propagate in the bulk while the Higgs field (and other SM fields) is localized on the brane where the *warp factor*¹⁰ is small. This non-trivial warp factor is the main ingredient that helps to solve the hierarchy problem by "warping down" the Planck scale. For more clarifications see the TASI lectures by Sundrum [37] and Gherghetta [38].

It is worth mentioning that to comply with various experimental observations many variants of the RS model have been adduced. However, from the experimental data from LHC it is evident that even if warped extra dimension (in any variant) exists in Nature, the size of it (*i.e.*, the compactification radius) is smaller than the TeV^{-1} scale [39,40].

1.4 Universal Extra Dimension

Amongst the many variants of extra-dimensional models, Universal Extra Dimensions (UED) proposed by Appelquist et al. [32] is the main focus of this thesis. The *universal* in UED reflects the fact that all of the Standard Model (SM) fields can access the extra dimension instead of some being confined to a boundary as in the case of ADD and RS model. Although UED is devoid of the virtue of solving the hierarchy problem which some other extra-dimensional models do address, there is a wide range of phenomenological motivations for this model.

Proton stability is one of the perplexing issues in particle physics. In SM the existence of dimension six baryon and lepton number violating operators can cause proton decay. Now, to maintain the constraints of proton lifetime in an SM-only theory leads to a cut-

¹⁰Warp factor is a measure of the curvature (warping) along the extra dimension.

off which is unnatural in many aspects. However, by the very construction of the UED model, the operators leading to rapid proton can be forbidden [41]. This is unlike some other BSM physics (*e.g.*, SUSY) where *ad hoc* introduction of some symmetry is required to alleviate the problem of rapid proton decay. The existence of three generation of fermions can also be explained in a version of UED model from the requirement of gauge anomaly cancellation in higher dimension [42]. The issue of gauge coupling unification is also well addressed in these types of theories. Normally they predict a unification scale which is substantially below the usual GUT scale [43–46]. But above all the most pressing motivation for UED comes from the fact that it provides, in a natural way, a stable, electrically neutral and colorless state which can qualify as a viable dark matter candidate. For a detailed review on this subject please see [47]. Moreover a flip side of the scenario is that it shares striking similarities, barring a few subtle differences, with SUSY [48]. So in a collider experiment it requires careful analysis to distinguish between these two scenarios [49].

1.4.1 Basic features

We will consider one extra spatial dimension (y). The problems with extra temporal dimension has been noted in the previous section. In UED, this extra spatial dimension is accessible to all of the SM fields. Now, the extra spatial dimension is compactified on a circle (S^1) of radius R . The inherent meaning of the earlier statement is that in the extra spatial dimension y , we identify two points which are separated by a distance $2\pi R$, *i.e.*, $y \sim y + 2\pi R$. Clearly this type of periodicity will have further implications which we will elucidate later. We denote our coordinates as,

$$x^M = \{x^\mu, y\}, \quad (1.18)$$

where x^μ ($\mu = 0, 1, 2, 3$) indicates the usual 4-dimensional (4D) non-compact space-time coordinates and y denotes the compact extra spatial dimension. The metric convention we will be using is the following,

$$g_{MN} = \text{diag}(+1, -1, -1, -1, -1), \quad (1.19)$$

which represents a flat metric. Had there been any coordinate dependence in the metric we would get a non-flat space.

To illustrate the effect of the identification $y \sim y + 2\pi R$, consider a real scalar field in 5-dimension (5D), $\Phi(x, y)$. Since in the extra dimension the points y and $y + 2\pi R$ are

identified, the field $\Phi(x, y)$ satisfies the condition: $\Phi(x, y) = \Phi(x, y + 2\pi R)$. Due to this periodicity in the y -coordinate, we can expand the 5D field in an infinite series of Fourier modes as,

$$\Phi(x, y) = \frac{1}{\sqrt{2\pi R}} \sum_{n=-\infty}^{\infty} \phi^{(n)}(x) e^{\frac{iny}{R}}, \quad (1.20)$$

where $1/\sqrt{2\pi R}$ is just a normalization factor. This also reminds us that the dimensionality of the 5D fields are different from that of 4D fields. Here $\phi^{(n)}(x)$ is called the n -th Kaluza-Klein (KK) mode. The zeroth mode $\phi^{(0)}$ will be identified as the SM field. Now to clarify some more issues, consider the 5D action of a real scalar field, given by,

$$\mathcal{S}_{5D} = \frac{1}{2} \int d^4x \int_0^{2\pi R} dy \left[\partial_M \Phi(x, y) \partial^M \Phi(x, y) - m_0^2 \Phi^2(x, y) \right], \quad (1.21)$$

where m_0 can be regarded as the zero-mode mass. The 4D action can be obtained by dimensional reduction of the 5D action by performing the integration over the compactified extra dimension. Plugging the expansion of $\Phi(x, y)$ into Eq. 1.21 and performing the integration one can get the effective 4D action to be,

$$\mathcal{S}_{4D} = \frac{1}{2} \sum_n \int d^4x \left[\partial_\mu \phi^{(n)}(x) \partial^\mu \phi^{(n)}(x) - \left(m_0^2 + \frac{n^2}{R^2} \right) (\phi^{(n)}(x))^2 \right]. \quad (1.22)$$

Thus the n -th KK mode $\phi^{(n)}(x)$ has mass,

$$m_n = \sqrt{m_0^2 + \frac{n^2}{R^2}}. \quad (1.23)$$

So, the smaller the compactification radius R , the larger the mass of the n -th mode. Also, Eq. 1.22 asserts that the 5D theory is equivalent to a theory with an infinite tower of 4D fields with masses m_n . This recasting of the 5D theory into a 4D theory is called KK decomposition. In an alternate way [50], instead of substituting Eq. 1.20 in Eq. 1.21, one can straightaway vary the 5D action to get the equation of motion and then solve them to obtain the mass relation as well as the KK expansion of the fields.

Till now we have used a real scalar field to illustrate the situation. Generalizing this to gauge fields and fermions is straightforward. But special care is to be taken for the case of fermions. This is due to the fact that defining chirality operator in odd number of dimension is not possible. Consider a massless fermion field $\Psi(x, y)$ in 5D. It will satisfy the Dirac equation $i\partial_M \Gamma^M \Psi(x, y) = 0$, where Γ_M satisfies the Clifford algebra,

$$\{\Gamma^M, \Gamma^N\} = 2\eta^{MN}, \quad (1.24)$$

where η^{MN} is the Minkowski metric in 5D. Now in the 5D case,

$$\Gamma^M = (\gamma^\mu, i\gamma_5). \quad (1.25)$$

Since γ_5 is being included among the Dirac matrices of 5D and there is no other matrix with the anti-commuting properties of γ_5 , there is no explicit chirality in 5D theory. Actually, in any dimension (even or odd), say n , we have n -number of gamma matrices Γ^a ($a = 1, 2, \dots, n$), satisfying $\{\Gamma^a, \Gamma^b\} = 2\eta^{ab}$. Then a generalized γ_5 can be defined as,

$$\Gamma^{n+1} = \Gamma^1 \Gamma^2 \dots \Gamma^n. \quad (1.26)$$

Then for even number of dimension, *i.e.*, $n = 2p$, Γ^{n+1} will be nilpotent ($(\Gamma^{n+1})^2 = 1$) and anti-commute with all Γ^a ,

$$\{\Gamma^{n+1}, \Gamma^a\} = 0, \quad \forall a = 1, 2, \dots, 2p. \quad (1.27)$$

However for odd number of dimension, $n = 2p + 1$,

$$[\Gamma^{n+1}, \Gamma^a] = 0, \quad \forall a = 1, 2, \dots, 2p + 1, \quad (1.28)$$

and then by Schur's lemma Γ^{n+1} is just a multiple of unit matrix. Thus in odd number of dimensions defining chiral fermion is not possible. Consequently, the fermions in odd number of dimension will necessarily be vector-like. Even though we are interested in the effective 4D theory, this problem will haunt us even after we integrate out the extra dimension, in the sense that now even the zero modes, which we will identify as the SM fields, will be vector-like which is in stark difference with the observations. To ameliorate this problem we need to further modify the space. We need to orbifold the compactified dimension. This is nothing but imposing one more identification $y \sim -y$. Orbifolding

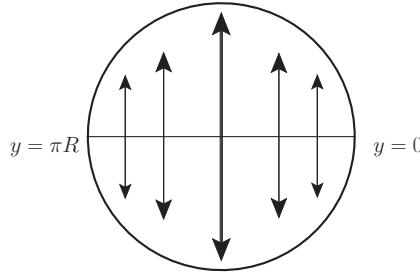


Figure 1.3: Pictorial description of orbifolding.

essentially makes the circle an interval of length πR with two endpoints 0 and πR , which

are basically fixed points of the manifold. After the orbifold compactification the resulting space is called an S^1/\mathbb{Z}_2 orbifold. Now, we can specify the transformation properties of the fields under this orbifold projection. An appropriate choice of this transformation property eliminates the phenomenologically undesirable degrees of freedom (DoF) at the zero modes level. For example, consider a generic field $\Phi(x, y)$, then

$$\Phi(x, y) \xrightarrow{y \rightarrow -y} \Phi(x, -y) = \pm \Phi(x, y). \quad (1.29)$$

The ‘even’(‘odd’) type field is defined by the $+(-)$ value in Eq. 1.29 and is denoted by Φ^+ (Φ^-). It can be shown that the even (odd) field satisfy Neumann (Dirichlet) boundary conditions, $\partial_y \Phi^+|_{y=0, \pi R} = 0$ ($\Phi^-|_{y=0, \pi R} = 0$). The KK decompositions of even and odd fields are given by,

$$\Phi^+(x, y) = \frac{1}{\sqrt{\pi R}} \phi^{(0)+}(x) + \sqrt{\frac{2}{\pi R}} \sum_{n=1}^{\infty} \phi^{(n)+}(x) \cos \frac{ny}{R}, \quad (1.30)$$

$$\Phi^-(x, y) = \sqrt{\frac{2}{\pi R}} \sum_{n=1}^{\infty} \phi^{(n)-}(x) \sin \frac{ny}{R}. \quad (1.31)$$

Clearly, zero mode of the odd field is then disallowed. Likewise by imposing appropriate transformation properties on the fermions we can obtain zero mode chiral (instead of getting vector-like) fermion in the 4D theory.

A generic gauge field in 5D can be written as, $A_M(x, y)$ ($M = 0, 1, 2, 3, 4$). However from now on we will use the index ‘5’ for the fourth spatial component. Thus a 5D gauge boson has five components, the usual $A_\mu(x, y)$ ($\mu = 0, 1, 2, 3$) and $A_5(x, y)$. The fifth component $A_5(x, y)$ corresponds to the polarization of the gauge field along the extra dimension and from 4D point of view, after compactification, this just behaves as a tower of spinless KK modes. Also this A_5 will have no zero mode and will be an odd field. Thus the boundary conditions for various components of $A_M(x, y)$ are, $\partial_y A_\mu|_{y=0, \pi R} = 0$ and $A_5|_{y=0, \pi R} = 0$. So the KK decomposition of $A_\mu(x, y)$ will be like Eq. 1.30 and that of $A_5(x, y)$ will be like Eq. 1.31.

In passing it is worth-mentioning that the presence of this fifth component of gauge field A_5 can play crucial role in determining the unitarity of the 5D theory [51]. Interestingly, in the pre-Higgs discovery era Higgs-less models were constructed based on this idea [52, 53].

1.4.2 KK parity

The KK number of a particle is a measure of its momentum in fifth dimension, *i.e.*, $p_5 = n/R$. Unlike the 4D momentum, p_5 is not a conserved quantity. The damage is done by the orbifold compactification which breaks the translational invariance along the extra dimension, rendering p_5 , *viz.* KK number, being violated. Even after the breaking of KK number there remains an accidental discrete symmetry, called KK parity, which is the translational symmetry $y \rightarrow y - \pi R$. From Eqs. 1.30 and 1.31 it is evident that under this transformation the even KK modes are invariant while the odd KK modes flip their sign. Thus for the n -th level particle KK parity is $(-1)^n$. KK parity is a multiplicative quantum number. One important point to keep in mind here is that the discrete symmetry, KK parity is *not* the \mathbb{Z}_2 of S^1/\mathbb{Z}_2 . Evidently all SM particles are then of even KK parity. A few phenomenological consequences of KK parity conservation are,

- stability of Lightest Kaluza-Klein Particle (LKP),
- in collider experiments, odd KK level particles can be produced only pairwise,
- all direct couplings of SM particles to even number KK states are loop suppressed.

All of these points will be elaborated in due time. Normally in the minimal version of UED, KK parity remains a good symmetry. But it can be broken by the introduction of explicit KK parity violating interactions (which nevertheless respect other symmetries *e.g.*, gauge, Lorentz etc.) on the orbifold fixed points. In passing it is worth mentioning that KK parity is somewhat analogous to the discrete symmetry, called R-parity, in the context of SUSY.

1.4.3 Standard Model in 5D

Accoutered with the basic tenets of extra-dimensional theories, we are now in a position to discuss the scenario where the SM is embedded in 5D with one extra spatial dimension and all SM fields can propagate in the bulk of this 5D. Even though SM will be embedded in 5D the gauge structure of the theory will remain intact, *i.e.*, the usual $SU(3)_c \otimes SU(2)_L \otimes U(1)_Y$. The 5D gauge fields for these gauge groups are G_M^a , W_M^a and B_M , where a represents the non-Abelian gauge index. As for the fermion fields they are simple 5D fermion fields satisfying appropriate parity transformations to ensure chiral fermions in 4D. Actually in SM, there is no left handed $SU(2)_L$ -singlet fermion and

right handed $SU(2)_L$ -doublet fermion. Thus in UED the SM doublet (Ψ) and singlet (ψ) fermions are the zero modes in the expansions¹¹

$$\Psi(x, y) = \frac{1}{\sqrt{\pi R}} \left[\Psi_L^{(0)} + \sqrt{2} \sum_{n=1}^{\infty} \left(\Psi_L^{(n)}(x) \cos \frac{ny}{R} + \Psi_R^{(n)}(x) \sin \frac{ny}{R} \right) \right], \quad (1.32a)$$

$$\psi(x, y) = \frac{1}{\sqrt{\pi R}} \left[\psi_R^{(0)} + \sqrt{2} \sum_{n=1}^{\infty} \left(\psi_R^{(n)}(x) \cos \frac{ny}{R} + \psi_L^{(n)}(x) \sin \frac{ny}{R} \right) \right]. \quad (1.32b)$$

These fields satisfy $\Psi(x, y) = -\gamma_5 \Psi(x, -y)$ and $\psi(x, y) = +\gamma_5 \psi(x, -y)$ which ensures that the zero modes *i.e.*, the SM fermions, appear with correct chirality.

Now we will describe the action for the 5D UED. In the following we write the action for various sectors separately to avoid cluttering. Here we will follow the notations of [54].

$$\mathcal{S}_{\text{gauge}} = \int d^4x \int_0^{\pi R} dy \left[-\frac{1}{4} B_{MN} B^{MN} - \frac{1}{4} W_{MN}^a W^{aMN} - \frac{1}{4} G_{MN}^i G^{iMN} \right], \quad (1.33a)$$

$$\mathcal{S}_{\text{GF}} = \int d^4x \int_0^{\pi R} dy \left[-\frac{1}{2\xi} (\partial_\mu B^\mu - \xi \partial_5 B_5)^2 - \frac{1}{2\xi} (\partial_\mu W^{a\mu} - \xi \partial_5 W_5^a)^2 - \frac{1}{2\xi} (\partial_\mu G^{i\mu} - \xi \partial_5 G_5^i)^2 \right], \quad (1.33b)$$

$$\mathcal{S}_{\text{lepton}} = \int d^4x \int_0^{\pi R} dy \sum_{j=\text{generation}} [i\bar{L}_j \not{D} L_j + i\bar{e}_j \not{D} e_j], \quad (1.33c)$$

$$\mathcal{S}_{\text{quark}} = \int d^4x \int_0^{\pi R} dy \sum_{j=\text{generation}} [i\bar{Q}_j \not{D} Q_j + i\bar{u}_j \not{D} u_j + i\bar{d}_j \not{D} d_j], \quad (1.33d)$$

$$\mathcal{S}_{\text{Yuk}} = \int d^4x \int_0^{\pi R} dy \sum_{i,j=\text{generation}} \left[-\hat{Y}_{ij}^u \bar{Q}_i \tilde{H} u_j - \hat{Y}_{ij}^d \bar{Q}_i H d_j - \hat{Y}_{ij}^l \bar{L}_i H e_j \right], \quad (1.33e)$$

$$\mathcal{S}_{\text{Higgs}} = \int d^4x \int_0^{\pi R} dy \left[(D_M H)^\dagger (D^M H) - \hat{\mu}^2 H^\dagger H - \hat{\lambda} (H^\dagger H)^2 \right]. \quad (1.33f)$$

The field strength tensor for the gauge fields, B_M , W_M^a and G_M^i are given by,

$$B_{MN} = \partial_M B_N - \partial_N B_M, \quad (1.34a)$$

$$W_{MN}^a = \partial_M W_N^a - \partial_N W_M^a + \hat{g}_2 \epsilon^{abc} W_M^b W_N^c, \quad (1.34b)$$

$$G_{MN}^i = \partial_M G_N^i - \partial_N G_M^i + \hat{g}_3 f^{ijk} G_M^j G_N^k. \quad (1.34c)$$

¹¹The chirality projection operators for the 4D modes of any fermionic field Ψ , is defined in a similar fashion, see footnote 2.

Here ϵ^{abc} and f^{abc} are structure constants for $SU(2)_L$ and $SU(3)_c$ respectively. Also, \hat{g}_i ($i = 1, 2, 3$) are the 5D gauge couplings for $U(1)$, $SU(2)_L$ and $SU(3)_c$ gauge groups. Unlike its 4D counterparts, these 5D couplings are dimensionful parameters. As will be illustrated later, there exists a scaling relation between the couplings in 4D and those of 5D. In the context of UED, this relation is,

$$g_i = \frac{\hat{g}_i}{\sqrt{\pi R}}, \quad (1.35)$$

where g_i represents the usual 4D coupling. An important observation from Eq. 1.35 is that the 5D coupling has negative mass dimension. This is a well-known fact that theories which have couplings with negative mass dimension are not renormalizable. Thus we arrive at the well accorded maxim that extra-dimensional theories are non-renormalizable.

The guiding principle for the construction of the gauge fixing action, \mathcal{S}_{GF} , is to prohibit A_μ - A_5 mixing and this is ensured by the very form of \mathcal{S}_{GF} given in Eq. 1.33b.

In Eqs. 1.33c and 1.33d, the $\not{D} = \Gamma^M D_M$, where Γ^M is defined in Eq. 1.25 and D_M represents the covariant derivative. Since covariant derivatives, in a way, determine the interaction between the fermion and the gauge boson, the explicit form of D_M will be dictated by the interaction properties of the corresponding fermionic field. For example, the covariant derivative for the quarks are given by,

$$D_M = \partial_M - i\hat{g}_1 \frac{Y_q}{2} B_M - i\hat{g}_2 \frac{\sigma^a}{2} W_M^a - i\hat{g}_3 \frac{\lambda^i}{2} G_M^i, \quad (1.36)$$

where sum over repeated gauge indices is implied. The hypercharge, Y , assignments of fermions are the same as that of SM, *i.e.*, $Y_Q = 1/3$, $Y_u = 4/3$, $Y_d = -2/3$, $Y_L = -1$ and $Y_e = -2$. Also σ^a ($a = 1, 2, 3$) are Pauli matrices and λ^i ($i = 1, 2, 3, \dots, 8$) are Gell-Mann matrices which are related to the generators of $SU(2)_L$ and $SU(3)_c$ respectively. Various Y_{ij} s in Eq. 1.33e are just the 5D Yukawa couplings and we define \tilde{H} , used in Eq. 1.33f, as $\tilde{H} \equiv i\sigma^2 H^*$.

1.4.4 Particle content and interactions

In Sec. 1.4.1 we have seen that from 4D perspective the effect of 5D will be reflected as the presence of an infinite KK tower of 4D fields with the lowest lying KK states, *i.e.*, the zero modes, being the SM particles. So the particle content of UED will be the SM particles, augmented by the KK tower of each species of those particles. Now, since the KK tower is infinite there is no harm in the assumption that there are infinite number of particles in UED. But as we go to higher and higher rungs of the KK tower the particles become so heavy (see Eq. 1.23) that they will not result in any observable consequences. Thus for any

practical purpose the effect of first few KK level is important. In passing we also recall the fact that for fermions only the zero modes are chiral but non-zero KK level fermions are always vector-like.

In SM the masses of particles vary from¹² MeV to GeV range. We have already mentioned that m_0 in Eq. 1.23 represents the zero mode or SM mass. Also, for a very small compactification radius ($1/R \sim \text{TeV}$), it is n^2/R^2 which is the dominant part in Eq. 1.23. As a consequence, even if the zero mode masses of various particles are different, non-zero mode masses will be autocratically dictated by $1/R$ and this being very large compared to the masses of SM particles, *all* of the particles in a non-zero KK level will be highly degenerate in mass. Later we will see that radiative corrections result in a non-degenerate mass spectrum.

Now we turn our attention to the interactions between various particles in UED. Calculating these interactions is also straightforward. In the coupling extraction process, however, we have to make sure that the couplings in zero mode sector come exactly like the SM couplings. So the procedure to calculate any coupling in UED is the following.

- Pick the corresponding action from the set of Eqs. 1.33.
- Collect the concerned interaction term between the fields.
- Write all the fields in terms of their respective KK expansion, keeping general mode numbers.
- Lastly, perform the y -integral to get the effective 4D coupling.

For example, suppose we want to calculate the interaction between fermions and gauge bosons. Now, this coupling comes from the fermion kinetic term, $i\bar{\chi}(x, y)\Gamma^M D_M\chi(x, y)$, where $\chi(x, y)$ is any arbitrary 5D fermionic field. Then,

$$i\bar{\chi}(x, y)\Gamma^M D_M\chi(x, y) = i\bar{\chi}(x, y)\gamma^\mu D_\mu\chi(x, y) + i\bar{\chi}(x, y)(i\gamma^5)D_5\chi(x, y). \quad (1.37)$$

For the time being, concentrate on the first term only. We write, illustratively, $D_\mu = \partial_\mu - i\hat{g}A_\mu$. Hence, the interaction between gauge field A_μ and fermion χ will be $\hat{g}\bar{\chi}(x, y)A_\mu(x, y)\chi(x, y)$. Then plug the KK expansion of each field in this term.

$$\hat{g} \int d^4x \int_0^{\pi R} dy \sum_{p,q,r} \left[\left(\frac{1}{\sqrt{\pi R}} \bar{\chi}^{(0)}(x) + \frac{\sqrt{2}}{\sqrt{\pi R}} \sum_p \left\{ \bar{\chi}_+^{(p)}(x) \cos \frac{py}{R} + \bar{\chi}_-^{(p)}(x) \sin \frac{py}{R} \right\} \right) \right]$$

¹²Leaving neutrinos from the considerations, as their exact masses are not yet measured but are assumed to be very small.

$$\begin{aligned}
& \times \gamma_\mu \left(\frac{1}{\sqrt{\pi R}} A^{\mu(0)}(x) + \frac{\sqrt{2}}{\sqrt{\pi R}} \sum_q \left\{ A_+^{\mu(q)}(x) \cos \frac{qy}{R} + A_-^{\mu(q)}(x) \sin \frac{qy}{R} \right\} \right) \\
& \times \left(\frac{1}{\sqrt{\pi R}} \bar{\chi}^{(0)}(x) + \frac{\sqrt{2}}{\sqrt{\pi R}} \sum_r \left\{ \chi_+^{(r)}(x) \cos \frac{ry}{R} + \chi_-^{(r)}(x) \sin \frac{ry}{R} \right\} \right) \Big]. \quad (1.38)
\end{aligned}$$

From this equation we can extract the coupling between χ and A_μ for any arbitrary KK level, *i.e.*, the coefficient of $\bar{\chi}^{(p)} A^{(q)} \chi^{(r)}$. The zero mode coupling can be obtained for $p = q = r = 0$, and can be written from Eq. 1.38,

$$\begin{aligned}
& \frac{\hat{g}}{(\pi R)^{3/2}} \int d^4x \int_0^{\pi R} dy \bar{\chi}^{(0)}(x) \gamma_\mu A^{\mu(0)}(x) \chi^{(0)}(x) \\
& = \frac{\hat{g}}{\sqrt{\pi R}} \int d^4x \bar{\chi}^{(0)}(x) \gamma_\mu A^{\mu(0)}(x) \chi^{(0)}(x) \\
& = g \int d^4x \bar{\chi}^{(0)}(x) \gamma_\mu A^{\mu(0)}(x) \chi^{(0)}(x). \quad (1.39)
\end{aligned}$$

Thus we will get the right zero mode coupling if $g = \hat{g}/\sqrt{\pi R}$, which is the correct scaling between 4D and 5D coupling, as we mentioned in Eq. 1.35. It can be shown, following similar steps, that KK number violating couplings are vanishing. Thus a second level particle can not have any tree level interaction with two zeroth level particles. Such a coupling is, however, present at loop level. In the last chapter we will discuss one scenario of this sort. Also we will see later, that this type of 2-0-0 coupling is possible, even at tree level, in the non-minimal version of UED.

The method of coupling extraction, mentioned here, is thus the standard procedure to obtain couplings between appropriate fields. Similar method will be used in the case of non-minimal version of UED also.

1.5 Structure of this thesis

In this section we will briefly describe the build-up of this thesis. In the following Chapter 2 we present an overview of the minimal and non-minimal UED. Chapter 3 consists of basics of dark matter and its observational implications on UED. Sections 3.3.2 and 3.4.2 in that chapter is based on the original work [55]. Chapters 4 and 5 are based on the original works [56] and [57]. Finally in Chapter 6 we conclude.

Chapter 2

Minimal and Non-minimal Universal Extra Dimension

In the previous chapter we have described the UED model. We also pointed out that for non-zero KK level the mass spectrum is highly degenerate. In this chapter we will briefly discuss, following [58], how radiative corrections lift the degeneracy. In the later part of the chapter we will review the non-minimal version of UED and set the notations and conventions for subsequent chapters.

2.1 Minimal Universal Extra Dimension

2.1.1 Radiative corrections

We have seen that the mass of the n -th mode particle is given by $\sqrt{m_0^2 + (n/R)^2}$. However, this is just the outcome of 5D Lorentz invariance (LI) of the tree level Lagrangian. Under radiative corrections this relation will be modified as $\sqrt{m_0^2 + (n/R)^2 + \delta m_n^2}$, where δm_n is the correction in mass coming from radiative corrections. The mass correction comes from the higher order contributions to the two-point correlation functions. There are two types of contributions to these mass corrections.

- Bulk corrections coming from compactification.
- Corrections due to orbifolding

The *first* type of correction comes from the S^1 compactification which breaks the 5D LI globally. Due to this type of non-local effect there can be loops which wind around the circle of the compactified dimension, see Fig. 2.1. The contributions coming from this type of loops are well defined and finite.

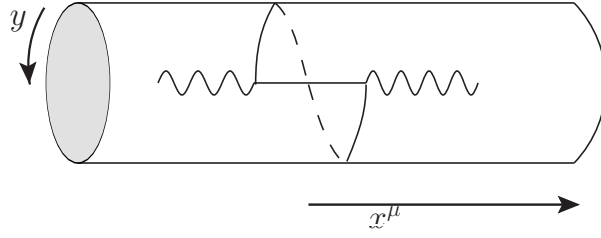


Figure 2.1: An example of a loop winding around the extra dimension.

The *second* type of correction is mandated by the orbifold compactification S^1/\mathbb{Z}_2 . Actually, orbifolding introduces fixed points ($y = 0$ and $y = \pi R$ in our case) in the manifold and they lead to additional breaking of 5D LI. This is a local effect. Radiative corrections of a field theory in S^1/\mathbb{Z}_2 orbifold has been calculated in [59]. Unlike bulk contribution, the mass shift coming from this orbifold correction is no longer finite, but logarithmically divergent. That means counterterms, localized at the orbifold fixed points, are needed to renormalize them. At this point one simplifying assumption, that the boundary terms at the cut-off Λ are small, is made. Then there is no mixing between different KK level particles and each mode receives, in addition to the bulk correction, a shift in its mass that is logarithmically dependent on the cut-off Λ .

The scenario with the assumption of vanishing boundary terms at the cut-off Λ is termed as *minimal UED (mUED)*. In the case of non-minimal UED this assumption will be relaxed.

Combining the above mentioned two types of corrections the total mass shift δm_n for various particles are given by [58],

$$\delta m_{Q^{(n)}} = \frac{n}{16\pi^2 R} \left(6g_3^2 + \frac{27}{8}g_2^2 + \frac{1}{8}g_1^2 \right) \ln(\Lambda R), \quad (2.1a)$$

$$\delta m_{u^{(n)}} = \frac{n}{16\pi^2 R} (6g_3^2 + 2g_1^2) \ln(\Lambda R), \quad (2.1b)$$

$$\delta m_{d^{(n)}} = \frac{n}{16\pi^2 R} \left(6g_3^2 + \frac{1}{2}g_1^2 \right) \ln(\Lambda R), \quad (2.1c)$$

$$\delta m_{L^{(n)}} = \frac{n}{16\pi^2 R} \left(\frac{27}{8}g_2^2 + \frac{9}{8}g_1^2 \right) \ln(\Lambda R), \quad (2.1d)$$

$$\delta m_{e^{(n)}} = \frac{n}{16\pi^2 R} \frac{9}{2}g_1^2 \ln(\Lambda R), \quad (2.1e)$$

$$\delta m_{B^{(n)}}^2 = \frac{g_1^2}{16\pi^2 R^2} \left(-\frac{39}{2} \frac{\zeta(3)}{\pi^2} - \frac{n^2}{3} \ln(\Lambda R) \right), \quad (2.1f)$$

$$\delta m_{W^{(n)}}^2 = \frac{g_2^2}{16\pi^2 R^2} \left(-\frac{5}{2} \frac{\zeta(3)}{\pi^2} + 15n^2 \ln(\Lambda R) \right), \quad (2.1g)$$

$$\delta m_{g^{(n)}}^2 = \frac{g_3^2}{16\pi^2 R^2} \left(-\frac{3}{2} \frac{\zeta(3)}{\pi^2} + 23n^2 \ln(\Lambda R) \right), \quad (2.1h)$$

$$\delta m_{H^{(n)}}^2 = \frac{n^2}{16\pi^2 R^2} \left(3g_2^2 + \frac{3}{2}g_1^2 - 2\lambda_h \right) \ln(\Lambda R), \quad (2.1i)$$

where g_1 , g_2 and g_3 are the gauge couplings for the $U(1)_Y$, $SU(2)_L$ and $SU(3)_c$ groups respectively and λ_h is the Higgs quartic coupling. The factor $\zeta(3) = \sum_{n=1}^{\infty} n^{-3} \approx 1.20205\dots$, is the third Riemann zeta function. The factor $\ln(\Lambda R)$ in the Eqs. 2.1 comes from the orbifold corrections and the Λ -independent contributions are from bulk corrections. Actually, the factor is $\ln\left(\frac{\Lambda}{\mu}\right)$ where μ is the renormalization scale. Generally μ is approximately taken as the mass of the corresponding KK mode. The factor ΛR counts the number of KK levels below Λ . If the contributions from Yukawa coupling is also considered (which is significant for top quark), then $SU(2)$ doublet quark T and singlet t receive corrections,

$$\delta_{\text{Yuk}} m_{T^{(n)}} = \frac{n}{16\pi^2 R} \left(-\frac{3}{2} y_t^2 \right) \ln(\Lambda R), \quad (2.2a)$$

$$\delta_{\text{Yuk}} m_{t^{(n)}} = \frac{n}{16\pi^2 R} \left(-3y_t^2 \right) \ln(\Lambda R). \quad (2.2b)$$

Thus to get the radiatively corrected mass for top quark of n -th mode we need to add these with appropriate corrections presented in Eq. 2.1. Also since the non-zero KK level fermions are vector-like so appropriate eigenstates and mass eigenvalues of the KK fermions can be obtained by diagonalizing the mass matrix of the form,

$$\begin{pmatrix} \frac{n}{R} + \delta_{\text{tot}} m_{F^{(n)}} & m_f \\ m_f & -\frac{n}{R} - \delta_{\text{tot}} m_{f^{(n)}} \end{pmatrix}, \quad (2.3)$$

where m_f is the zero mode mass obtained from EWSB and δ_{tot} represents the total correction arising from bulk, boundary as well as Yukawa corrections that are mentioned in Eqs. 2.1 and 2.2.

KK mass eigenstates and the eigenvalues of photon and Z-boson are obtained, in the similar spirit of SM, by diagonalizing the mass squared matrix \mathcal{M}_{GB} in the $B^{(n)}$ and $W^{3(n)}$ basis,

$$\begin{pmatrix} \left(\frac{n^2}{R^2} + \delta m_{W^{3(n)}}^2 \right) + \frac{1}{4} g_2^2 v^2 & -\frac{1}{4} g_1 g_2 v^2 \\ -\frac{1}{4} g_1 g_2 v^2 & \left(\frac{n^2}{R^2} + \delta m_{B^{(n)}}^2 \right) + \frac{1}{4} g_1^2 v^2 \end{pmatrix} \quad (2.4)$$

Clearly for the zeroth level the diagonal entries will have only v^2 -dependent terms, and then the eigenvalues of this matrix will be $\{0, (g_1^2 + g_2^2)v^2/4\}$ where zero is the mass eigenvalue of the SM photon and $(g_1^2 + g_2^2)v^2/4$ is the mass squared eigenvalue of the SM Z -boson and the vacuum expectation value (vev) of Higgs, $v = 246$ GeV. For the non-zero mode particles the full matrix in Eq. 2.4 is to be used. Evidently, for the KK particles, the Weinberg mixing angle, θ_n will also be different from that of zero mode particles and is given by,

$$\theta_n = \frac{1}{2} \tan^{-1} \left(\frac{g_1 g_2 v^2}{2 [\delta m_{W^{3(n)}}^2 - \delta m_{B^{(n)}}^2 + \frac{v^2}{4} (g_2^2 - g_1^2)]} \right). \quad (2.5)$$

As it stands, θ_n is small which makes the KK photon more $B^{(n)}$ -like and KK Z -boson more $W^{3(n)}$ -like. They are often used interchangeably.

Unlike 4D SM, in mUED the KK W and Z -boson acquire their masses by absorbing the linear combination of the fifth component of the gauge fields and the KK Goldstone bosons. After this for each KK level there remains four scalar states: two charged scalars $H^{(n)\pm}$, CP-even neutral scalar $H^{(n)}$ and CP-odd neutral scalar $A_0^{(n)}$. Clearly, the zero modes $H^{(0)\pm}$ and $A_0^{(0)}$ are the usual Goldstone bosons in the SM. The one loop corrected masses of these extra scalar states are,

$$m_{H^{(n)\pm}}^2 = \frac{n^2}{R^2} + m_{W^{(0)}}^2 + \delta m_{H^{(n)}}^2, \quad (2.6a)$$

$$m_{A_0^{(n)}}^2 = \frac{n^2}{R^2} + m_{Z^{(0)}}^2 + \delta m_{A_0^{(n)}}^2, \quad (2.6b)$$

where $\delta m_{H^{(n)}}^2$ is given by Eq. 2.1i.

2.1.2 Mass spectrum

After the discussion of radiative corrections of masses for various species of particles we are now in a position to discuss the particle spectrum of the full one loop corrected mUED. We have seen in the previous section that the shift in mass is different for different types of particles (see Eqs. 2.1). Then for non-zero KK level particle spectrum will no longer be degenerate. Clearly, now the phenomenology of the model will be quite different from what would have been the case for the tree level degenerate spectrum. In Fig. 2.2 (taken from [58]) an illustrative spectrum, for a definite choice of mUED parameters (m_H , $1/R$ and Λ)¹, for the first KK level has been shown.

¹Here m_H is the mass of SM Higgs boson. After the discovery of Higgs, [20,21] and subsequent analysis [60], $m_H = 125.9 \pm 0.4$ GeV.

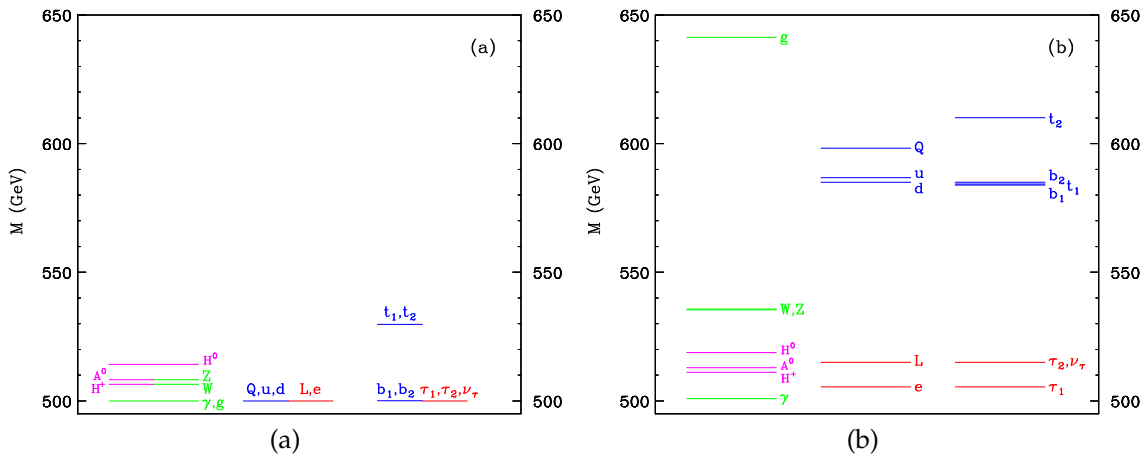


Figure 2.2: (From [58]). Particle spectrum for the first level KK particles at tree level (left) and after one loop correction (right). Assuming Higgs mass $m_H = 120$ GeV, $1/R = 500$ GeV and $\Lambda R = 20$.

An important observation is that at any specific level the mass of KK photon ($\gamma^{(n)}$) receives the merest contribution from radiative corrections. The upshot of this observation is that the first level photon, *i.e.*, $\gamma^{(1)}$ (or $B^{(1)}$, so to say) is the lightest KK particle (LKP). $B^{(1)}$ is a particle with odd KK parity. The decay of this particle to any KK level particle is kinematically forbidden and to SM particles is forbidden due to the conservation of KK parity. Thus $B^{(1)}$ is a stable particle and it has all the properties to qualify as a suitable dark matter candidate. We will discuss more about this in Chapter 3.

2.2 Non-minimal Universal Extra Dimension

In the previous section 2.1 we have discussed how the radiative correction modify the mass spectrum of the model. Also we have seen that the orbifold corrections are logarithmically divergent and to remove these divergences boundary localized counterterms are needed. A general form of these type of terms would be,

$$r\{\delta(y) + \delta(y - \pi R)\} \times (\text{appropriate field combinations}) \quad (2.7)$$

The two Dirac delta functions assure the localization. Now as a counterterm (Eq. 2.7), the parameter r can be chosen such that the divergent contribution from orbifold corrections are just canceled out at a scale, say Λ_{arb} . Indeed without any loss of generalization, one can take $\Lambda_{arb} = \Lambda$, where Λ is the cut-off scale. But then again, in time of renormalization

group (RG) running from Λ down to the electroweak scale these terms will be induced radiatively. So, from the point of view of effective field theory, a constant like r has to be considered as a free parameter of the theory and experimental data are to be used to put constraint on it. However, these boundary localized terms (BLT) obey 4D LI and gauge symmetries of SM. Actually every bulk term in the action will have their corresponding BLTs. In the following we will write these BLTs and study their effects. This scenario is called non-minimal UED (nmUED) where the ‘non-minimality’ reflects the fact that assumption of vanishing BLTs at the cut-off scale is relaxed. Various physical aspects of these BLTs are discussed in [61–66].

2.2.1 Model description

In this section we will discuss the basic features of nmUED. We are going to consider a 5D theory, compactified on S^1/\mathbb{Z}_2 , with additional kinetic terms localized at the boundaries at $y = 0$ and $y = \pi R$. The action for various fields in the presence of boundary localized kinetic terms (BLKT) are given by [67],

$$\mathcal{S}_{\text{gauge}} = -\frac{1}{4} \int d^4x \int_0^{\pi R} dy \sum_a [F_{MN}^a F^{aMN} + r_a \{\delta(y) + \delta(y - \pi R)\} F_{\mu\nu}^a F^{a\mu\nu}], \quad (2.8a)$$

$$\begin{aligned} \mathcal{S}_{\text{lepton}} = \int d^4x \int_0^{\pi R} dy \sum_{j=\text{generation}} \left[i\bar{L}_j \Gamma^M D_M L_j + r_f \{\delta(y) + \delta(y - \pi R)\} \phi_{jL}^\dagger i\bar{\sigma}^\mu D_\mu \phi_{jL} \right. \\ \left. + i\bar{e}_j \Gamma^M D_M e_j + r_f \{\delta(y) + \delta(y - \pi R)\} \chi_{jR}^\dagger i\bar{\sigma}^\mu D_\mu \chi_{jR} \right], \end{aligned} \quad (2.8b)$$

$$\begin{aligned} \mathcal{S}_{\text{quark}} = \int d^4x \int_0^{\pi R} dy \sum_{j=\text{generation}} \left[i\bar{Q}_j \Gamma^M D_M Q_j + r_f \{\delta(y) + \delta(y - \pi R)\} \phi_{jL}^{Q\dagger} i\bar{\sigma}^\mu D_\mu \phi_{jL}^Q \right. \\ \left. + i\bar{u}_j \Gamma^M D_M u_j + r_f \{\delta(y) + \delta(y - \pi R)\} \chi_{jR}^{u\dagger} i\bar{\sigma}^\mu D_\mu \chi_{jR}^u \right. \\ \left. + i\bar{d}_j \Gamma^M D_M d_j + r_f \{\delta(y) + \delta(y - \pi R)\} \chi_{jR}^{d\dagger} i\bar{\sigma}^\mu D_\mu \chi_{jR}^d \right], \end{aligned} \quad (2.8c)$$

$$\begin{aligned} \mathcal{S}_{\text{Higgs}} = \int d^4x \int_0^{\pi R} dy \left[(D_M H)^\dagger (D^M H) - \hat{\mu}^2 H^\dagger H - \hat{\lambda} (H^\dagger H)^2 \right. \\ \left. + r_H \{\delta(y) + \delta(y - \pi R)\} (D_\mu H)^\dagger D^\mu H \right]. \end{aligned} \quad (2.8d)$$

Here in Eqs. 2.8a, a represents the gauge group index. We will use r_B , r_W , r_G as the BLKT parameters for $U(1)_Y$, $SU(2)_L$, $SU(3)_c$ gauge bosons respectively. The fields labeled by ϕ and χ , in Eqs. 2.8b and 2.8c, will be described shortly.

One important point to note here is that these type of symmetric BLTs preserve KK parity. Asymmetric BLT is the case where the BLT parameters, r , are different at the two boundaries, *i.e.*,

$$\underbrace{r\{\delta(y) + \delta(y - \pi R)\}}_{\text{Symmetric BLT}} \quad \text{and} \quad \underbrace{\{r_1\delta(y) + r_2\delta(y - \pi R)\}}_{\text{Asymmetric BLT}}.$$

Asymmetric BLTs violate KK parity [68]. Very trivially this can be shown as follows. The KK parity is actually a translational symmetry under the transformation, $y \rightarrow y - \pi R$. For symmetric BLTs:

$$\begin{aligned} r\{\delta(y) + \delta(y - \pi R)\} &\rightarrow r\{\delta(y - \pi R) + \delta(y - 2\pi R)\} \\ &= r\{\delta(y - \pi R) + \delta(y)\}, \end{aligned} \quad (2.9)$$

and for asymmetric BLTs,

$$\begin{aligned} \{r_1\delta(y) + r_2\delta(y - \pi R)\} &\rightarrow \{r_1\delta(y - \pi R) + r_2\delta(y - 2\pi R)\} \\ &= \{r_1\delta(y - \pi R) + r_2\delta(y)\}, \end{aligned} \quad (2.10)$$

Thus we see from Eqs. 2.9 and 2.10 that under $y \rightarrow y - \pi R$ the symmetric BLT case remains invariant, ensuring the conservation of KK parity. But asymmetric BLTs violate KK parity. Although KK parity violation would lead to unstable LKP and kill one good motivation of the universal extra dimensional scenario, but it may also give rise to some interesting phenomenology in the context of collider physics. Some recent studies in this line can be found in [69–71]. In passing we also note that in the literature (*e.g.*, [67, 72, 73]) some other form of BLT has been used, like $r\{\delta(y - L) + \delta(y + L)\}$ with $L = \pi R/2$. Clearly in those cases the orbifold fixed points are at $y = \pm L$. By a simple mapping $y \rightarrow y + \frac{\pi R}{2}$ the results from here to that of reference [67, 72] can be obtained, provided other conventions are taken care of appropriately.

Now we will take, for illustrative purpose, the fermionic action with BLTs and discuss some of the basic features of nmUED. We will follow [55] here. The 5D action for typical free fermion fields Ψ_L and Ψ_R whose zero modes are the chiral projections of an SM fermion is given by [53],

$$\begin{aligned} \mathcal{S}_f = \int d^4x \int_0^{\pi R} dy &\left[\bar{\Psi}_L i\Gamma^M \partial_M \Psi_L + r_f \{\delta(y) + \delta(y - \pi R)\} \phi_L^\dagger i\bar{\sigma}^\mu \partial_\mu \phi_L \right. \\ &\left. + \bar{\Psi}_R i\Gamma^M \partial_M \Psi_R + r_f \{\delta(y) + \delta(y - \pi R)\} \chi_R^\dagger i\bar{\sigma}^\mu \partial_\mu \chi_R \right], \end{aligned} \quad (2.11)$$

with $\sigma^\mu = (\mathbf{1}, \vec{\sigma})$ and $\bar{\sigma}^\mu = (\mathbf{1}, -\vec{\sigma})$, $\vec{\sigma}$ being the 2×2 Pauli matrices. Here we take same BLKT parameter, r_f for both the fields Ψ_L and Ψ_R . The 5D fermion fields can be expressed using two component chiral spinors [53]²,

$$\Psi_L(x, y) = \begin{pmatrix} \phi_L(x, y) \\ \chi_L(x, y) \end{pmatrix} = \sum_{n=0}^{\infty} \begin{pmatrix} \phi^{(n)}(x) f_L^{(n)}(y) \\ \chi^{(n)}(x) g_L^{(n)}(y) \end{pmatrix}, \quad (2.12a)$$

$$\Psi_R(x, y) = \begin{pmatrix} \phi_R(x, y) \\ \chi_R(x, y) \end{pmatrix} = \sum_{n=0}^{\infty} \begin{pmatrix} \phi^{(n)}(x) f_R^{(n)}(y) \\ \chi^{(n)}(x) g_R^{(n)}(y) \end{pmatrix}. \quad (2.12b)$$

Now, using Eq. 2.12a and variation of the action \mathcal{S}_f , we get the coupled differential equations for the y -dependent wave functions of Ψ ,

$$m_n g_L^{(n)} + \partial_y f_L^{(n)} = 0, \quad (2.13a)$$

$$[1 + r_f \{\delta(y) + \delta(y - \pi R)\}] m_n f_L^{(n)} - \partial_y g_L^{(n)} = 0. \quad (2.13b)$$

Similarly, using Eq. 2.12b, one can get,

$$m_n f_R^{(n)} - \partial_y g_R^{(n)} = 0, \quad (2.14a)$$

$$[1 + r_f \{\delta(y) + \delta(y - \pi R)\}] m_n g_R^{(n)} + \partial_y f_R^{(n)} = 0. \quad (2.14b)$$

We can now eliminate $g_L^{(n)}$ and $f_R^{(n)}$ from Eqs. 2.13 and 2.14, to get,

$$\partial_y^2 f_L^{(n)} + [1 + r_f \{\delta(y) + \delta(y - \pi R)\}] m_n^2 f_L^{(n)} = 0, \quad (2.15a)$$

$$\partial_y^2 g_R^{(n)} + [1 + r_f \{\delta(y) + \delta(y - \pi R)\}] m_n^2 g_R^{(n)} = 0. \quad (2.15b)$$

Clearly, $f_L^{(n)}$ and $g_R^{(n)}$ satisfies similar EoM. To find the solutions of these functions we impose the boundary conditions [68],

$$f_L^{(n)}|_{0^-} = f_L^{(n)}|_{0^+}, \quad f_L^{(n)}|_{\pi R^-} = f_L^{(n)}|_{\pi R^+}, \quad (2.16a)$$

$$\partial_y f_L^{(n)}|_{0^+} - \partial_y f_L^{(n)}|_{0^-} = -r_f m_n^2 f_L^{(n)}|_0, \quad (2.16b)$$

$$\partial_y f_L^{(n)}|_{\pi R^+} - \partial_y f_L^{(n)}|_{\pi R^-} = -r_f m_n^2 f_L^{(n)}|_{\pi R}. \quad (2.16c)$$

Using these boundary conditions we get the solution,

$$f_L^{(n)} = N_n \left[\cos(m_n y) - \frac{r_f m_n}{2} \sin(m_n y) \right], \quad \text{for } y \in [0, \pi R), \quad (2.17)$$

where N_n is some normalization factor. Evidently, the same solution will hold for $g_R^{(n)}$. As for $f_R^{(n)}$ and $g_L^{(n)}$, we can now use Eq. 2.13a and 2.14a and use the form of Eq. 2.17 to solve

²The Dirac γ -matrices are in the chiral representation with $\gamma_5 = \text{diag}(-1, 1)$

for $g_L^{(n)}$ and $f_R^{(n)}$ respectively. The masses m_n ($n = 0, 1, 2, \dots$) satisfy the transcendental equation [68],

$$(r_f^2 m_n^2 - 4) \tan(m_n \pi R) = 4r_f m_n. \quad (2.18)$$

Also $f_L^{(n)}$ and $g_L^{(n)}$ satisfy the following orthonormality relations,

$$\int_0^{\pi R} dy [1 + r_f \{\delta(y) + \delta(y - \pi R)\}] f_L^{(m)}(y) f_L^{(n)}(y) = \delta^{mn}, \quad (2.19a)$$

$$\int_0^{\pi R} dy g_L^{(m)}(y) g_L^{(n)}(y) = \delta^{mn}. \quad (2.19b)$$

These equations can be used to get the normalization factor for each mode function. For example, the normalization factor, N_n in Eq. 2.17, comes out to be,

$$N_n = \sqrt{\frac{2}{\pi R}} \left(\frac{1}{\sqrt{1 + \frac{r_f}{\pi R} + \frac{r_f^2 m_n^2}{4}}} \right). \quad (2.20)$$

A quick glance at Eqs. 2.17 and 2.20 reveals that in the limit $r_f \rightarrow 0$ we get back the familiar result of mUED. Before proceeding further we would like to spend some time on the mass determining transcendental equation, Eq. 2.18. Recall that in the case of UED, the mass of n -th KK mode is n/R (if no bulk mass is present) and after the radiative corrections n/R gets modified accordingly. But now, in case of nmUED, the mass of the n -th mode is given by the solution of transcendental equation 2.18. Also the mass of n -th mode depends on the BLT parameter, r and thus the mass of the n -th mode can no longer be presented in a closed form. The masses are now calculated by numerically solving Eq. 2.18. It can be shown by explicit calculation that the mode functions for gauge and scalar fields also satisfy analogous differential equations (cf. Eq. 2.15), boundary conditions (cf. Eq. 2.16) and consequently have similar forms (cf. Eq. 2.17). So the masses of n -th mode of gauge and scalar fields will also be given by equations analogous to Eq. 2.18 with appropriate BLT parameters (*e.g.*, r_{Gauge} or r_H etc.). Now we write the Eq. 2.18 with a general BLT parameter r as,

$$(r^2 m_n^2 - 4) \tan(m_n \pi R) = 4r m_n, \quad (2.21)$$

and from this,

$$\frac{r m_n}{2} = \frac{\cos(m_n \pi R) \pm 1}{\sin(m_n \pi R)}. \quad (2.22)$$

Hence,

$$\frac{r m_n}{2} = \begin{cases} \cot\left(\frac{m_n \pi R}{2}\right) & \text{for positive case,} \\ -\tan\left(\frac{m_n \pi R}{2}\right) & \text{for negative case.} \end{cases} \quad (2.23)$$

Also this is easy to convince oneself from the sequential mode-wise solution of Eq. 2.21 that the solutions for even n comes from the tangent case while those for odd n follows from the cotangent case. Thus we can write,

$$\frac{rm_n}{2} = \begin{cases} \cot\left(\frac{m_n\pi R}{2}\right) & \text{for } n : \text{odd,} \\ -\tan\left(\frac{m_n\pi R}{2}\right) & \text{for } n : \text{even.} \end{cases} \quad (2.24)$$

As an aside, we note that using the solutions for mode functions (cf. Eq. 2.17) and Eq. 2.24 one can write,

$$f(y) = N_n \times \begin{cases} -\frac{\sin\left\{m_n\left(y-\frac{\pi R}{2}\right)\right\}}{\sin\left(\frac{m_n\pi R}{2}\right)} & \text{for } n : \text{odd,} \\ \frac{\cos\left\{m_n\left(y-\frac{\pi R}{2}\right)\right\}}{\cos\left(\frac{m_n\pi R}{2}\right)} & \text{for } n : \text{even.} \end{cases} \quad (2.25)$$

This form of mode functions are similar to the forms used in [66] and also with the replacement $y \rightarrow y + \frac{\pi R}{2}$ we can obtain the convention of [67,72,73].

Now we would like to investigate how m_n depends on r . To see this, for convenience, we define the dimensionless variables,

$$M^{(n)} = m_n R \text{ and } R_{\text{BLT}} = \frac{r}{R}. \quad (2.26)$$

For illustration consider only $n = 1$ modes. In Fig. 2.3 we plot $M^{(1)}$ as a function of R_{BLT} as obtained from the first equation in Eq. 2.24. For any choice of R_{BLT} there is a unique

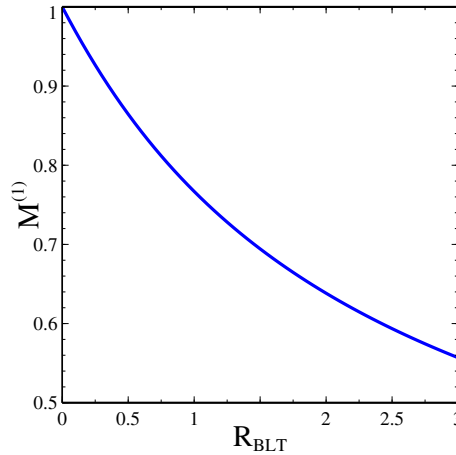


Figure 2.3: Variation of $M^{(1)} = m_1 R$ with BLT strength $R_{\text{BLT}} = r/R$. Larger R_{BLT} yields a smaller mass. This result applies to any type of fields when their corresponding BLTs are symmetric.

$M^{(1)} = m_1 R$. It is noteworthy that when $R_{\text{BLT}} = 0$, *i.e.*, in the absence of BLT, one gets

$m_1 = 1/R$, as expected. Moreover, m_1 monotonically decreases as the BLT strength, R_{BLT} increases. Clearly, the mass spectrum of nmUED thus depends on what BLT parameters are present in the theory. Of immediate consequence is the fact that the identity of LKP, which for obvious reasons is an $n = 1$ KK excitation, will be determined by the largest BLT parameter in entire field content. An elaborate discussion of this point will be given in the next chapter.

We have seen that the presence of BLTs modify the masses of the KK particles from their UED values. This is true for the couplings as well. In subsection 1.4.4 we have shown how to calculate the interactions between various KK level particles in the case of UED. Again if we take that very example, then in the context of nmUED, the cosine and sine in Eq. 1.38 will now be replaced by the mode functions given in Eq. 2.25. Evidently the modification in the coupling will be dependent on the BLT parameters which enter, even at the mode function level, in two places: explicitly in the normalization factor, N_n and implicitly in the m_n . At any time it is straightforward to revert to the UED case from nmUED, simply by taking the limit, $r \rightarrow 0$.

Thus we see nmUED differs from UED in two perspicuous ways. Due to the presence of BLTs, firstly the mass spectrum and secondly the couplings alter from its UED values, depending on the BLT parameters. It is to be noted that the mUED is an intermediate state between UED and nmUED, as in mUED only the corrections to the masses are taken into account, but the couplings are rendered as that of UED case.

Chapter 3

Dark Matter & Non-minimal Universal Extra Dimension

3.1 Dark Matter

From various astrophysical observations it has become evident that there exists, in the universe, a lion's share of matter content which can not be constituted out of our known building blocks of matter, *i.e.*, the fundamental particles of SM. Apropos of this, the unknown matter content of the universe, for which there are several evidences as detailed below, is called dark matter (DM). Actually, according to the observations of Planck [74], our universe consists of 4.9% ordinary matter (constituted out of SM particles), 26.8% dark matter and 68.3% dark energy. From the particle physics point of view, it is thus imperative to solve the DM conundrum by identifying, at least theoretically, some suitable DM candidate.

In this chapter we will see how nmUED fares when it is subjected to the constraints from DM observations. We will preface this by a brief introduction of DM: evidences of its existence, basic properties and a few candidates from various BSM scenarios. The standard calculation of thermal relic density of DM and direct detection methods will also be discussed in subsequent subsections.

Some of the good reviews and books on DM and related literature are [47, 75–81].

3.1.1 Evidences

It has long been established that in the universe there is matter which is non-luminous and not visible in telescopes. Later it was also ascertained that most of it is non-baryonic. In this subsection we will discuss some of the compelling evidences that consolidate this

paradigm.

Galactic rotation curves

The earliest astrophysical evidence of DM come from the study of rotation curves in spiral galaxies. F. Zwicky [82] observed that the outer constituents of the Coma cluster were moving far too quickly than what can be explained by the visible cluster mass. To reconcile this observation with the virial theorem, one has to postulate that the cluster contains another large component of mass which is invisible, *viz.*, *dark matter*. An example of such

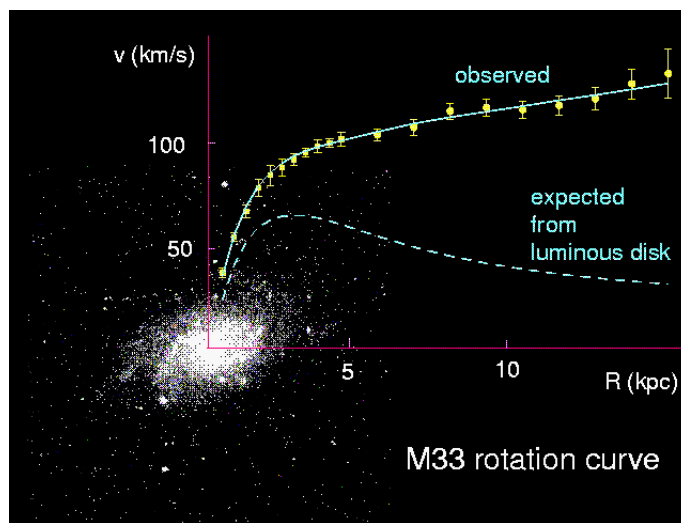


Figure 3.1: The observed rotation curve of the dwarf spiral galaxy M33. The dashed line is predicted purely on the basis of luminous stellar disc. The observed curve is flatter than the predicted one. This suggests the presence of a halo of dark matter, extending to large galactic radii. (From [77]).

anomalous velocity distribution has been shown in Fig. 3.1. These galactic rotation curves are important not only to establish the presence of DM, but also it can be used to obtain the local density of the DM halo, which is a very important quantity in the context of DM detection.

Another observation from spiral galaxies is the Tully-Fisher relation [83],

$$L \propto v_{\max}^{\beta}, \quad \beta = 3 \sim 4, \quad (3.1)$$

where L is the luminosity of the galaxy and v_{\max} is the maximum circular velocity of the constituent members. This relation can be explained using virial theorem only if the existence of DM is taken into account [84].

Gravitational lensing and Bullet cluster

Gravitational lensing is the bending (or *lensing*) of light due to the presence of massive objects. This is a general-relativistic phenomenon. Now, galaxy clusters being very massive structures show this effect. Due to this, a background object appear brighter than it otherwise would (see, *e.g.*, [85,86]). The dark matter present in the galaxy cluster, though not visible, contributes significantly to the total mass of the cluster. The best evidence to date for the existence of DM comes from the weak lensing observations of famous Bullet Cluster (1E0657-558), a unique cluster merger [87], where the lensing effect shows a large amount of dark matter. On top of it, another property of DM comes out of this cluster merger, that is, the DM halos have passed right through both the gas clouds and appear almost undisturbed after the collision. But the visible gas clouds of both clusters have undergone characteristic changes. It becomes evident from this, that the DM interacts with luminous matter as well as itself, very weakly.

Other astrophysical observations

There are many other observations which put the evidence of DM on a stronger footing. Big bang nucleosynthesis (BBN), in the parlance of standard big bang cosmology, allows us to measure the primordial baryon density of the universe. On the other hand from the measurements of the cosmic microwave background (CMB) power spectra and large-scale structure of the universe the matter density of the universe can be obtained. From recent experimental observations [74,88] it is evident that the baryonic density and total matter density are different. This mandates that the DM is necessarily non-baryonic.

3.1.2 Basic properties

The existence of DM is now established almost definitely. The observations that provide doubtless evidence for the existence of DM also shed light on some of the obvious properties of DM. So a theory which attempts to put forward any DM candidate must satisfy these requirements. Below we enlist some of the properties that any dark matter candidate should abide by.

- The DM must be dark, *i.e.*, it should have no (or extremely weak) interactions with photons. So it must be *electrically neutral*. Otherwise it would be able to emit photons which could have modified observations from astrophysical objects, like quasars.
- The DM should have very *small self-interactions*.

- The interaction between DM and baryons should also be weak. Observations of baryonic acoustic oscillation (BAO) and CMB angular power spectrum suggest this.
- The DM must be stable. To put it another way, DM must have lifetime larger than the age of the universe. Actually, from the search for the decay products of DM one can put bounds on the decay width of the DM.
- Large scale structure formation requires the DM to be "cold" enough which is already non-relativistic.
- DM can not be made up of SM particles as most of them are charged. Within the ambit of SM only neutrinos can be a potential DM candidate. Actually it *does* contribute in the relic density of DM minutely. But it can not be the ultimate candidate satisfying all observations. Neutrinos are very light particles. Although its mass has not been measured exactly, but it is of the order of electron volt or smaller [89]. With this small mass it can not contribute significantly to the matter density of universe. See chapter 5 of [75] for a discussion. From the Gunn-Tremaine bound [90] we know that massive galactic halos can not be made up of neutrinos of mass ≤ 1 MeV. Moreover, being so light neutrinos are still relativistic and they constitute what is called *hot* dark matter. This type of hot DM can not explain the galaxy formation rate of the universe after the big bang.

Thus it becomes evident that SM can not accommodate a viable DM candidate. But it is also worth noting that although observations tend to implicate that DM is non-baryonic, there are exotic baryonic objects *e.g.*, white dwarfs, neutron stars, super-massive black holes which comprise Massive Compact Halo Objects (MACHO) [91, 92], if not ruled out, are not favorable as baryonic DM candidates.

3.1.3 A few candidates

Now-a-days the most attractive, and rightfully so, non-baryonic cold dark matter candidates are weakly interacting massive particles (WIMP), χ . They are elementary particles arising from many BSM theories. Normally WIMPs are heavy ($\sim \mathcal{O}(\text{GeV-TeV})$) elementary particles and till now our colliders are not energetic enough to create them. But at the time of Big Bang they were produced copiously along with a slew of other particles. In the next subsection 3.2.1 we will discuss the standard method of calculating the relic abundance of this WIMP DM.

For completeness, now we are going to mention a few BSM scenarios where appropriate WIMP can arise. The list, however, is not at all exhaustive and for more details see *e.g.*, [77, 93]. Any BSM theory, that tries to address DM problem, has to have a stable particle in its particle spectrum. It is a general theme of these type of theories that they are endowed with some discrete symmetry that makes the lightest symmetry-odd particle stable. That particle, if satisfies the relevant cosmological observational data, will be identified as the DM candidate of that model. In the following we will discuss such examples.

Axion

Although its not WIMP type DM, but axion is one of the leading non-baryonic cold DM candidates. The idea of axion, a light pseudoscalar boson, was put forward to solve the strong CP problem [94]. A number of astrophysical observations and laboratory experiments put bound on axion mass to be $\sim 10^{-4} - 10^{-5}$ eV. Even though the mass is so small they are still cold as their production is non-thermal. Some reviews and recent studies can be found in [95–101].

Supersymmetry

By far the most popular and extensively studied BSM scenario is Supersymmetry (SUSY). In supersymmetric theories every SM particle has its super-partner particle differing in spin by half. In most versions of SUSY, there is a conserved discrete symmetry, R -parity, to fill up the requirement of proton stability, *i.e.*, to avoid baryon number violating processes. It is defined as,

$$R = (-1)^{3(B-L)+2S}. \quad (3.2)$$

Here B and L is baryon and lepton number respectively and S is the spin of the particle. For SM particles $R = 1$ and for supersymmetric particles $R = -1$. In the minimal supersymmetric standard model (MSSM) a linear combination of the super-partner of photon, Z -boson and neutral Higgs, called neutralino is the lightest supersymmetric particle (LSP). Neutralino is of fermionic nature. This can serve as a good DM candidate. Some of the recent studies on neutralino LSP are [102–105]. However, there are other variants of SUSY model where the DM candidate is not neutralino but some other supersymmetric particle (sneutrino or gravitino for example).

Inert Higgs Doublet Model

Two Higgs doublet model (2HDM) is a simple extension of SM. In 2HDM there is one extra Higgs doublet in addition to the SM Higgs doublet. This model is attractive because it is a minimal extension to SM which can accommodate additional source of CP violation which is needed to explain the baryon asymmetry of the universe. Also there are other motivations. In a version of 2HDM, named as inert Higgs doublet model (IDM) [106] one unbroken \mathbb{Z}_2 symmetry assures the stability of the lightest neutral scalar (or pseudoscalar) particle. A recent study of this DM candidate can be found in [107].

mUED and nmUED

We have already pointed out in subsection 2.1.2 that in mUED the first KK level photon, $\gamma^{(1)}$ (or effectively $B^{(1)}$) is the LKP. The stability of LKP is ensured by the conservation of KK parity. Various aspects of LKP as a dark matter has been discussed in [108–119].

In the case of nmUED the identity of LKP is no longer fixed, it can change depending on the BLT parameter. Due to this flexibility, either of $\gamma^{(1)}$ (or $B^{(1)}$), $Z^{(1)}$ (or $W_3^{(1)}$), $\nu^{(1)}$ and $H^{(1)}$ [66, 120] can be the DM candidate. In a later section we will study the details of the $B^{(1)}$ and $W_3^{(1)}$ LKP case based on the results obtained in [55].

Actually there are a lot of BSM theories which predict a suitable DM particle. In the above we just mentioned a few. We are now going to give a brief summary of the standard relic density calculation. This will also set the notations and conventions for the later section 3.3.2 where we will discuss the nmUED case in a detailed manner.

3.2 Relic density

3.2.1 Standard calculation of relic density

A brief history of WIMPs is as follows. After its production such particles remain in thermal equilibrium and in abundance when the temperature of the universe is greater than the mass of the particle, m_χ . The equilibrium abundance (or density) of these particles is maintained by the annihilation of these particles with their anti-particles, $\bar{\chi}$ into other lighter particles (X), ($\chi\bar{\chi} \rightarrow X\bar{X}$) and vice versa, ($X\bar{X} \rightarrow \chi\bar{\chi}$). But the temperature of the universe decreases and when it becomes less than m_χ , the equilibrium abundance drops. Clearly the annihilation ($\chi\bar{\chi} \rightarrow X\bar{X}$) rate will also drop. At the point when the annihilation rate falls below the expansion rate of the universe, H , the interactions maintaining

the thermal equilibrium "freeze out". Since the χ s are stable (*i.e.*, they can not decay) then after the freeze out the abundance of them also become fixed and what remains afterward is just the *thermal relic* of WIMPs. In the following we will describe how to calculate the relic density following standard equilibrium thermodynamics [75].

It is a fairly good approximation that the early universe was in thermal equilibrium. The number density of the particle, χ , in thermal equilibrium is given by,

$$n_{eq} = \frac{g}{(2\pi)^3} \int d^3p f(\vec{p}), \quad (3.3)$$

where g is the internal degrees of freedom (DoF) of χ and $f(\vec{p})$ is the phase space distribution function and is given by usual Fermi-Dirac (FD) or Bose-Einstein (BE) distribution,

$$f(\vec{p}) = \frac{1}{\exp\left(\frac{E-\mu}{T}\right) \pm 1}, \quad (3.4)$$

where '+' is for FD statistics and '-' for BE statistics and μ is the chemical potential of the corresponding species.

In the relativistic limit ($T \gg m$) and $T \gg \mu$,

$$n_{eq} = \begin{cases} \left(\frac{\zeta(3)}{\pi^2}\right) gT^3 & \text{for BE statistics,} \\ \left(\frac{3\zeta(3)}{4\pi^2}\right) gT^3 & \text{for FD statistics,} \end{cases} \quad (3.5)$$

and in the non-relativistic limit ($m \gg T$), both for FD and BE species,

$$n_{eq} = g \left(\frac{mT}{2\pi}\right)^{3/2} \exp\left(\frac{m-\mu}{T}\right). \quad (3.6)$$

The evolution, with time (or temperature), of the number density of χ is given by the Boltzmann equation,

$$\frac{dn}{dt} = -3Hn - \langle\sigma v\rangle(n^2 - n_{eq}^2), \quad (3.7)$$

where

$$H = \frac{1}{a} \frac{da}{dt} \quad (3.8)$$

is the Hubble parameter (a is the scale factor of the universe) and $\langle\sigma v\rangle$ is the thermally averaged annihilation cross section times relative velocity. The first term in the right-hand side of Eq. 3.7 accounts for the reduction of number density due to the expansion of the universe. The second term takes care of decrease (or increase) in n due to the interaction of χ with other particles in the spectrum. After solving Eq. 3.7 we can calculate the contribution of χ in the energy density of the universe by defining the quantity, Ω_χ as,

$$\Omega_\chi h^2 \equiv \frac{\rho_\chi}{\rho_c} = \frac{m_\chi n}{\rho_c}, \quad (3.9)$$

where h is the Hubble parameter in the units of $100 \text{ km s}^{-1} \text{ Mpc}^{-1}$ and ρ_c is the critical density of the universe and is given by,

$$\rho_c = \frac{3H^2}{8\pi G_N}. \quad (3.10)$$

At the point when the annihilation rate $\Gamma = n\langle\sigma v\rangle \lesssim H$, the annihilation of χ s ceases and the relic abundance remains fixed afterward. At the freeze out temperature the annihilation cross section can be expanded in powers of squared relative velocity,

$$\sigma v = a + bv^2 + \dots, \quad (3.11)$$

where the first term comes from the s -wave annihilation and the second from both s and p -wave annihilation. A nice discussion on the these type annihilation cross section in the low velocity limit can be found in [121]. In most of the cases these first two terms in the expansion are enough to produce a fair estimate of the relic density. With appropriate approximations Eq. 3.7 can be solved analytically and the relic density is given by [75, 108, 110, 122],

$$\Omega_\chi h^2 \approx \frac{1.04 \times 10^9 / 1\text{GeV}}{M_{\text{Pl}}} \frac{x_F}{\sqrt{g_*(x_F)}} \frac{1}{a + \frac{3b}{x_F}}, \quad (3.12)$$

where M_{Pl} is the Planck mass and $g_*(x_F)$ is the total number of relativistic DoF at the freeze out temperature. Here $x_F (= m/T_F, T_F$ being the freeze out temperature) is solved from the equation,

$$x_F = \ln \left(\frac{15}{8} \sqrt{\frac{5}{2}} \frac{g}{2\pi^3} \frac{m M_{\text{Pl}} (a + 6b/x_F)}{\sqrt{g_*(x_F) x_F}} \right). \quad (3.13)$$

However, there are three important exceptions to the validity of the above mentioned prescription¹ [76, 123],

- annihilation near mass thresholds (*i.e.*, kinematically forbidden channels at $T = 0$, but can be significant at higher temperatures),
- coannihilations (*i.e.*, when there are particles which are slightly heavier than χ and affect the number density of χ), and
- resonances in the annihilation cross section (*i.e.*, when the m_χ is half the mass of the particle exchanged in the s -channel annihilation process).

Systematic treatment of finite temperature corrections takes care of the first case. But this marginally affects the relic density. The latter two cases depend significantly on the particle spectrum and thus on the parameters of the theory.

¹In the relevant parameter space of mUED or nmUED, only coannihilation will play an important role.

3.2.2 Coannihilation

In the particle spectrum of the theory if there are particles nearly degenerate with the relic particle then the freeze out of these particles occurs almost at the same epoch when the relic particle χ decouples and can affect the relic abundance of χ . For example, consider there are N particle species, χ_i ($i = 1, 2, \dots, N$) and $m_i < m_j$ if $i < j$, i.e., χ_1 is the lightest particle. The number density n_i of each species χ_i will obey appropriate Boltzmann equations. Moreover, all the heavier particles (χ_i with $i > 1$) will ultimately decay to χ_1 . So from any number N_i of χ_i particles we end up getting exactly N_i number of χ_1 at the end of the decay chain. Thus to determine the relic abundance of χ_1 it is meaningful to study the evolution of the number density $n(= \sum_j n_j)$ instead of each number density separately. The Boltzmann equation will be modified from the form we have given in Eq. 3.7 as,

$$\frac{dn}{dt} = -3Hn - \langle \sigma_{\text{eff}} v \rangle (n^2 - n_{\text{eq}}^2). \quad (3.14)$$

The quantity σ_{eff} is given by,

$$\sigma_{\text{eff}}(x) = \frac{1}{g_{\text{eff}}^2} \sum_{i,j=1}^N \sigma_{ij} F_i F_j \quad (3.15)$$

where

$$g_{\text{eff}}(x) = \sum_{i=1}^N F_i(x), \quad (3.16a)$$

$$F_i(x) = g_i (1 + \Delta_i)^{3/2} \exp(-x\Delta_i), \quad (3.16b)$$

with

$$\Delta_i = \frac{m_i - m_1}{m_1} \quad \text{and} \quad x = \frac{m}{T}. \quad (3.17)$$

Here $\sigma_{ij} \equiv \sigma(\chi_i \chi_j \rightarrow \text{SM})$ and g_i is the number of internal DoF of the species χ_i taking part in the annihilation or coannihilation process. In the non-relativistic limit we have, $\langle \sigma_{\text{eff}} v \rangle \sim a_{\text{eff}}(x) + b_{\text{eff}}(x)v^2 + \mathcal{O}(v^4)$. The approximate expression for the relic density will now become,

$$\Omega_\chi h^2 \approx \frac{1.04 \times 10^9 / 1\text{GeV}}{M_{\text{Pl}}} \frac{x_F}{\sqrt{g_*(x_F)}} \frac{1}{I_a + \frac{3I_b}{x_F}}, \quad (3.18)$$

where $I_{a,b}$ are given by,

$$I_a = x_F \int_{x_F}^{\infty} a_{\text{eff}}(x) x^{-2} dx, \quad (3.19a)$$

$$I_b = 2x_F^2 \int_{x_F}^{\infty} b_{\text{eff}}(x)x^{-3}dx. \quad (3.19b)$$

The freeze out temperature is given by,

$$x_F = \ln \left(\frac{15}{8} \sqrt{\frac{5}{2}} \frac{g_{\text{eff}}(x_F)}{2\pi^3} \frac{m_1 M_{\text{Pl}} (a_{\text{eff}}(x_F) + 6b_{\text{eff}}(x_F)/x_F)}{\sqrt{g_*(x_F)x_F}} \right). \quad (3.20)$$

After this discussion on relic density calculation we are now in a position to look at mUED and nmUED in the light of dark matter observations.

3.3 Relic density in mUED and nmUED

In this section we will discuss the relic density constraints on mUED and nmUED. As has been already mentioned earlier, in mUED, $B^{(1)}$ is the dark matter candidate and in nmUED the identity of DM is not fixed. We will first see in the case of mUED, if $B^{(1)}$ is the LKP then how it satisfies the relic density observation, *i.e.*, how do the observations put constraint on the parameters of mUED. In the later part we will see how those constraints can be relaxed if we consider the nmUED. We will also discuss how well-suited other possible candidates in nmUED are.

3.3.1 mUED

In the context of mUED, we know that the LKP is the first KK level photon, $\gamma^{(1)}$ which due to a small mixing angle behaves purely like the first KK level $U(1)_Y$ gauge boson $B^{(1)}$. After radiative correction its mass gets the smallest correction and it remains the LKP. Even in mUED departing from the standard scenario if one *by hand* relaxes the restriction that fields which experience only the $U(1)_Y$ interaction are lighter than those of the fields which experience the $SU(2)$ interaction, then $W_3^{(1)}$ (*i.e.*, first KK level Z -boson) or level one KK neutrino $\nu^{(1)}$ can be considered as the LKP [108, 109]. As it stands, $\nu^{(1)}$ is ruled out as an LKP from DM direct detection experiments [109]. Another less popular candidate for LKP is first level KK graviton. The problem is that since KK graviton will have very feeble gravitational interaction only, their inefficient annihilation will lead to overclosure of the universe. Also there are other stringent constraints on KK graviton as the LKP [124]. Another possibility is to add extra fields, *e.g.*, right handed neutrinos, in the already existing spectrum. Such possibilities and their advantages have been discussed in [125–127]. Below we will present the case of $\gamma^{(1)}$ (or $B^{(1)}$) and $Z^{(1)}$ (or $W_3^{(1)}$) LKP following [108, 110, 117].

Actually these are variants of mUED model where the mass spectra is not kept as it is obtained after radiative corrections and the usual practice is to take a different LKP ($\nu^{(1)}$ or $Z^{(1)}$ or $H^{(1)}$ ²), purely from phenomenological point of view, and study their effects. Not only the identity of LKP but also the mass splitting (e.g., Δ_{q_1} in [117]) is put in by hand.

In the case of $B^{(1)}$ LKP, the relevant cross sections are the annihilation of $B^{(1)}$ pairs into fermions and into Higgs boson. If the EWSB effects are neglected then there are no channels into vector bosons. If the coannihilation processes are neglected then from the observed value of relic density the allowed mass for $B^{(1)}$ lies in the range 900 – 1200 GeV. With coannihilation effects taken into account this bound decreases. Considering only the coannihilation of first level singlet electron $e_R^{(1)}$ with $B^{(1)}$, the allowed band of $m_{B^{(1)}}$ becomes 600 – 1050 GeV [108], depending on the mass splitting $\Delta_{e_R^{(1)}}$. A more elaborate study, done in [110], with a modified data set and taking coannihilation processes for other set of particles as well, reveals that the allowed range of $m_{B^{(1)}}$ should be 500 – 600 GeV which is in good agreement with an independent study done in [114]. In a similar study [117] on a variant of mUED model with $B^{(1)}$ LKP it is shown (left panel of Fig. 3.2) that allowed range $m_{B^{(1)}}$ (presented as m_{γ_1} in the figure) is from 500–1600 GeV depending on the mass splitting of $B^{(1)}$ with $q^{(1)}$.

The case of $Z^{(1)}$ (or $W_3^{(1)}$) LKP in the context of a variant of mUED³ has been discussed in [117]. Due to the larger value of weak gauge coupling the annihilation cross section of $Z^{(1)}$ is relatively large. The relic density as a function of $Z^{(1)}$ mass, $m_{Z^{(1)}}$ has been shown in Fig. 3.2 (right panel). It is evident from this figure that quark coannihilation processes increase the effective cross section reducing the relic density and thus the allowed band of $m_{Z^{(1)}}$ consistent with data becomes 1800 – 2700 GeV depending on the mass splitting with first KK level quarks which in this case are the next to lightest LKPs (NLKP). We will see a similar effect in the case of nmUED too.

It is worth mentioning that the inclusion of second KK level particles, in the calculation, changes many of the bounds mentioned earlier. Actually the second level particles can be exchanged in an s -channel annihilation of two level one particles. For example, in $B^{(1)}B^{(1)}$ annihilation, second level Higgs $H^{(2)}$ can be exchanged in s -channel. So there is a possibility of enhancement in annihilation cross section near resonance. Due to this, there is significant reduction in relic abundance [111, 112, 116]. The second level particles can affect the relic density not only through s -channel resonance but also they can be singly

²See e.g., [128] for $H^{(1)}$ LKP study.

³For a different discussion of $Z^{(1)}$ LKP see, for example, [129]

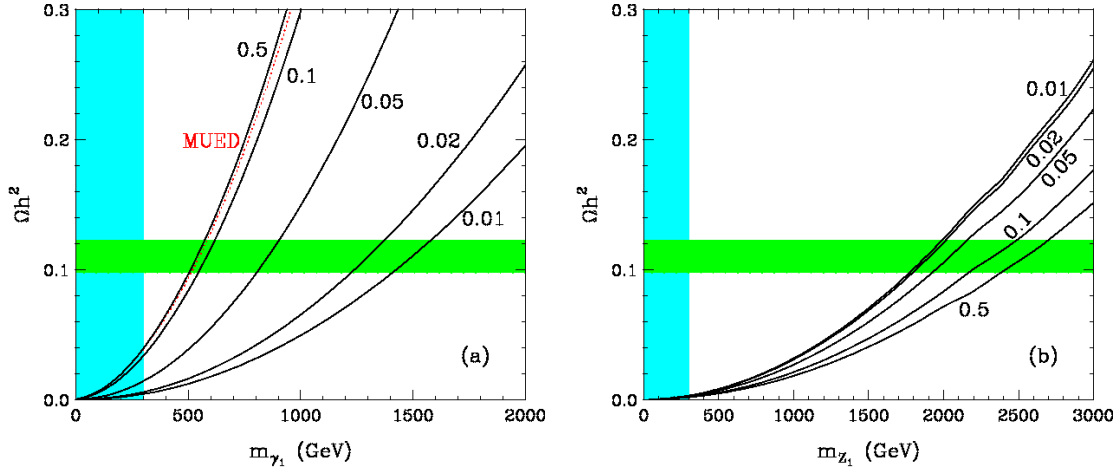


Figure 3.2: Relic density of LKP (i) $\gamma^{(1)}$ (left) and (ii) $Z^{(1)}$ (right) as a function of LKP mass. The green band gives 2σ allowed region from WMAP 5yr data [130], $\Omega_{\text{CDM}}h^2 \in (0.1037, 0.1161)$ and the vertical cyan band excludes the mass of LKP from precision data. Here KK singlet and doublet quarks are assumed to be degenerate and the mass of the level one quarks are varied by hand, such that $\Delta_{q_1} = 0.01, 0.02, 0.05, 0.1$ and 0.5 . Also $Z^{(1)}$ and $W^{(1)\pm}$ are taken to be degenerate. The red dotted line gives the result of full mUED calculation including all coannihilation processes. Adapted from [117].

produced in association with SM particle in the final state and subsequently this level two particle decays to SM particles through loop induced processes. In such a scenario coannihilation processes can even dominate over the annihilation processes which in turn reduce the relic density. Considering these points, in a recent study [118], it is pointed out that the preferred compactification scale ($1/R$) and thus the mass of the LKP should be 1.3 TeV. However in non-minimal version of UED the LKP can have masses much lower than this bound while satisfying other constraints.

3.3.2 nmUED

We are now going to discuss the nmUED scenario. We have described the model in Sec. 2.2. The action is given in Eqs. 2.8. We have already mentioned that in nmUED the mass spectrum and couplings are dependent on the BLT parameters (r_X for the field X). We will use the dimensionless parameter $R_X (= r_X/R)$, where R is the compactification radius. We will concentrate on the bosonic LKP states:⁴ $B^{(1)}$ and $W_3^{(1)}$. The discussion of this subsection will follow [55].

⁴Depending on the BLT parameter $\nu^{(1)}$ or $H^{(1)}$ can also be LKP.

From our earlier discussion it is evident that $M_{(1)} (= m_1 R)$ is determined entirely by the BLT parameter, R_{BLT} , and the compactification radius R . The gauge coupling plays no role. Therefore the earlier discussion applies for both $W_3^{(1)}$ and $B^{(1)}$ as long as the appropriate BLT parameters are used. Which of them will be identified as LKP is determined purely by the choice of the respective BLT parameters. In the subsequent part of this subsection we investigate the prospects of these WIMPs playing the role of the dark matter particle.

On the electroweak gauge boson mass matrix

Before going to the details of DM study it is important to clarify some of the points regarding the masses of $B^{(1)}$ and $W_3^{(1)}$. It is imperative to see how the inclusion of zero mode masses (which we did not discuss in the subsection 2.2.1) affect the masses and mixing of $W_3^{(1)}$ and $B^{(1)}$. In a 5D theory the electroweak gauge boson eigenstates with BLKT have been discussed in the literature [66]. It can be easily verified that for the range of BLKT parameters which we will consider the states of different KK level, n , mix negligibly. Further, only if the BLKT parameters for the B and W gauge bosons are exactly equal (or their difference is very small) the mixing between $B^{(1)}$ and $W_3^{(1)}$ is substantial, it being equal to the zero-mode weak mixing angle in the case of equality. If $(r_B - r_W)/R$ is of order 0.1 (or larger) this mixing is negligible. This can be verified from the mass matrix which we now discuss.

The mass matrix for the $n = 1$ neutral electroweak gauge bosons including spontaneous electroweak symmetry breaking, as well as the extra-dimensional contribution (discussed in Sec. 2.2) is⁵:

$$\mathcal{M}_{W_3^{(1)}B^{(1)}} = \begin{pmatrix} \frac{g_2^2 v^2}{4} \frac{S_W}{S_H} I_{W_3 W_3} + m_{W_3}^2 & -\frac{g_2 g_1 v^2}{4} \frac{\sqrt{S_W S_B}}{S_H} I_{W_3 B} \\ -\frac{g_2 g_1 v^2}{4} \frac{\sqrt{S_W S_B}}{S_H} I_{W_3 B} & \frac{g_1^2 v^2}{4} \frac{S_B}{S_H} I_{BB} + m_{B^{(1)}}^2 \end{pmatrix} \quad (3.21)$$

where

$$I_{ij} = \int_0^{\pi R} (1 + r_H \{\delta(y) + \delta(y - \pi R)\}) a_i^{(1)}(y) a_j^{(1)}(y) dy, \quad (i, j = W_3, B). \quad (3.22)$$

Above, r_H is the strength of the Higgs scalar BLKT and $R_H = r_H/R$. Also,

$$a_{W_3}^{(1)}(y) = N_{W_3}^{(1)} \left[\cos \left(m_{W_3}^{(1)} y \right) - \frac{r_W m_{W_3}^{(1)}}{2} \sin \left(m_{W_3}^{(1)} y \right) \right], \quad (3.23a)$$

⁵Here $m_{W_3}^{(1)}$ and $m_{B^{(1)}}$ stand for the extra-dimensional mass contribution m_1 , obtained from solving the mass determining transcendental equation, for the $n = 1$, W_3 and B states, respectively.

$$a_B^{(1)}(y) = N_B^{(1)} \left[\cos(m_{B^{(1)}} y) - \frac{r_B m_{B^{(1)}}}{2} \sin(m_{B^{(1)}} y) \right], \quad (3.23b)$$

with $N_{W_3}^{(1)}$, $N_B^{(1)}$ being normalization factors as in Eq. 2.20. The 5D gauge couplings \hat{g}_2, \hat{g}_1 and the vacuum expectation value (vev) \hat{v} are related to the 4D couplings g_2, g_1 respectively and the vev v through

$$\hat{g}_2 = g_2 \sqrt{\pi R S_W}, \quad \hat{g}_1 = g_1 \sqrt{\pi R S_B}, \quad \hat{v} = v / \sqrt{\pi R S_H}, \quad (3.24)$$

where

$$S_W = \left(1 + \frac{R_W}{\pi} \right), \quad S_B = \left(1 + \frac{R_B}{\pi} \right), \quad S_H = \left(1 + \frac{R_H}{\pi} \right). \quad (3.25)$$

A few comments about the mass matrix, $\mathcal{M}_{W_3^{(1)} B^{(1)}}$ in Eq. 3.21 are in order. The matrix is given in the $W_3^{(1)} - B^{(1)}$ basis⁶. As an estimate of the relative magnitudes of the terms in $\mathcal{M}_{W_3^{(1)} B^{(1)}}$, notice that the S_i are $\mathcal{O}(1)$ as are the overlap integrals I_{ij} . Hence the contributions to the mass matrix from the EWSB are $\mathcal{O}(v^2)$. The extra-dimensional contributions, $m_{(W_3/B)^{(1)}}^2$, are of the order of $(1/R)^2$ and are always dominant by far. As a consequence these terms affect significantly the mass eigenvalues and the mixing is negligible for $(R_W - R_B) \sim 0.1$ or larger⁷. So, in our discussion below we take $B^{(1)}$ and $W_3^{(1)}$ to be the neutral electroweak gauge eigenstates. This is similar to the case in mUED. The contributions to the masses from the EWSB are insignificant and hence dropped. It is verified that for the cases of our interest there is negligible dependence of the results on the Higgs BLKT strength, r_H . In our calculations we keep $R_H = 0.1$ throughout.

Dark matter study

Since in nmUED masses of the KK-excitations are determined by the BLT parameters, it is the choice of these BLT parameters which determine whether or not the mass of any KK-excitation would lie close to the relic particle mass ($\Delta_i \leq 10\%$) so that their coannihilation process could contribute significantly. In our analysis we have chosen the BLKT parameters for quarks, gluons and right-handed leptons such that their masses are sufficiently larger than the $B^{(1)}$ mass and their contributions to coannihilation are negligible. With this choice the only relevant coannihilation processes are those of KK-excitations of the left-handed lepton doublets.

⁶It can be easily checked that the mixing with states of $n \neq 1$ is very small.

⁷If $R_W = R_B$ then the dominant diagonal terms become equal and keep the mixing unaffected and simply make a constant shift in the masses of the eigenstates. In this case the mixing between $W_3^{(1)}$ and $B^{(1)}$ is just like the Standard Model with $\tan \theta = g_1/g_2$.

$B^{(1)}$ annihilation	$B^{(1)}$ -lepton scattering
$B^{(1)}B^{(1)} \rightarrow f\bar{f}$	$\nu_L^{(1)}B^{(1)} \rightarrow W^+\ell^-$
$B^{(1)}B^{(1)} \rightarrow h^+h^-$	$\bar{\nu}_L^{(1)}B^{(1)} \rightarrow W^-\ell^+$
	$\nu_L^{(1)}B^{(1)} \rightarrow Z\nu_\ell$
	$\bar{\nu}_L^{(1)}B^{(1)} \rightarrow Z\bar{\nu}_\ell$
	$\ell_L^{(1)-}B^{(1)} \rightarrow W^-\nu_\ell$
	$\ell_L^{(1)+}B^{(1)} \rightarrow W^+\bar{\nu}_\ell$
	$\ell_L^{(1)-}B^{(1)} \rightarrow Z\ell^-$
	$\ell_L^{(1)+}B^{(1)} \rightarrow W^+\bar{\nu}_\ell$

Table 3.1: The $B^{(1)}$ annihilation and relevant $B^{(1)}$ -lepton scattering process that are important for the relic density calculation of $B^{(1)}$.

In Tables 3.1-3.3 the relevant processes which are used to calculate effective cross section, σ_{eff} , have been listed. Some of the couplings between the level one KK particles and SM particles will get modification in nmUED in view of non-trivial mode functions of the KK excitations⁸. Consequently, the cross sections of some of the processes which are contributing in σ_{eff} will accordingly be scaled up or down with respect to their mUED values.

$\nu^{(1)}$ annihilation and scattering	$\ell^{(1)}$ annihilation and scattering
$\nu_L^{(1)}\bar{\nu}_L^{(1)} \rightarrow f\bar{f}$	$\ell_L^{(1)+}\ell_L^{(1)-} \rightarrow h^+h^-$
$\nu_L^{(1)}\bar{\nu}_L^{(1)} \rightarrow h^+h^-$	$\ell_L^{(1)+}\ell_L^{(1)-} \rightarrow ZZ, Z\gamma, \gamma\gamma$
$\nu_L^{(1)}\bar{\nu}_L^{(1)} \rightarrow ZZ$	$\ell_L^{(1)+}\ell_L^{(1)-} \rightarrow W^+W^-$
$\nu_L^{(1)}\bar{\nu}_L^{(1)} \rightarrow W^+W^-$	$\ell_L^{(1)\pm}\ell_L^{(1)\pm} \rightarrow \ell^\pm\ell^\pm$
$\nu_L^{(1)}\nu_L^{(1)} \rightarrow \nu_\ell\nu_\ell$	$\ell_L^{(1)\pm}\ell_L^{(1)\pm} \rightarrow \ell^\pm\ell'^\pm$
$\nu_L^{(1)}\nu_L^{\prime(1)} \rightarrow \nu_\ell\nu'_\ell$	$\ell_L^{(1)\pm}\ell_L^{\prime(1)\mp} \rightarrow \ell^\pm\ell'^\mp$
$\nu_L^{(1)}\bar{\nu}_L^{\prime(1)} \rightarrow \nu_\ell\bar{\nu}'_\ell$	$\ell_L^{(1)+}\ell_L^{\prime(1)-} \rightarrow f\bar{f} \text{ or } \ell_R^+\ell_R^-$
$\nu_L^{(1)}\bar{\nu}_L^{\prime(1)} \rightarrow \ell^-\ell'^+$	$\ell_L^{(1)+}\ell_L^{\prime(1)-} \rightarrow \nu_\ell\bar{\nu}_\ell \text{ or } \ell_L^+\ell_L^-$
$\nu_L^{(1)}\bar{\nu}_L^{(1)} \rightarrow \ell^+\ell^-$	$\ell_L^{(1)+}\ell_L^{\prime(1)-} \rightarrow \nu_\ell\bar{\nu}'_\ell$

Table 3.2: The $\nu^{(1)}$ and $\ell^{(1)}$ annihilation and scattering processes which contribute to the relic density calculation.

⁸Such interactions with the Feynman rules are listed in the Appendix at the end of this chapter.

Now we are going to discuss the results for each LKP case ($B^{(1)}$ and $W_3^{(1)}$) separately.

$\nu^{(1)} - \ell^{(1)}$ scattering	
$\nu_L^{(1)} \ell_L^{\prime(1)} \rightarrow \nu_\ell \ell'$	$\ell_L^{(1)-} \bar{\nu}_L^{(1)} \rightarrow f \bar{f}'$
$\ell_L^{(1)-} \bar{\nu}_L^{(1)} \rightarrow h^- h^0$	$\ell_L^{(1)-} \bar{\nu}_L^{(1)} \rightarrow \gamma W^-$
$\ell_L^{(1)-} \bar{\nu}_L^{(1)} \rightarrow ZW^-$	$\ell_L^{(1)-} \bar{\nu}_L^{(1)} \rightarrow \ell^- \bar{\nu}_\ell$
$\ell_L^{(1)-} \nu_L^{(1)} \rightarrow \ell^- \nu_\ell$	$\nu_L^{(1)} \ell_L^{\prime(1)} \rightarrow \nu_{\ell'} \ell^-$
$\nu_L^{(1)} \ell_L^{\prime(1)} \rightarrow \nu_\ell \ell'^-$	$\bar{\nu}_L^{(1)} \ell_L^{\prime(1)} \rightarrow \bar{\nu}_\ell \ell'^-$

Table 3.3: The $\nu^{(1)}-\ell^{(1)}$ scattering processes which contribute to the relic density calculation.

Results for $B^{(1)}$ LKP

In mUED the oft-chosen DM candidate is $B^{(1)}$. Here for this choice the modifications in the mass spectrum and the couplings will be used to estimate the relic density in nmUED. The main outcome of this analysis has been presented in Fig. 3.3 where in the three panels R_B is chosen differently. Variation of Ωh^2 with the mass of $B^{(1)}$ has been plotted for different choices of the fermion BLKT parameter, R_f . As mentioned above, the BLKT parameters for gluons, quarks and right-handed fermions are so chosen that the masses of these KK-excitations are well above that of the $B^{(1)}$. Consequently, they will not play any role in the determination of relic density of $B^{(1)}$. Furthermore, it is checked that Ωh^2 is nearly insensitive to the choice of r_H , the Higgs BLKT parameter.

At this point we would like to make a comment about the choice of parameter values in the plots in Fig. 3.3. In each panel R_B has a fixed value. Thus by changing R^{-1} , the mass $m_{B^{(1)}}$ is being varied along the x -axes. To make it certain that $B^{(1)}$ is the LKP, $n = 1$ KK-lepton masses should be greater than $m_{B^{(1)}}$. This can be achieved if R_f (chosen same for all three left-handed lepton doublets) is smaller than R_B in every panel. In each panel, we also show the values of Δ_f corresponding to five (equi-spaced) choices of R_f .

It is worth mentioning that while calculating σ_{eff} we have taken level one leptons, $\ell_L^{(1)}$ and $\nu_L^{(1)}$ as mass degenerate and they are the NLKPs assuming all other KK modes being heavy enough so that their contribution in coannihilation can be neglected. For a given value of R^{-1} , it is found that the cross sections of the processes listed in Tables 3.1 - 3.3 are higher compared to the corresponding rates in mUED. Relatively lower values of the $n = 1$ KK-masses and enhanced couplings in nmUED are responsible for the higher

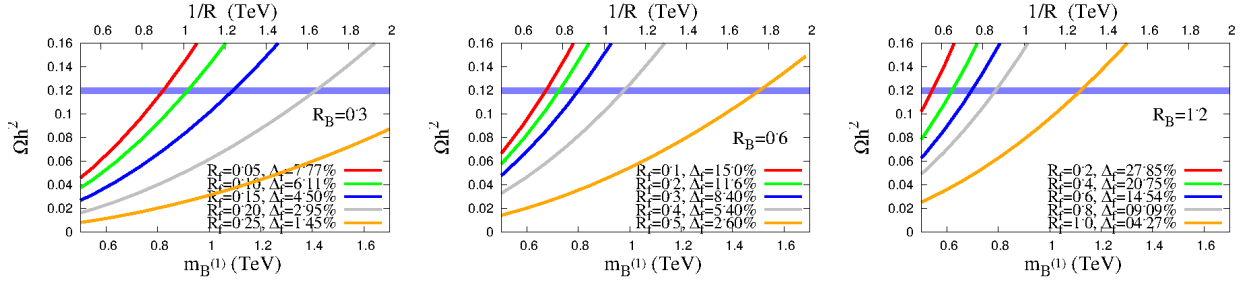


Figure 3.3: Variation of Ωh^2 with relic particle mass, $m_{B(1)}$. Curves for different choices of the fermion BLKT parameter R_f are shown and the corresponding Δ_f indicated. The narrow horizontal blue band corresponds to the 1σ allowed range of relic particle density from Planck data [74]. The allowed $1/R$ (or $m_{B(1)}$) can be read off from the intersections of the curves with the allowed band. The three panels are for different choices of R_B , the BLKT parameter for B .

reaction rates for a given value of R^{-1} . Thus the numerical value of the relic density in nmUED is always less than in mUED as long as the BLKT parameters are positive (as used in our analysis).

It is possibly useful to mention here the magnitudes of the coefficients I_a and I_b in Eq. 3.18 which reflect the model dynamics. For the choices that we have made for R_B and R_f , I_a and I_b are in the range of (1 – 10) pb. Both I_a and I_b decrease with increasing $m_{B(1)}$.

One can see from Fig. 3.3 that Ωh^2 increases with increase of R^{-1} or R_B . Both increases serve to reduce $m_{B(1)}$ and also enhance the couplings. In contrast, Ωh^2 decreases with increasing R_f , the fermion BLKT coefficient. Unlike in mUED, the allowed range of R^{-1} depends on R_f in nmUED. This is expected, as R_f moves away from R_B the splitting in mass between $B^{(1)}$ and fermions, Δ_f , increases (noted in the figures) and coannihilation becomes less important.

It is seen from Fig. 3.3 that depending on the choice of R_B and R_f the allowed range of R^{-1} can be as much as 0.6 TeV to 2 TeV or even more, while remaining consistent with the observed dark matter limits. It should be kept in mind that in nmUED the mass of the LKP is actually a little lower than R^{-1} as seen in the lower x -axes in the panels and also illustrated in Fig. 2.3.

In passing we would like to comment on the upper bounds on R^{-1} that arise by demanding that the LKP does not overclose the universe. This can happen if $\Omega h^2 \approx 0.48$. Some sample results are presented in Table 3.4. To be conservative, the smallest R_f has been chosen for every R_B (which implies the largest Δ_f) in Fig. 3.3. For larger R_f the

LKP	R_B or R_W	R_f	Δ_f	R^{-1} (in TeV)	$m_{B^{(1)}} \text{ or } m_{W_3^{(1)}}$ (in TeV)
$B^{(1)}$	0.3	0.05	7.7%	1.9	1.7
	0.6	0.1	15%	1.7	1.4
	1.2	0.2	27.8%	1.5	1.1
$W_3^{(1)}$	0.6	-	-	10.0	8.4

Table 3.4: Upper bound on R^{-1} from overclosure of the universe ($\Omega h^2 = 0.48$). The masses of the LKP for the limiting R^{-1} are also presented. For the $W_3^{(1)}$ LKP case only the process $W_3^{(1)} W_3^{(1)} \rightarrow W^+ W^-$ is taken into account. Including coannihilation will further enhance the upper bound in this case.

upper bound on R^{-1} is increased.

The observed 1σ limits of Ωh^2 , that we have used, are very restrictive. In Fig. 3.4 we have presented the regions consistent with the observed range of Ωh^2 in the $m_{B^{(1)}}-m_{f^{(1)}}$ plane. While deriving these limits it is assumed that $B^{(1)}$ is the *only* relic particle in the model. Fig. 3.4 reveals that a very narrow region in the $m_{B^{(1)}} - m_{f^{(1)}}$ plane – *between* the two curves in each panel – is allowed by the data. In view of the present precision of

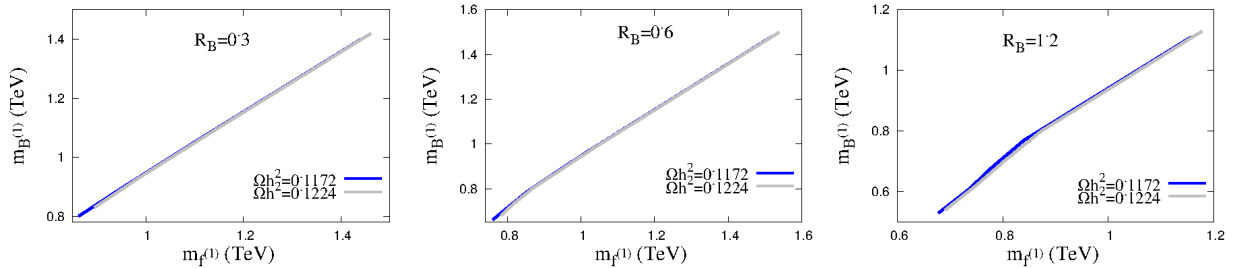


Figure 3.4: Allowed region in the $m_{f^{(1)}} - m_{B^{(1)}}$ plane that satisfies the observed Ωh^2 limits. The three panels are for different choices of R_B . Only the narrow strip *between* the two curves is allowed from the relic density constraints.

cosmological measurements, when translated to the $m_{B^{(1)}}-m_{f^{(1)}}$ plane one has essentially reduced the allowed region to almost a line. The plots in Fig. 3.4 shows that the allowed range is very close to the $m_{B^{(1)}} = m_{f^{(1)}}$ line. The region above this line is not interesting in the sense that there $f^{(1)}$ becomes the LKP and since we take BLKT parameters for both left handed neutrinos as well as leptons to be same we would get charged fermion LKP.

Results for $W_3^{(1)}$ LKP

The masses of the $n > 0$ KK-states are determined by their respective BLKT parameters r_i or equivalently $R_i = r_i/R$. Thus to avoid a fermion LKP one must choose $R_B, R_W > R_f$. Besides the just discussed case of $R_B > R_W$, corresponding to $B^{(1)}$ LKP, one should also consider $R_W > R_B$ which makes $W_3^{(1)}$ the dark matter candidate⁹. In such a case it is found that the annihilation cross section is large (notably because of the process $W_3^{(1)}W_3^{(1)} \rightarrow W^+W^-$) and therefore the relic density is too small¹⁰. The relic density as

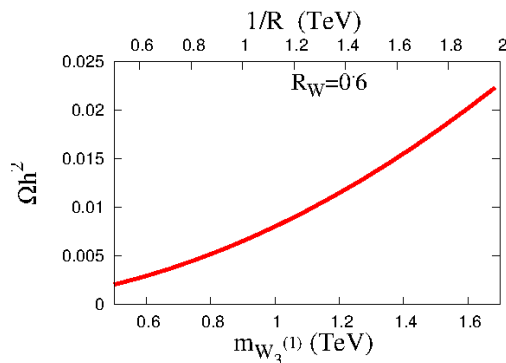


Figure 3.5: Variation of the relic density with $m_{W_3^{(1)}}$ in the case of $W_3^{(1)}$ LKP. The current observed value (~ 0.12) disfavors this alternative.

a function of the $W_3^{(1)}$ mass, $m_{W_3^{(1)}}$ is shown in Fig. 3.5 for a typical value of $R_W = 0.6$. It is important to note that the obtained relic density is far below the observed [74] value (around 0.12). For $R_W = 0.6$ the lower (upper) bounds on Ωh^2 – which are outside the range of the figure – correspond to $R^{-1} = 4.66$ (4.7) TeV with the respective $W_3^{(1)}$ masses 3.92 (4.04) TeV. This establishes that $W_3^{(1)}$ would not be an attractive dark matter candidate for easy detection at the LHC unless the DM consists of several components and $W_3^{(1)}$ is one of them¹¹.

3.4 Direct Dark Matter Detection in mUED and nmUED

Once the evidence of dark matter has been proved with certainty from various observations, the next exigent issue in the DM paradigm is to detect it and pinpoint its other characteristic features. Presently various DM search strategies are operative *e.g.*, collider

⁹For a different discussion of the $W_3^{(1)}$ LKP see, for example, [129].

¹⁰The coannihilation in this case has not been considered as it would further reduce the relic density.

¹¹The overclosure bound on R^{-1} for $R_W = 0.6$ is 10 TeV (see Table 3.4).

searches, indirect searches (searching for annihilation products of DM which have features allowing for a discrimination from other astrophysical background sources) and direct searches (scattering of DM particles off ordinary matter). We will begin this section with a brief exposition to the direct detection methods of WIMPs. Then in the later parts its implications on mUED and nmUED will be examined. Actually from Fig. 3.6 it is ev-

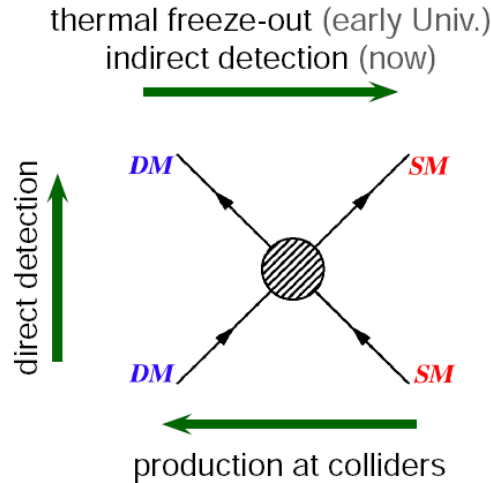


Figure 3.6: Schematic presentation of DM interaction (taken from [131]).

ident that the amplitude for DM annihilation to SM particles is related to the amplitude for elastic scattering of DM particles from SM particles by crossing symmetry. Thus it is expected that the DM will have small, but non-zero coupling to atomic nuclei through the coupling to quarks. Now, assuming a certain DM distribution in our galaxy, such experiments can be devised where DM particle scatters off a target nucleus and releases an amount of energy which will be measured as the recoil of the target nucleus or ionization of the target medium¹².

The calculation of DM-nuclei interaction proceeds through three important steps. The first step involves the calculation of interactions of DM with quarks and gluons. Although straightforward, this procedure is marred with model parameter uncertainties as these creep in at various stages of the calculations. In the second step these microscopic interactions are to be translated to the interactions of DM with nucleons. To perform this one needs the matrix elements of quark and gluon operators in a nucleon state. At this comes in uncertainty stemmed from nuclear physics. The last step requires adding up the DM-nucleon interactions to obtain the DM-nucleus interactions by using nuclear wave

¹²See, for example [132] for an overview of various experimental setups.

functions. Various nuclear form factors are to be used in this step, leaving scope of more nuclear physics uncertainty¹³. One important aspect of this calculation is that the scattering of DM happens in extreme non-relativistic limit. It is straightforward to show that in this limit the axial vector current leads to interaction between quark spin and DM particle spin, also vector and tensor currents take the form of scalar interactions. Thus there are two types of interactions that the DM-nucleus elastic scattering proceeds through, namely, spin independent or scalar interactions and spin dependent interactions. In the spin independent interaction the mass of nucleus plays the major role whereas for the case of spin dependent interaction it is the spin of the nucleus [134]. It may so happen that a specific DM candidate (*e.g.*, neutralino in the case of SUSY or $B^{(1)}$ in the case of mUED or nmUED) has both scalar as well as spin dependent interactions. In that case the full elastic scattering cross section is the sum of these two interactions.

There are many experiments, operative presently (and in the past), which are trying to search DM by direct detection method. They fall into different classes depending on the detection technique and detector material, for example cryogenic crystal experiments (*e.g.*, CDMS [135], EDELWEISS [136], CRESST [137]), scintillator experiments (*e.g.*, DAMA [138]), noble liquid experiments (*e.g.*, XENON [139, 140], LUX [141]) etc. In our study of nmUED (subsection 3.4.2, following [55]) we will compare our results with the XENON experiment. Before going to nmUED it will not be out of place to mention a few things about the direct detection studies in the context of mUED.

3.4.1 mUED

In mUED the detection prospect of $B^{(1)}$ LKP has been discussed in [142] followed by subsequent studies in [109, 117]. In [142], taking $B^{(1)}$ to be the LKP it has been shown that the scalar cross sections are suppressed with respect to the spin dependent one. As we will see in the next subsection this is the case for nmUED too.

In Fig. 3.7 it is illustrated that the cross sections can be increased up to one order depending on the mass splitting $\Delta_{q^{(1)}}$ which has been varied by hand. The cross sections are below the reach of currently running experiments. Experiments with improved sensitivity will be required to probe the scenario.

In a variant of mUED, the first level KK neutrino, $\nu^{(1)}$ is also considered to be the LKP [109]. But it has been shown that this case is not viable as to be consistent with the observations of experiments like, EDELWEISS [143] or CDMS [144] the $\nu^{(1)}$ LKP should

¹³For a nice pedagogic review on direct detection see, *e.g.*, [133]

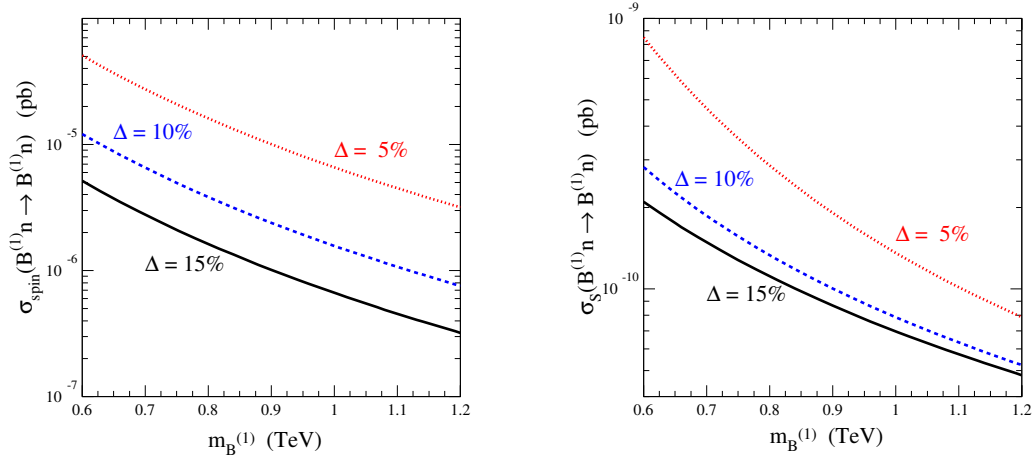


Figure 3.7: Spin dependent and scalar LKP-nucleon cross section as a function of $B^{(1)}$ mass for $\Delta_{q^{(1)}} = 5, 10, 15\%$ and $m_H = 120$ GeV. Adapted from [109].

have a mass $\gtrsim 50$ TeV. But relic density calculations do not favor the $\nu^{(1)}$ masses to be greater than 10 TeV. The direct detection study of the $W_3^{(1)}$ (or $Z^{(1)}$) LKP has been performed in [117, 145].

3.4.2 nmUED

In this subsection we will consider nmUED and how the DM direct detection experiments constrain it. At this point it would be useful to recall that the main difference with the mUED scenario will come through the BLKT parameters which modify the mass spectra as well as couplings. The discussion of this subsection will closely follow [55].

We would like to elaborate on the prospects of direct detection of $B^{(1)}$ at an experiment such as XENON [140, 146]. The actual event rates at such an experiment will not be estimated; instead, we will present the spin dependent and spin independent cross sections of $B^{(1)}$ scattering off Xenon nuclei ($A = 131$, $Z = 54$). Event rates and cross sections of DM in the context of mUED have been obtained in ref. [109, 142]. As masses and also the couplings in nmUED show a distinctive departure from the corresponding quantities in UED, we wish to revisit the calculation.

We have already mentioned that the scattering cross section of dark matter off nuclei is ultimately related to its scattering from quarks. Also in the non-relativistic limit the total cross section can have two components: the spin-independent (*i.e.*, scalar) and spin-

dependent parts.

The spin independent part of the scattering cross section of $B^{(1)}$ with a nucleus of mass m_N with atomic number Z and mass number A at zero momentum transfer is given by,

$$\sigma_0^{\text{scalar}} = \frac{m_N^2}{4\pi(m_{B^{(1)}} + m_N)^2} \left(Z f_p^{B^{(1)}} + (A - Z) f_n^{B^{(1)}} \right)^2, \quad (3.26)$$

where

$$f_{p,n}^{B^{(1)}} = m_{p,n} \sum_q \frac{\gamma_q + \beta_q}{m_q} f_{T_q}^{(p,n)}. \quad (3.27)$$

The subscript p and n refers to the proton and neutron respectively. In our numerical calculations we have used $f_{T_q}^{(p,n)} = \langle q\bar{q} \rangle_{p,n}(m_q/m_{p,n})$, that relate the quark-level cross sections to that for the nucleons, as given in [76]. The model dependence of the specific dark matter candidate is captured in the quantities γ_q and β_q which here represent the interaction of $B^{(1)}$ with quarks, mediated via the SM Higgs exchange and $n = 1$ KK-fermion exchange respectively. We find that

$$\gamma_q = -\frac{g_1'^2}{2} \left(\frac{m_q}{m_h^2} \right), \quad \text{and} \quad \beta_q = -\tilde{g}_1^2 (Y_{qL}^2 + Y_{qR}^2) \frac{m_q (m_{B^{(1)}}^2 + m_{q^{(1)}}^2)}{(m_{B^{(1)}}^2 - m_{q^{(1)}}^2)^2}, \quad (3.28)$$

with

$$g_1'^2 = g_1^2 \pi R \left(1 + \frac{R_B}{\pi} \right) \frac{1}{\sqrt{1 + \frac{R_H}{\pi}}} I_{B^{(1)}B^{(1)}h^{(0)}}, \quad (3.29)$$

where $I_{B^{(1)}B^{(1)}h^{(0)}}$ is given in Eq. 3.37.

$$\tilde{g}_1 = g_1 \sqrt{\pi R \left(1 + \frac{R_B}{\pi} \right)} I_{B^{(1)}q^{(1)}q^{(0)}}, \quad (3.30)$$

where $I_{B^{(1)}q^{(1)}q^{(0)}}$ is given in Eq. 3.35. Numerically γ_q is almost insensitive to $m_{B^{(1)}}$ and about two orders of magnitude larger than β_q .

The corresponding spin-dependent cross section is given by:

$$\sigma_0^{\text{spin}} = \frac{2}{3\pi} (\mu^2 \tilde{g}_1^4) \left(\frac{a_p \langle S_p \rangle + a_n \langle S_n \rangle}{m_{B^{(1)}}^2 - m_{q^{(1)}}^2} \right)^2 \frac{(J+1)}{J}, \quad (3.31)$$

where μ is the reduced mass of the target nucleus and LKP system and the other nuclear parameters can be found in [76]. In particular,

$$a_p = \frac{17}{36} \Delta u + \frac{5}{36} (\Delta d + \Delta s) \quad \text{and} \quad a_n = \frac{17}{36} \Delta d + \frac{5}{36} (\Delta u + \Delta s) \quad (3.32)$$

Following [109], in our calculations we have used the central values of $\Delta u = 0.78 \pm 0.02$, $\Delta d = -0.48 \pm 0.02$ and $\Delta s = -0.15 \pm 0.02$.

Experimental results are often presented in terms of *effective* dark matter-nucleon scattering cross sections given by:

$$\sigma_{p,n}^{\text{scalar}} = \sigma_0 \frac{m_{p,n}^2}{\mu^2} \frac{1}{A^2}, \quad (3.33a)$$

$$\sigma_{p,n}^{\text{spin}} = \frac{\tilde{g}_1^4}{2\pi} \frac{\mu_{p,n}^2 a_{p,n}^2}{(m_{B^{(1)}}^2 - m_{q^{(1)}}^2)^2}, \quad (3.33b)$$

where $\mu_{p,n}$ is the reduced mass of the WIMP-nucleon system.

We can now turn to the numerical results for the spin-dependent and scalar WIMP-nucleon cross section for Xenon. The cross sections will be presented as a function of the LKP ($B^{(1)}$) mass which is fixed by R^{-1} and the BLKT parameter R_B . For the direct detection the relevant parton level processes involve the interaction of $B^{(1)}$ with quarks. The relevant Feynman diagrams for these processes are shown in Fig. 3.8. We see that

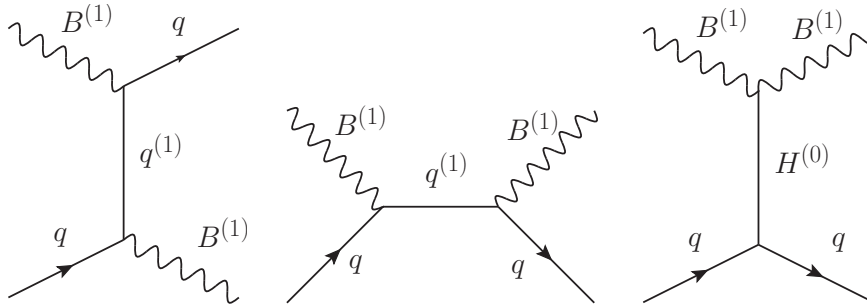


Figure 3.8: The Feynman diagrams for $B^{(1)}$ and quark scattering.

the first KK level quarks, $q^{(1)}$, can come as intermediate particles in $B^{(1)}$ -quark scattering processes. For simplicity we keep the mass of the level one quarks much higher than the mass of $B^{(1)}$ as well as first level leptons. Due to this choice the first level quarks can not contribute significantly in the relic density of $B^{(1)}$ via coannihilation, *i.e.*, the $\Delta_{q^{(1)}}$ becomes larger. To serve this purpose we take the BLKT strength of quarks, R_q to be less than zero¹⁴. For a fixed value of R_B (*i.e.*, any one panel) we show the region bounded by curves of $R_q = 0$ and $-\pi/2$.

Scattering rates of the the LKP off nucleons are presented in Fig. 3.9 (scalar cross section, σ_n^{scalar}) and in Fig. 3.10 (spin dependent cross section, σ_n^{spin}). Over the range of input

¹⁴High negative BLKTs can result in tachyonic modes. The limit to circumvent a tachyonic zero mode is [72], $R_X > -\pi/2$. In our choice of BLKT parameters we respect this limit.

parameters we have considered, σ_n^{scalar} decreases by three orders of magnitude from 10^{-43} cm^2 to 10^{-46} cm^2 while σ_n^{spin} varies from 10^{-41} – 10^{-45} cm^2 . It would be relevant here to mention that the values of the spin dependent LKP scattering cross sections are well below the sensitivity of the XENON experiment in the relevant mass range of our case¹⁵. As for the spin independent or scalar cross sections, the XENON bound [140] can be evaded in the region where R_q is negative.

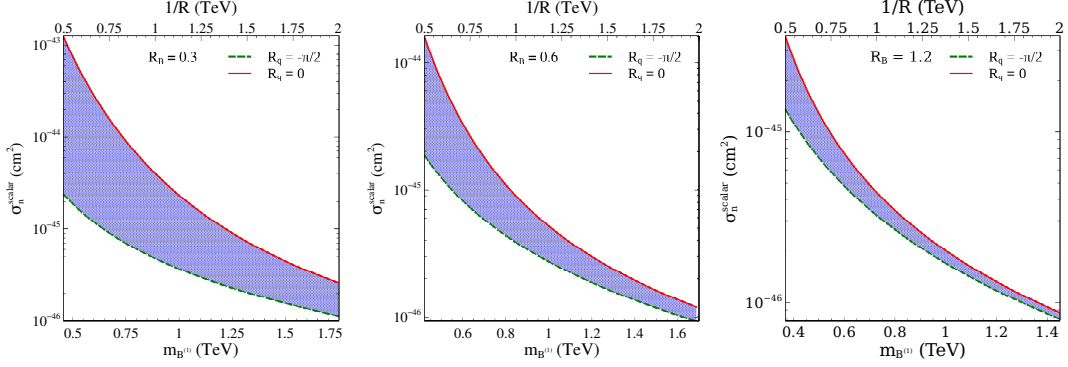


Figure 3.9: Variation of the scalar $B^{(1)}$ -nucleon cross section with relic particle mass for Xenon. The three panels are for three values of R_B . The shaded (blue) region represents the cross section for a continuous variation of R_q within the range bounded by the two curves.

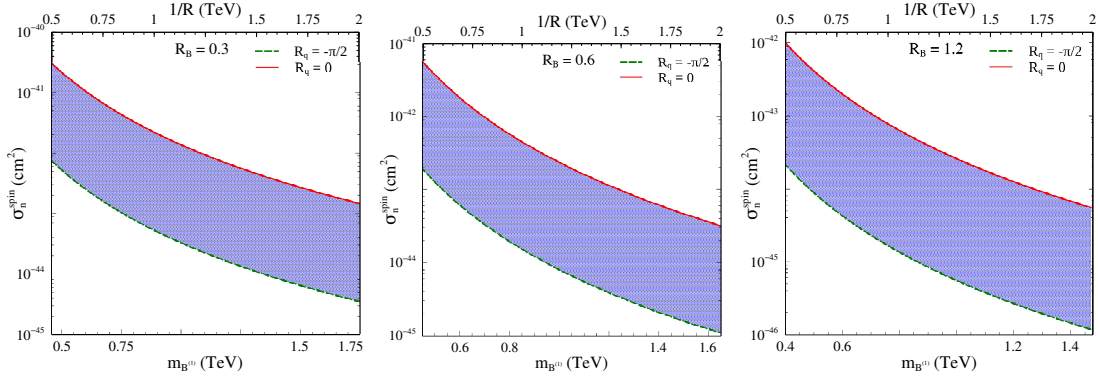


Figure 3.10: Variation of the spin dependent $B^{(1)}$ -nucleon cross section with relic particle mass for Xenon. The three panels are for three values of R_B . The shaded (blue) region shows the cross section for a continuous variation of R_q within the range bounded by the two curves.

¹⁵For the range of WIMP masses in Fig. 3.10, sensitivity of the XENON experiment [146] for the scalar cross section is above 10^{-40} cm^2 .

The plots in Figs. 3.9 and 3.10 for the dark matter cross sections appear somewhat different from those given for mUED in [109] and [142]. This is due to the fact that in nmUED, in contrast to the mUED, the mass of $B^{(1)}$ as well as its couplings are dependent on the BLKT parameters and this in turn modifies the cross sections in comparison to the mUED. However the overall nature (e.g., the dependence on $\Delta_{q^{(1)}}$ etc.) remains the same.

The nature of variation of the DM scattering cross sections as presented in Figs. 3.9 and 3.10 can be seen to follow from Eq. 3.33. BLKT parameter dependence creeps into σ_n^{spin} via the $\left(m_{q^{(1)}}^2 - m_{B^{(1)}}^2\right)^2$ factor in the denominator along with \tilde{g}_1 . The scalar cross section, σ_n^{scalar} has a more complicated dependence on the BLKT parameters. While $\frac{\gamma_q}{m_q}$ is almost independent of BLKT parameters, $\frac{\beta_q}{m_q}$ increases with $m_{B^{(1)}}$ and R_f . However, the γ_q contribution dominates and thus the combination $\frac{(-\gamma_q - \beta_q)}{m_q}$ changes slowly with $m_{B^{(1)}}$ and R_f . An overall factor of $m_{B^{(1)}}^2$ in the denominator of σ_0 (see Eq. 3.26), accounts for the rapid decrease of the scalar cross section, which falls monotonically in Fig. 3.9.

3.5 Summary and Conclusions

In this chapter we discussed the generalization of the UED model where the extra four-dimensional kinetic terms located at the two fixed points are of a strength which is a free parameter and varies from particle to particle. To ensure the conservation of a \mathbf{Z}_2 symmetry, called *KK parity*, the strengths are taken equal at the two fixed points. This ensures the stability of the LKP. The BLKT parameters determine the wave-functions of the KK-excitations in the fifth dimension, y , as well as their masses. Moreover, the non-trivial y -dependence of the wave-functions affects the couplings of the KK-excitations; these are also controlled by the BLKT parameters. We allow different BLKT strengths for the various SM particles and ensure that $B^{(1)}$ is the LKP. We also examine the alternative case of a $W_3^{(1)}$ LKP but find that the relic density is too small for a WIMP mass ~ 1 TeV. We conclude that $W_3^{(1)}$ cannot serve the role of a single component dark matter when its mass is within the LHC reach. We make a note of the bounds on the LKP dark matter particle mass which follow from the overclosure of the universe.

In this work we consider dark matter in this nmUED scenario retaining the impact of BLKT parameters on the masses *and* the couplings. We show that the range of relic densities preferred by the Planck data places stringent restrictions on the BLKT strengths of the gauge bosons and fermions and these get correlated. We find that in this process the allowed range of the compactification scale R^{-1} is much relaxed from its narrow UED prediction of 0.5 – 0.6 TeV.

We discussed the prospects of direct detection of the nmUED dark matter candidate keeping the relic density constraints in mind. As an example, we evaluate the spin-dependent and spin-independent scattering cross section of dark matter off Xenon nuclei. Our calculations indicate that the signal is well below the existing limits set by the XENON experiment.

Appendix

In this Appendix we note the Feynman rules for the $n = 1$ Kaluza-Klein excitations. Each of these vertices involves a nontrivial coupling determined by the five-dimensional wave-functions of the KK-excitations. These couplings are listed separately below. Besides these Feynman rules and couplings, only the SM rules are required.

Overlap integrals:

Here we list the overlap integrals which appear in the Feynman rules given below.

$$I_{B^{(1)}f^{(1)}f^{(0)}} = \int_0^{\pi R} [1 + r_f \{\delta(y) + \delta(y - \pi R)\}] a_B^{(1)} f^{(1)} f^{(0)} dy. \quad (3.34)$$

$$I_{B^{(1)}H^{(1)}H^{(0)}} = \int_0^{\pi R} [1 + r_H \{\delta(y) + \delta(y - \pi R)\}] a_B^{(1)} H^{(1)} H^{(0)} dy. \quad (3.35)$$

$$I_{B^{(1)2}H^{(0)2}} = \int_0^{\pi R} [1 + r_H \{\delta(y) + \delta(y - \pi R)\}] a_B^{(1)2} H^{(0)2} dy. \quad (3.36)$$

$$I_{B^{(1)}B^{(1)}H^{(0)}} = \int_0^{\pi R} [1 + r_H \{\delta(y) + \delta(y - \pi R)\}] a_B^{(1)} a_B^{(1)} H^{(0)} dy. \quad (3.37)$$

$$I_{W^{(1)}f^{(1)}f^{(0)}} = \int_0^{\pi R} [1 + r_f \{\delta(y) + \delta(y - \pi R)\}] a_W^{(1)} f^{(1)} f^{(0)} dy. \quad (3.38)$$

where $a_B^{(n)}(y)$, $f^{(n)}(y)$ are the the wave-functions for the gauge boson and fermion fields introduced earlier, and $H^{(n)}(y)$ is the same for the Higgs field.

Feynman Rules:

The $B^{(1)} f^{(1)} f^{(0)}$ vertex

$$\equiv -i \left(g_1 \sqrt{\pi R \left(1 + \frac{R_B}{\pi} \right)} \times I_{B^{(1)} f^{(1)} f^{(0)}} \right) \gamma^\mu (P_L Y_L + P_R Y_R)$$

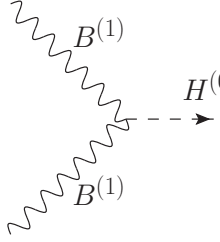
The $B^{(1)} H^{(1)} H^{(0)}$ vertex

$$\equiv -i \left(g_1 \sqrt{\pi R \left(1 + \frac{R_B}{\pi} \right)} \times I_{B^{(1)} H^{(1)} H^{(0)}} \right) Y_H (p_\mu^- - p_\mu^+)$$

The $B^{(1)} B^{(1)} H^{(0)} H^{(0)}$ vertex

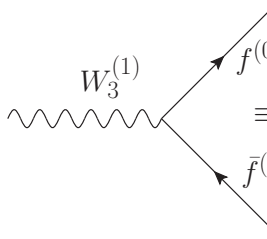
$$\equiv -2i \left(g_1^2 \pi R \left(1 + \frac{R_B}{\pi} \right) \times I_{B^{(1)} B^{(1)} H^{(0)} H^{(0)}} \right) \eta_{\mu\nu} Y_H^2$$

The $B^{(1)}B^{(1)}H^{(0)}$ vertex

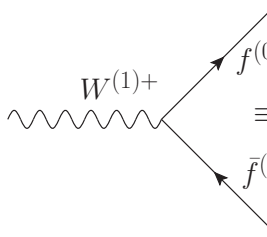


$$\equiv -2i \left(g_1^2 \pi R \left(1 + \frac{R_B}{\pi} \right) \times I_{B^{(1)}B^{(1)}H^{(0)}} \right) \times \frac{v}{\sqrt{1 + \frac{R_H}{\pi}}} Y_H^2$$

The $W^{(1)}f^{(1)}f^{(0)}$ vertices



$$\equiv -i \left(g_2 \sqrt{\pi R \left(1 + \frac{R_W}{\pi} \right)} \times I_{W^{(1)}f^{(1)}f^{(0)}} \right) \gamma^\mu T_3 P_L$$



$$\equiv -i \left(g_2 \sqrt{\pi R \left(1 + \frac{R_W}{\pi} \right)} \times I_{W^{(1)}f^{(1)}f^{(0)}} \right) \frac{\gamma^\mu}{\sqrt{2}} P_L$$

Chapter 4

Non-minimal Universal Extra Dimension Confronting Higgs Data

By now it is almost evident that the observed scalar boson at CERN as reported by ATLAS [20] and CMS [21] collaborations has properties that are close to the Standard Model (SM) Higgs, *i.e.*, it almost behaves like a spin zero [147] and dominantly CP-even field [148–151]. However, present trends indicate substantial constraints on New Physics (NP) scenarios that result in a modification of the Higgs production cross sections and branching ratios. The loop-induced Higgs couplings to the photon and the gluon are of particular interest as they are susceptible to considerable corrections from TeV scale NP. Indeed the impact of these couplings has been explored extensively in the recent past [152]. Aficionados of TeV scale NP scenarios have been compelled to move to more general versions of specific models typically with a larger parameter space to accommodate these experimental constraints.

In this chapter we will discuss the constraints coming from the LHC Higgs data on the UED scenario. However, generalizing to models with BLKT, *i.e.*, nmUED, [66] that arise naturally due to the cut-off dependent radiative corrections, facilitates a considerable recovery of the constrained parameter space.

We begin by reviewing the formalism to study the Higgs couplings $gg \rightarrow H$ and $H \rightarrow \gamma\gamma$, including possible contributions from new states beyond the SM. Then we compute in turn the contributions from UED and nmUED scenarios and compare with present experimental values. This chapter follows largely from [56].

4.1 Loop-induced Higgs couplings

At the LHC, the Higgs production chiefly proceeds through the gluon fusion process $gg \rightarrow H$, driven by the fermion (dominant effect comes from top quark) triangle loop [153]. Similarly an important decay mode for a 125 GeV Higgs is the di-photon channel. This proceeds through a fermion and a W -boson loop within SM. New states with correct quantum numbers can show up as virtual particles in these loops and may lead to a sizable correction of the effective couplings. The corresponding decay width and cross section, including possible contributions from new massive states are given below [154],

$$\Gamma_{H \rightarrow \gamma\gamma} = \frac{G_F \alpha^2 m_H^3}{128 \sqrt{2} \pi^3} \left| A_W(\tau_W) + 3 \left(\frac{2}{3} \right)^2 A_t(\tau_t) + N_{c, \text{NP}} Q_{\text{NP}}^2 \mathcal{A}_{\text{NP}}(\tau_{\text{NP}}) \right|^2, \quad (4.1a)$$

$$\sigma_{gg \rightarrow H} = \frac{G_F \alpha_s^2 m_H^3}{16 \sqrt{2} \pi^3} \left| \frac{1}{2} A_t(\tau_t) + C(r_{\text{NP}}) \mathcal{A}_{\text{NP}}(\tau_{\text{NP}}) \right|^2, \quad (4.1b)$$

where

$$\mathcal{A}_{\text{NP}}(\tau_{\text{NP}}) = \sum_{\text{NP}} \frac{v}{m_{\text{NP}}} \frac{\partial m_{\text{NP}}}{\partial v} A_{F,V,S}(\tau_{\text{NP}}). \quad (4.2)$$

In these expressions $\tau_i = m_H^2/4m_i^2$, and the function $A_X(\tau_X)$ represents the amplitude when the particle X is running in the loop. Here $N_{c, \text{NP}}$ is the number of color states in the color representation and Q_{NP} is the electric charge of the particle in the loop and $C(r_{\text{NP}})$ is an appropriate group theoretic factor.

In SM the masses of all the particles are proportional to the vev of the Higgs field, v_{SM} . The couplings of the SM particles to Higgs can be written as,

$$y_{H\bar{f}f}^{\text{SM}} = \frac{m_f}{v_{\text{SM}}} \text{ for fermions,} \quad (4.3a)$$

$$g_{H\phi\phi}^{\text{SM}} = \frac{2m_\phi^2}{v_{\text{SM}}} \text{ for bosons.} \quad (4.3b)$$

It is evident that the contribution of a state in the loops depends on the spin statistics of that state (F, V and S stand for fermions, vector bosons and scalars respectively). The various contributions are given as [155],

$$A_F(\tau) = \frac{2}{\tau^2} (\tau + (\tau - 1)f(\tau)), \quad (4.4a)$$

$$A_V(\tau) = -\frac{1}{\tau^2} (2\tau^2 + 3\tau + 3(2\tau - 1)f(\tau)), \quad (4.4b)$$

$$A_S(\tau) = -\frac{1}{\tau^2} (\tau - f(\tau)), \quad (4.4c)$$

where, $f(\tau) = (\sin^{-1} \sqrt{\tau})^2$. In the light Higgs limit, *i.e.*, $m_H \ll 2m_i$, we get, $A_F \sim 4/3$, $A_V \sim -7$, $A_S \sim 1/3$.

Normally the masses of the NP particles are not proportional to Higgs vev, but receive a small correction from it. For example, the KK particles acquire the mass from compactification with minute contribution from EWSB. Hence the coupling to the Higgs boson can in general be written as,

$$y_{H\bar{f}f} = \frac{\partial m_f(v)}{\partial v}, \quad g_{H\phi\phi} = \frac{\partial m_\phi^2(v)}{\partial v}. \quad (4.5)$$

Thus in the amplitude the NP contribution can be written as,

$$A_F^{\text{NP}} = \frac{y_{H\bar{f}f}^{\text{NP}}}{y_{H\bar{f}f}^{\text{SM}}} A_F \quad \text{for fermions,} \quad (4.6a)$$

$$A_{V,S}^{\text{NP}} = \frac{y_{H\phi\phi}^{\text{NP}}}{y_{H\phi\phi}^{\text{SM}}} A_{V,S} \quad \text{for bosons,} \quad (4.6b)$$

and these can be expressed in a generalized form by Eq. 4.2.

It will be useful to define two dimensionless parameters, $C_{gg} = \sigma_{gg \rightarrow H}^{\text{NP}} / \sigma_{gg \rightarrow H}^{\text{SM}}$ and $C_{\gamma\gamma} = \Gamma_{H \rightarrow \gamma\gamma}^{\text{NP}} / \Gamma_{H \rightarrow \gamma\gamma}^{\text{SM}}$, to compare the correction induced by NP scenarios with experimentally allowed values. The best fit values for C_{gg} and $C_{\gamma\gamma}$ from the LHC Higgs results were computed in [152]. We are going to use the numerical values quoted in [156]: $\sqrt{C_{gg}} = 0.88 \pm 0.11$ and $\sqrt{C_{\gamma\gamma}} = 1.18 \pm 0.12$.

4.2 mUED results

In this section we will talk about the constraints that are imposed on the UED model after the discovery of Higgs boson. Since then, many studies have been performed to examine various implications on this model [157–161]¹. We have introduced the UED model in Sec. 1.4. Recall that in UED the extra spatial dimension is compactified on an S^1/\mathbb{Z}_2 orbifold and all the SM fields can propagate in the extra dimension. In this chapter we will take the convention that the orbifold fixed points are at $y = \pm\pi R/2$ instead of being $y = 0, \pi R$. The relevant part of the action for our study in this chapter can be written as,

$$\mathcal{S} = \int_{-L}^L dy \int d^4x \left[-\frac{1}{4} \sum_g F_{MN}^g F^{gMN} \right]$$

¹Some of the earlier studies in this field can be found in [162–164]

$$\begin{aligned}
 & + (D_M H)^\dagger D^M H - \hat{\mu}^2 H^\dagger H - \hat{\lambda} (H^\dagger H)^2 \\
 & + i\bar{Q}_3 \not{D} Q_3 + i\bar{u}_3 \not{D} u_3 \\
 & - \left\{ i\hat{\lambda}_5^u \bar{Q}_3 \tilde{H} u_3 + \text{h.c.} \right\},
 \end{aligned} \tag{4.7}$$

where $L = \pi R/2$ and the summation in the first term is over all the gauge groups. Here Q_3 and u_3 represent the third generation quarks and λ_5^u is the corresponding Yukawa coupling. Other symbols are defined in Sec. 1.4.

We are interested in the contribution of the KK excitations that may show up as virtual particles and modify the loop level couplings of the zero mode scalar field (*i.e.*, SM Higgs field) with the photon and gluon. The contribution from the entire KK top tower is a convergent sum which can be computed in closed form in the light Higgs approximation by using Eq. 4.2 is given by [154],

$$\mathcal{A}_t^{NP} \sim \frac{8}{6} \left\{ \frac{\pi m_t}{R} \coth \left(\frac{\pi m_t}{R} \right) - 1 \right\}. \tag{4.8}$$

To consider the effect of the KK W -boson in the loop, one needs to be careful to also incorporate the contribution from the additional scalar states present in the spectrum. These are states that are a linear combinations of KK excitations of the fifth component of the gauge bosons $W_5^{(n)}$ and the KK excitations of the Goldstone modes $G^{(n)}$, that are orthogonal to the longitudinal component of the massive $W_\mu^{(n)}$ boson. A systematic study of this within the light Higgs approximation gives us,

$$\mathcal{A}_W^{NP} \sim -\frac{20}{6} \left\{ \frac{\pi m_W}{R} \coth \left(\frac{\pi m_W}{R} \right) - 1 \right\}. \tag{4.9}$$

Using these expressions in Eq. 4.1, we compute the corrections to the Higgs couplings as a function of the radius of compactification of the fifth spatial dimension.

From Fig. 4.1 we find that the measurement of the Higgs coupling to gluons at 95% confidence disfavors $1/R < 1.3$ TeV. The constraints from the effective couplings to photons are smaller primarily owing to the partial cancellation of the contributions between the KK fermions and KK gauge-Goldstone bosons. This is in consonance with other constraints, which are typically stringent, from the oblique corrections estimated to be around: $1/R > 0.8$ TeV [165]. The bounds from direct searches at colliders lead to subdominant or comparable constraints [166], owing to the relatively compressed mass spectrum within this class of models. Recent LHC Higgs mass bounds can constrain UED from the renormalization group running of the physical parameters [167]. The vacuum stability bounds on UED can be found in [157]. It may be noted that an exclusion limit at

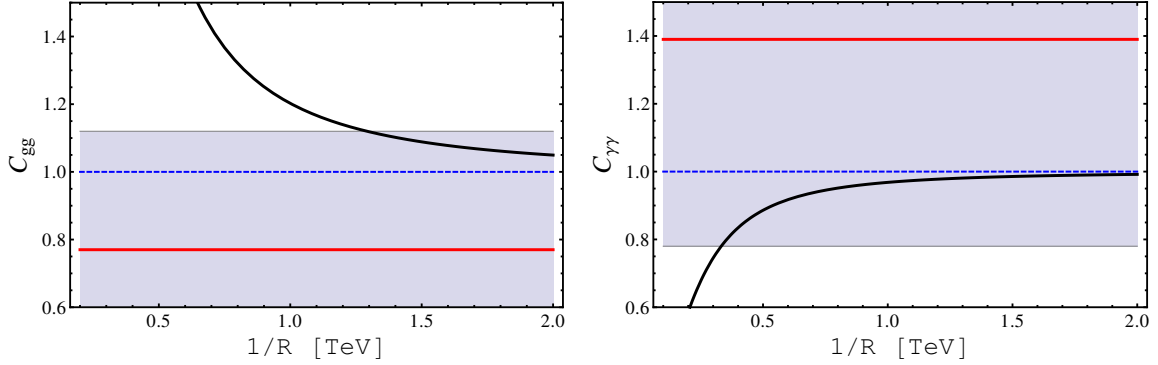


Figure 4.1: The ratios of the Higgs couplings in UED scenario to their SM values are plotted as functions of the inverse radius of compactification of the extra dimension ($1/R$). The blue (shaded) bands represent the 95% confidence level allowed values for these ratios [156], with the red (solid) horizontal lines representing the central values from LHC data. The blue (dashed) lines correspond to the SM points. The black (dark) curves are the UED predictions. We have assumed $m_H = 125$ GeV.

$1/R > 1.3$ TeV closes in on the overclosure limit from dark matter relic abundance in the minimal model [118]. A similar study [161] taking Higgs data into account also demonstrated that the lower bound on $1/R$ is 1.3 TeV at 95% confidence level. We will see in the next section 4.3 that this limit may be avoided in non-minimal models.

Thus it can be asserted that if the current trend of the Higgs data gets support in future with increased statistics, it will result in tighter bounds than from direct observations and pose a challenge to the parameter space of these models that is accessible to present and future collider experiments.

4.3 nmUED results

To consider the case of nmUED we need to introduce the appropriate BLTs. The relevant BLTs for this purpose will be the BLTs of fermionic and Yukawa sectors. The boundary localized part of the action will be given by²,

$$\begin{aligned} \mathcal{S}_{\text{BLT}} = \int_{-L}^L dy \int d^4x \left[r_Q \{ \delta(y-L) + \delta(y+L) \} (i\bar{Q}_3 \not{D} P_L Q_3 + i\bar{u}_3 \not{D} P_R u_3) \right. \\ \left. - r_Y \{ \delta(y-L) + \delta(y+L) \} (i\lambda_5^u \bar{Q}_3 \tilde{H} u_3 + \text{h.c.}) \right] \end{aligned} \quad (4.10)$$

Here we will consider the BLT strengths r_Q and r_Y at the weak scale to be free and independent parameters. As has been already mentioned, inclusion of these types of terms

²We will use the notations and conventions of [72] in this section.

can lead to deviations in the bulk profile, masses and the couplings of the bulk field. The KK masses are given by the subsequent roots of the following transcendental equations³,

$$r_Q m_n = \begin{cases} \cot\left(\frac{m_n \pi R}{2}\right) & \text{for } n : \text{ odd,} \\ -\tan\left(\frac{m_n \pi R}{2}\right) & \text{for } n : \text{ even.} \end{cases} \quad (4.11)$$

In the present scenario, the Yukawa sector that couples the fermions, with a non-trivial bulk profile, with the zero mode of the Higgs, which is assumed to be flat in the bulk, is of interest and can be written as,

$$\mathcal{S}_{\text{Yuk}} = -\frac{v\lambda}{\sqrt{2}} \int d^4x \left[\left(\bar{Q}_L^{(0)} u_R^{(0)} + r'_{Qnn} \bar{Q}_L^{(n)} u_R^{(n)} - R'_{Qnn} \bar{u}_L^{(n)} Q_R^{(n)} + \dots \right) + \text{h.c.} \right], \quad (4.12)$$

where, $r'_{Qnn}(r_Q, r_Y, m_n)$ and $R'_{Qnn}(r_Q, r_Y, m_n)$ are overlap integrals obtained by introducing the bulk profile of the fermions into Eq. 4.10 and integrating the fifth dimension. The effects of possible KK level mixing terms in Eq. 4.12 will be discussed separately. The overlap integrals can be adopted from the expression given in [72] and are given by,

$$r'_{Qnn}(\text{e/o}) = \frac{2r_Q + \pi R}{2r_Y + \pi R} \left(\frac{2r_Y + \frac{1}{A_{Q^{(n)}}^2} \left[\frac{\pi R}{2} \pm \frac{1}{2m_{Q^{(n)}}} \sin(m_{Q^{(n)}} \pi R) \right]}{2r_Q + \frac{1}{A_{Q^{(n)}}^2} \left[\frac{\pi R}{2} \pm \frac{1}{2m_{Q^{(n)}}} \sin(m_{Q^{(n)}} \pi R) \right]} \right), \quad (4.13a)$$

$$R'_{Qnn}(\text{e/o}) = \frac{2r_Q + \pi R}{2r_Y + \pi R} \left(\frac{2r_Y (B_{Q^{(n)}})^2 + \frac{1}{A_{Q^{(n)}}^2} \left[\frac{\pi R}{2} \mp \frac{1}{2m_{Q^{(n)}}} \sin(m_{Q^{(n)}} \pi R) \right]}{\frac{1}{A_{Q^{(n)}}^2} \left[\frac{\pi R}{2} \mp \frac{1}{2m_{Q^{(n)}}} \sin(m_{Q^{(n)}} \pi R) \right]} \right). \quad (4.13b)$$

The subscript (e/o) represents whether n is even or odd. $A_{Q^{(n)}} = \sin(m_{Q^{(n)}} \pi R/2)$, for n odd and $\cos(m_{Q^{(n)}} \pi R/2)$, for n even, similarly $B_{Q^{(n)}} = \cot(m_{Q^{(n)}} \pi R/2)$, for n odd and $\tan(m_{Q^{(n)}} \pi R/2)$, for n even and $m_{Q^{(n)}}$ is the n -th root of Eq. 4.11. The mass part of the action for the n -th KK excitation of the top quark can be written as,

$$S_{t^{(n)}} = - \int d^4x \left\{ \left[\bar{Q}_3^{(n)}, \bar{u}_3^{(n)} \right]_L \begin{bmatrix} m_{Q_3^{(n)}} & r'_{Qnn} \frac{v}{\sqrt{2}} \lambda_t \\ -R'_{Qnn} \frac{v}{\sqrt{2}} \lambda_t & m_{u_3^{(n)}} \end{bmatrix} \begin{bmatrix} Q_3^{(n)} \\ u_3^{(n)} \end{bmatrix}_R + \text{h.c.} \right\}. \quad (4.14)$$

In the above expressions we have assumed that in the 4D effective theory obtained by integrating out the fifth dimension, the bulk fields $Q_L(x, y)$ and $u_R(x, y)$ split into a massless zero mode and an infinite tower of massive 4D states given by $(Q_L^{(0)}, Q_L^{(n)}, Q_R^{(n)})$ and $(u_R^{(0)}, u_L^{(n)}, u_R^{(n)})$ respectively.

³Note that the equations given here differs by a factor of two in the left hand side of Eq. 2.24. The origin of this mismatch is just due to the conventions.

The introduction of the BLKT parameters lead to KK level mixing at the leading order in the Yukawa interactions. However the symmetric nature of the BLKT parameters as introduced in Eq. 4.10 confines the mixing within the odd or even modes, due to a residual unbroken KK parity in the theory. The mixing angle between the n -th KK level and $(n + 2l)$ -th KK level can be estimated as $\theta_{mix} \sim f(r_Y, r_Q, n, l)m_t R/2l$, where $f(r_Y, r_Q, n, l)$ schematically represents the corresponding overlap integrals. Though the mixing angle is suppressed by the new physics scale $(1/R)$, significant level mixing between zero mode and $n = 2$ KK states are possible in certain regions of the parameters space specially for smaller values of $1/R$ [72]. For the collider implications of this mixing in the top sector see [67].

We now turn our attention to make a careful study of this mixing. The relevant part of the action can be written as,

$$S_{t^{(0-2)}} = - \int d^4x \left\{ \left[\overline{Q}_3^{(0)}, \overline{Q}_3^{(2)}, \overline{u}_3^{(2)} \right]_L \begin{bmatrix} \frac{v}{\sqrt{2}} \lambda_t & 0 & r'_{Q02} \frac{v}{\sqrt{2}} \lambda_t \\ r'_{Q20} \frac{v}{\sqrt{2}} \lambda_t & m_{Q_3^{(2)}} & r'_{Q22} \frac{v}{\sqrt{2}} \lambda_t \\ 0 & -R'_{Q22} \frac{v}{\sqrt{2}} \lambda_t & m_{u_3^{(2)}} \end{bmatrix} \begin{bmatrix} u_3^{(0)} \\ Q_3^{(2)} \\ u_3^{(2)} \end{bmatrix}_R + \text{h.c.} \right\}, \quad (4.15)$$

where,

$$r'_{Q20} = \frac{2r_Q + \pi R}{2r_Y + \pi R} \left(\frac{1}{\sqrt{2r_Q + \pi R}} \frac{2(r_Y - r_Q)}{\sqrt{2r_Q + \frac{1}{A_{Q^{(2)}}^2} \left[\frac{\pi R}{2} + \frac{\sin(m_{Q^{(2)}} \pi R)}{2m_{Q^{(2)}}} \right]}} \right) \quad (4.16)$$

The overlap integral between the zero mode and second level, r'_{Q20} is symmetric in its last two indices. In Eq. 4.15, the identification of the lightest eigenvalue with the SM top with mass in the range⁴, $m_t = 173.07 \pm 0.52 \pm 0.72$ GeV [60] puts a severe constraint on the allowed BLKT parameters and consequently constrains the Higgs couplings that we will now discuss.

In order to obtain the Higgs couplings, we diagonalize the mass matrix in Eq. 4.14, that gives us the physical mass of the n -th KK excitations. One can use this to compute the Higgs cross section and decay width in the BLKT scenario by using Eqs. 4.1 and 4.2. We perform the KK summation numerically and terminate the procedure at $n = 20$, as the contribution decouples with higher KK number and becomes numerically insignificant beyond this. Note that the gauge and scalar parts of the Lagrangian are unaffected by the introduction of the BLKT action given in Eq. 4.10. For the gauge-Goldstone sector one

⁴According to the most recent analysis from the results of Tevatron [168], $m_t = 174.98 \pm 0.76$ GeV

can adopt the analytic expression in Eq. 4.9. As indicated above we take care to include the constraint from the mixing effect on the parameter space of the theory. We find that once the constraint on the top mass is imposed the numerical effect of the mixing on the Higgs coupling is insignificant. However we include the leading order contribution from the mixing effect by considering the 0-2 KK level mixing. This can be consistently included into the calculation by replacing the contribution of the second KK top to the sum in Eq. 4.2 by the following expression,

$$\mathcal{A}_{NP}^{(2)} = \frac{4}{3} \left[\sum_{j=1}^3 \frac{v}{m_j} \frac{\partial m_j}{\partial v} - 1 \right], \quad (4.17)$$

where, m_j ($j = 1, 2, 3$) are the three eigenvalues of the mass matrix in Eq. 4.15 with the lowest eigenvalue identified with SM top mass.

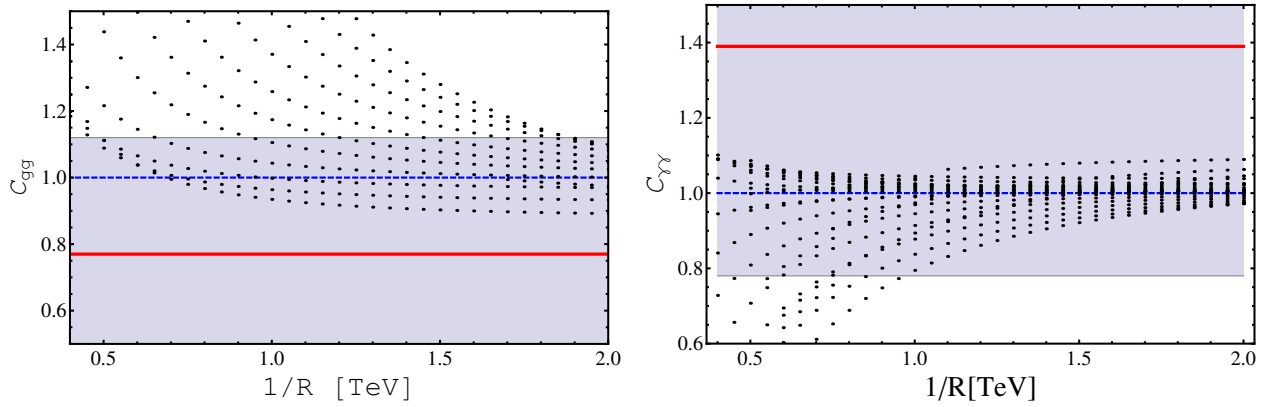


Figure 4.2: The ratios of the Higgs couplings in the BLKT scenario to their SM values are plotted as functions of the inverse radius of compactification of the extra dimension ($1/R$). The blue (shaded) bands represent the 95% confidence level allowed values for these ratios [156], with the red (light) horizontal lines representing the central values from LHC data. The blue (dashed) lines correspond to the SM points. The black (dark) points represent the BLKT results. We have assumed $m_h = 125$ GeV. The BLKT parameters r_Q and r_Y are varied within the range $[-\pi R/2, \pi R/2]$.

After the KK sum is done the ratios C_{gg} and $C_{\gamma\gamma}$ still remain functions of the BLKT parameters (r_Q, r_Y) and the inverse radius of compactification ($1/R$). We vary the BLKT parameters within the range $[-\pi R/2, \pi R/2]$ and obtain the corresponding scatter plots for C_{gg} and $C_{\gamma\gamma}$ as functions of $1/R$ in Fig. 4.2. As is expected the points form a band around the minimal UED prediction that corresponds to $r_Q = r_Y = 0$.

Crucially we find that in certain regions of the parameter space, the contribution from the KK fermions can change sign relative to the zero mode (SM) contribution. As can

be seen from the plot this reduces constraint from the coupling, which was at 1.3 TeV for mUED models, now becoming around 0.5 TeV. Significantly we find (see Fig. 4.1) that the mUED couplings are farther from the best fit line than the SM predictions in all regions of the parameter space. In the extended scenario with the BLKT parameters, we find (see Fig. 4.2) that in certain regions of the parameter space the couplings are closer to the best fit values than the SM. The limits on $1/R$, from dark matter relic density measurements and their direct detection at experiments within the BLKT framework, are rather model dependent and can lead to considerable relaxation over the minimal UED bound [55,73]. The corresponding constraints on this class of models from electroweak precision measurements can be found in [65,66,73].

4.4 Conclusion

In this chapter we presented the studies about the impact of Higgs couplings as measured at the LHC on Universal Extra Dimension models. We find that the minimal models are particularly constrained from the Higgs coupling to the gluon. We make a simple extension of the model by introducing relevant boundary localized kinetic terms. This leads to non-trivial 5D profiles for the bulk fields. The interactions are modified by the corresponding overlap integrals. In certain regions of the parameter space this can lead to better fitting of the experimental data implying a considerable relaxation of the experimental constraints.

Chapter 5

Signal of Second Level Kaluza-Klein Particles

In our discussion of UED (see Chapter 1) we mentioned that KK number, the incarnation of fifth dimensional momentum, is conserved at the tree level. Clearly, KK number violating processes will be loop-induced. An outcome of this is that the second KK level particles can decay to SM, *i.e.*, the zero mode, particles only via loop diagrams. Such KK number violating effective interactions are considered in [58]. A very important observation has been made based on these type of loop-induced second level decays in the context of dark matter [118]. In the present chapter (based on the original work [57]) we will take up the case of second level top quark and consider its loop-induced decay to SM top quark and Higgs boson.

We will first examine the loop-driven strong interaction mediated $t^{(2n)}t^{(0)}H^{(0)}$ coupling¹. The strength of this coupling is calculated and is used to compute the decay rate of a $2n$ -level top quark to a zero mode top quark and a Higgs boson. For the top quark KK excitation this Yukawa coupling driven decay mode will dominate over decays to other zero mode states, *e.g.*, those with weak gauge bosons in the final state. The comparison between this rate and the KK number conserving decay to a pair of n -level states has also been done. These findings can be used to explore the prospects of detecting an mUED signal through the pair production of $n = 2$ KK top quark at the future runs of the LHC.

In the next section we will set up the notations and conventions for this chapter. This will be followed by an estimation of the branching ratio of the decay of the $t^{(2n)}$ through this coupling.

¹The notation is schematic here and will be elaborated later.

5.1 Coupling of the $2n$ -level top quark to zero mode states

We have already mentioned that the 5D fields of UED are usually expressed in terms of a tower of 4-dimensional KK states. For example, the left- and right-chiral² quark fields of the i -th generation will be written as,

$$\mathcal{Q}_i(x, y) = \frac{\sqrt{2}}{\sqrt{2\pi R}} \left[\begin{pmatrix} u_i \\ d_i \end{pmatrix}_L(x) + \sqrt{2} \sum_{n=1}^{\infty} \left(Q_{iL}^{(n)}(x) \cos \frac{ny}{R} + Q_{iR}^{(n)}(x) \sin \frac{ny}{R} \right) \right], \quad (5.1)$$

$$\mathcal{U}_i(x, y) = \frac{\sqrt{2}}{\sqrt{2\pi R}} \left[u_{iR}(x) + \sqrt{2} \sum_{n=1}^{\infty} \left(U_{iR}^{(n)}(x) \cos \frac{ny}{R} + U_{iL}^{(n)}(x) \sin \frac{ny}{R} \right) \right]. \quad (5.2)$$

The expansion for $\mathcal{D}_i(x, y)$, containing d_{iR} , is similar to Eq. 5.2. The fields satisfy $\mathcal{Q}_i(x, y) = -\gamma_5 \mathcal{Q}_i(x, -y)$ and $\mathcal{U}_i(x, y) = +\gamma_5 \mathcal{U}_i(x, -y)$, $\mathcal{D}_i(x, y) = +\gamma_5 \mathcal{D}_i(x, -y)$ which ensure that the zero-modes are the SM quarks with the correct chirality. The notation used for the third generation is,

$$Q_{3L}^{(n)} \equiv \begin{pmatrix} t^{(n)} \\ b^{(n)} \end{pmatrix}_L, \quad U_{3R}^{(n)} \equiv t_R^{(n)}, \quad D_{3R}^{(n)} \equiv b_R^{(n)}, \quad (n = 0, 1, \dots), \quad (5.3a)$$

$$Q_{3R}^{(n)} \equiv \begin{pmatrix} T^{(n)} \\ B^{(n)} \end{pmatrix}_R, \quad U_{3L}^{(n)} \equiv T_L^{(n)}, \quad D_{3L}^{(n)} \equiv B_L^{(n)}, \quad (n = 1, 2, \dots). \quad (5.3b)$$

As for the SM third generation quarks, $t_L^{(0)}, b_L^{(0)}$ are the left-handed quarks while $t_R^{(0)}, b_R^{(0)}$ are similarly their right-handed counterparts.

We know that in UED the mass of the n -th level KK excitation is n/R irrespective of the other properties of the field so long as $1/R$ is much larger than the zero-mode mass, m_0 , which arises through the electroweak symmetry breaking. In mUED higher order corrections to these masses are included. In our calculation of the $t^{(2n)}t^{(0)}H^{(0)}$ coupling we use the lowest order (i.e., UED) masses of the KK states. However, when we calculate the decay rates in the next section we do include the mUED corrected masses.

The 4D theory, with the tower of Kaluza-Klein states, is valid up to the cut-off scale Λ . The magnitude of a coupling at Λ is determined by the theory which takes over beyond this energy and is to be regarded as a boundary condition for mUED. A common practice, pioneered, as noted earlier, in the context of masses of KK-states in minimal UED [58], is to take this boundary value of the coupling at Λ to be zero and obtain its magnitude at low

²The left- and right-chiral projectors are $(1 - \gamma_5)/2$ and $(1 + \gamma_5)/2$, respectively.

energy through calculable corrections³. We evaluate the KK-number violating couplings using the same principle.

As seen from Eq. 5.3, at any KK-level n , excepting $n = 0$, there are four top-quark excitations: $t_L^{(n)}, T_R^{(n)}, T_L^{(n)}$ and $t_R^{(n)}$, the first two being members of electroweak $SU(2)_L$ doublets while the last two are singlets. For the zero-modes there is no right-handed doublet member, $T_R^{(0)}$, nor a left-handed singlet, $T_L^{(0)}$.

The effective coupling which we want to calculate involves a decay of a $2n$ -level top quark to a zero mode top quark and a zero mode Higgs. The $SU(2)_L$ doublet nature of the Higgs permits only the following possibilities $t_R^{(2n)} t_L^{(0)} H^{(0)}$ and $t_L^{(2n)} t_R^{(0)} H^{(0)}$.

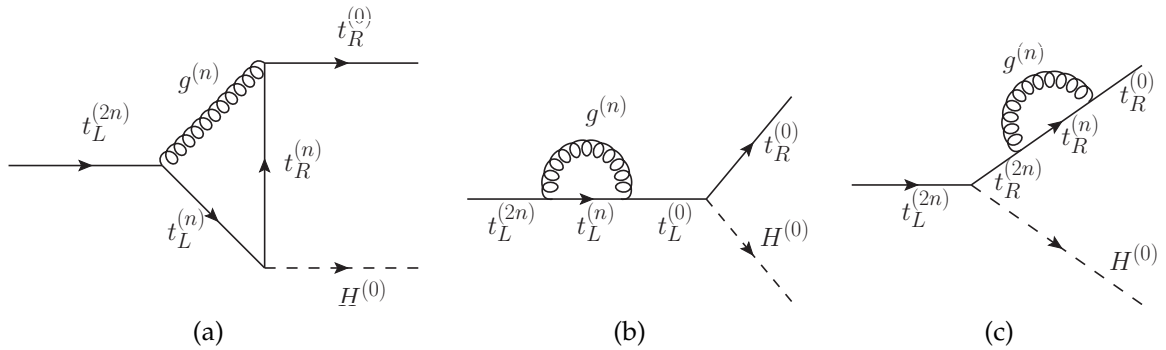


Figure 5.1: The dominant diagrams in the unitary gauge generating an effective $t_L^{(2n)} t_R^{(0)} H^{(0)}$ coupling.

We will now present some details of the calculation that is performed in the unitary gauge⁴. The dominant contributions to the second of these couplings⁵ will arise from the Feynman diagrams shown in Fig. 5.1. We ignore smaller contributions which are generated, for example, by virtual $W^{(1)\pm}$ exchange.

Each of the diagrams, Fig. 5.1a, 5.1b and 5.1c are individually divergent. We use Dimensional Regularisation to evaluate them. Using the techniques of Passarino-Veltman reduction [169] the contributions can be expressed after euclideanization in terms of scalar loop integrals which include the divergent pieces,

$$\frac{i}{\pi^2} \int d^n q \frac{1}{[q^2 + m^2]} = m^2(-\Delta - 1 + \ln m^2), \quad (5.4)$$

³It has been shown in [157, 167] that the present experimental observation constrains the cut-off to be rather small, *i.e.*, $\Lambda R < 10$.

⁴We have verified that identical results are obtained in the 't Hooft-Feynman gauge.

⁵The $t_R^{(2n)} t_L^{(0)} H^{(0)}$ coupling is obtained from similar diagrams – with $(L \leftrightarrow R)$ exchange – which we have not shown.

$$\frac{i}{\pi^2} \int d^n q \frac{1}{[q^2 + m^2][(q+p)^2 + m^2]} = \Delta + \text{finite terms} , \quad (5.5)$$

where

$$\Delta = -\frac{2}{n-4} + \gamma - \ln \pi , \quad \gamma = \text{Euler's constant} . \quad (5.6)$$

In Pauli-Villars regularization, the momentum integral in Eq. 5.4 is quadratically divergent while the one in Eq. 5.5 has a logarithmic behavior.

The effective couplings, that are obtained from the contributions from the diagrams in Fig. 5.1, can be presented by using an overall common factor,

$$\xi = -\left(\frac{g_3^2}{16\pi^2}\right) \frac{m_t}{v} (T_{ab}^c T_{ba}^c) . \quad (5.7)$$

Using Eqs. 5.4 and 5.5 we find the contribution from Fig. 5.1a to be,

$$\begin{aligned} -i\mathcal{M}_1 &= \xi \bar{u}_0(k_1) \left\{ -\frac{1}{M_n^2} [M_n^2(-\Delta - 1 + \ln M_n^2)] \right. \\ &\quad \left. + \Delta \left(4 - \frac{1}{M_n^2} \left[2M_n^2 - \frac{3}{2}M_{2n}^2 \right] \right) + \text{finite} \right\} \frac{1-\gamma_5}{2} u_2(p) . \end{aligned} \quad (5.8)$$

Similarly from Figs. 5.1b and 5.1c we respectively get,

$$\begin{aligned} -i\mathcal{M}_2 &= \xi \bar{u}_0(k_1) \left\{ \frac{M_{2n}^2}{M_{2n}^2 - M_0^2} \frac{1}{M_n^2} [M_n^2(-\Delta - 1 + \ln M_n^2)] \right. \\ &\quad \left. + \Delta \frac{1}{M_{2n}^2 - M_0^2} \left(-3M_{2n}^2 + \frac{1}{M_n^2} \left[\frac{1}{2}M_n^2 M_{2n}^2 - \frac{3}{2}M_{2n}^4 \right] + \text{finite} \right) \right\} \frac{1-\gamma_5}{2} u_2(p) , \end{aligned} \quad (5.9)$$

and

$$\begin{aligned} -i\mathcal{M}_3 &= \xi \bar{u}_0(k_1) \left\{ \frac{M_0^2}{M_0^2 - M_{2n}^2} \frac{1}{M_n^2} [M_n^2(-\Delta - 1 + \ln M_n^2)] \right. \\ &\quad \left. + \Delta \frac{1}{M_0^2 - M_{2n}^2} \left(-3M_0^2 + \frac{1}{M_n^2} \left[-\frac{1}{2}M_n^2 M_0^2 - \frac{3}{2}M_0^4 \right] + \text{finite} \right) \right\} \frac{1-\gamma_5}{2} u_2(p) . \end{aligned} \quad (5.10)$$

The leading (quadratic) divergences cancel out when Eqs. 5.8 - 5.10 are taken together. As mentioned earlier, in the spirit of mUED calculations the boundary value of the effective $t_L^{(2n)} t_R^{(0)} H^{(0)}$ coupling is taken as zero at the scale Λ . At lower energies, μ , the net contribution is logarithmically dependent on the energy scale – *i.e.*, proportional to $\ln(\Lambda/\mu)$. We thus get from Eqs. 5.8 - 5.10,

$$g_{t_L^{(2n)} t_R^{(0)} H^{(0)}}^{\text{eff}} = \xi \ln \left(\frac{\Lambda}{\mu} \right) \left\{ 1 + \frac{1}{M_n^2} \left[M_n^2 \left(-2 + \frac{1}{2} \frac{M_{2n}^2 + M_0^2}{M_{2n}^2 - M_0^2} \right) \right] \right\}$$

$$\begin{aligned}
 & \left. + \frac{3}{2} (M_{2n}^2 - (M_{2n}^2 + M_0^2)) \right\} \frac{1 - \gamma_5}{2} \\
 = & -\frac{1}{2} \xi \ln \left(\frac{\Lambda}{\mu} \right) \frac{1 - \gamma_5}{2} , \tag{5.11}
 \end{aligned}$$

where in the last step we have substituted $M_n = n/R$ for all n . Notice that the resultant coupling is independent of n .

5.2 Decays of a $2n$ -level top quark

After the discussion of the effective coupling we are now in a position to examine the decay rate of a $2n$ -level top quark induced through the coupling calculated in the previous section. We also compare it with other KK-number conserving decays that are allowed.

In general the decay width of a heavier fermion F of mass m_F decaying to a lighter fermion f and a scalar H with masses m_f and m_H is given by,

$$\begin{aligned}
 \Gamma(F \rightarrow fH) &= \frac{g_{\text{eff}}^2}{8\pi m_F^3} [(m_F - m_f)^2 - m_H^2] \\
 &\times \left\{ (m_F^2 - m_f^2 - m_H^2)^2 - 4m_H^2 m_f^2 \right\}^{1/2} , \tag{5.12}
 \end{aligned}$$

where g_{eff} is the effective Yukawa coupling between F , f and H .

For the case of our concern, using Eq. 5.11 we have

$$\Gamma \left(t_L^{(2n)} \rightarrow t_R^{(0)} H^{(0)} \right) = \left[\frac{1}{2} \xi \ln \left(\frac{\Lambda}{\mu} \right) \right]^2 \left(\frac{2n/R}{8\pi} \right) , \tag{5.13}$$

where the zero-mode masses are ignored in comparison to $2n/R$. We will identify the mass scale μ with $m_F = 2n/R$.

This decay rate has to be compared with the KK number conserving decays that proceed through tree level couplings. A typical example would be the decay $t_L^{(2n)} \rightarrow t_R^{(n)} H^{(n)}$. In this case the coupling strength is simply m_t/v . From the phase space considerations this decay is prohibited. But in mUED, due to the corrections in the KK state masses this channel opens up. Keeping only the strong interaction effects the corrected mass m_n^{corr} of the n -th level KK quark is given by [58],

$$m_n^{\text{corr}} = m_n \left[1 + \frac{3g_3^2}{8\pi^2} \ln \left(\frac{\Lambda}{\mu} \right) \right] . \tag{5.14}$$

This correction has the same form for quarks of both chirality. Clearly, the Higgs scalar and its excitations receive no corrections from the strong interactions. Now using

Eqs. 5.12 and 5.14 one can write,

$$\Gamma \left(t_L^{(2n)} \rightarrow t_R^{(n)} H^{(n)} \right) = \left(\frac{m_t}{v} \right)^2 \ln \left(\frac{\Lambda}{\mu} \right) \left(\frac{n/R}{16\pi} \right). \quad (5.15)$$

The decay width for more general channels, *e.g.*, $t_L^{(2n)} \rightarrow t_R^{(m)} H^{(2n-m)}$, can be easily obtained using the appropriate daughter particle masses in Eq. 5.12.

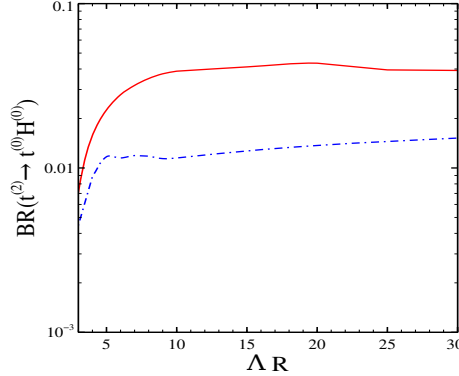


Figure 5.2: The branching ratio for the process $t^{(2)} \rightarrow t^{(0)} H^{(0)}$ as a function of ΛR . The red solid (blue dot-dashed) curve is for $t_L^{(2)}$ ($t_R^{(2)}$) decay.

Now, using Eqs. 5.7, 5.13 and 5.15 one can write,

$$\frac{\Gamma \left(t_L^{(2n)} \rightarrow t_R^{(0)} H^{(0)} \right)}{\Gamma \left(t_L^{(2n)} \rightarrow t_R^{(n)} H^{(n)} \right)} = \left[\left(\frac{g_3^2}{16\pi^2} \right) (T_{ab}^c T_{ba}^c) \right]^2 \ln \left(\frac{\Lambda}{\mu} \right) = \left[3 \left(\frac{\alpha_s}{4\pi} \right) \right]^2 \ln \left(\frac{\Lambda R}{2n} \right). \quad (5.16)$$

According to the recent practice, Λ is chosen such that $\Lambda R \sim 10$. To get meaningful results the masses of the KK particles must not exceed Λ . The implication of it in our case is that we need to stay in the limit where $n \leq 5$.

In the next section will examine the possibility of detection of the KK number non-conserving decay of $n = 2$ top quarks after their pair production at the LHC. The branching ratio for the decay $t^{(2)} \rightarrow t^{(0)} H^{(0)}$ taking into account all the KK-number conserving decay modes is shown in Fig. 5.2 as a function of the parameter ΛR . The red solid curve corresponds to the decay of a $t_L^{(2)}$ quark while the blue dot-dashed curve is for $t_R^{(2)}$ decay.

5.3 Detection prospect of the $n = 2$ top quark

In this section we discuss the manifestations of the $t_L^{(2n)} t_R^{(0)} H^{(0)}$ coupling that can be experimentally probed with particular reference to the LHC. We consider the pair production

of $t_{L,R}^{(2)} \bar{t}_{L,R}^{(2)}$ at the LHC and the subsequent decay of both of them through the $t_{L,R}^{(2)} t_{R,L}^{(0)} H^{(0)}$ coupling and compare this signal with the SM background. Assuming that both $n = 2$ top-quarks decay in the $t^{(0)} H^{(0)}$ mode the signal consists of two top quarks⁶ and two Higgs bosons such that the correct pairing leads to identical invariant masses for the two $t^{(0)} H^{(0)}$ pairs. We estimate the Standard Model background for this channel and find it to be insignificant, see the discussion below. However, with $\sqrt{s} = 13$ TeV the signal is small in number and inadequate for vindicating the strength of the coupling. On the other hand, with the HL-LHC option with the same \sqrt{s} with $\int \mathcal{L} dt = 3000 \text{ fb}^{-1}$ the signal could be viable. For the HE-LHC with $\sqrt{s} = 33$ TeV and $\int \mathcal{L} dt = 300 \text{ fb}^{-1}$ the reach would be more. The 100 TeV hadron Future Circular Collider (FCC) would surely do the best.

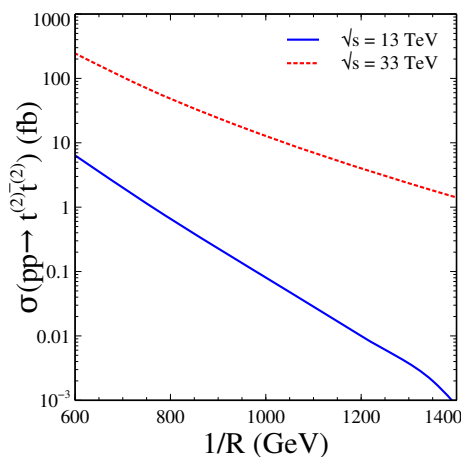


Figure 5.3: The production cross section for a $t^{(2)} \bar{t}^{(2)}$ pair at the LHC. The blue solid (red dashed) curve corresponds to $\sqrt{s} = 13$ TeV (33 TeV).

We add the couplings of our concern in the CalcHEP implementation of mUED [54, 165] to generate the events. A parton-level Monte Carlo has been utilized with the CTEQ6l [170] distribution functions. The renormalization scale (for α_s) and the factorization scale (for the parton distributions) are both taken as $2n/R$.

The production of the $t^{(2)} \bar{t}^{(2)}$ pair proceeds through gluon-gluon fusion – both s -channel and t -channel processes – as well as $q\bar{q}$ annihilation. We find that at the \sqrt{s} that we study the former dominate. The production cross sections for LHC running at $\sqrt{s} = 13$ TeV and in the future at 33 TeV are shown in Fig. 5.3.

The goal of this section is only to make a preliminary examination of this channel. So, we have refrained from including detailed detector simulation or indeed the subsequent

⁶Surely, one would be a top anti-quark but we forego this distinction for ease of presentation.

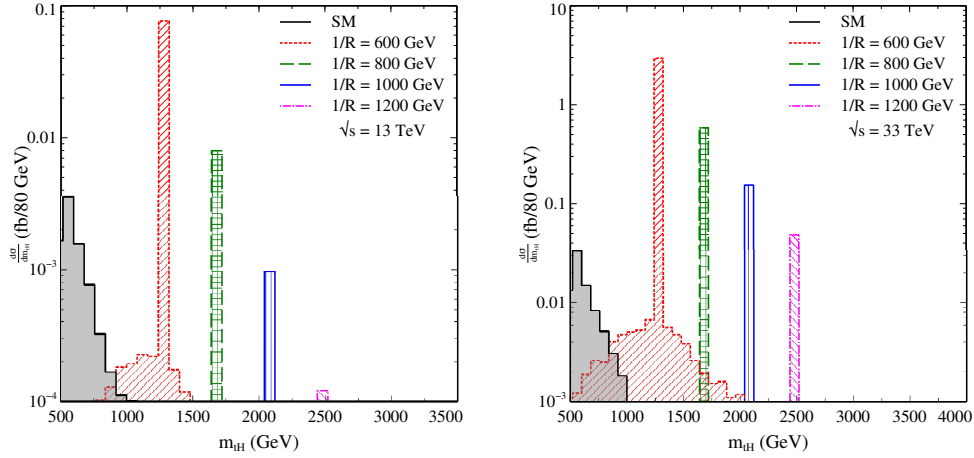


Figure 5.4: The cross section for the $(tH)(tH)$ signal at the LHC as a function of the $t^{(0)}H^{(0)}$ invariant mass. The histograms for different choices of $1/R$ (explained in the legend) and the SM background (shown shaded) at the LHC running at $\sqrt{s} = 13$ TeV (left) and 33 TeV (right).

decays of the top-quark or the Higgs bosons. We incorporate these effects by appropriate detection efficiency factors for these particles after applying kinematic cuts⁷. For all tracks we impose the following p_T and rapidity η cuts:

$$p_T > 25 \text{ GeV} , \quad |\eta| < 2.5 . \quad (5.17)$$

In addition, all four tracks are required to be isolated. For any two tracks i, j we require:

$$\Delta R_{ij} = \sqrt{(\Delta\eta)_{ij}^2 + (\Delta\phi)_{ij}^2} > 0.5 . \quad (5.18)$$

From the surviving events we pick those for which there are two distinct $t^{(0)}H^{(0)}$ pairs of the same invariant mass. We ensure that the p_T of the two reconstructed $t^{(2)}$ are balanced to within 10%.

In Fig. 5.4 is shown the cross section for the above process as a function of the $t^{(0)}H^{(0)}$ invariant mass. In the left (right) panel are the results for $\sqrt{s} = 13$ (33) TeV. The histograms correspond to the signal for $1/R = 600$ GeV (red dotted), 800 GeV (green dashed), 1000 GeV (blue solid), and 1200 GeV (pink dot-dashed). For both panels the SM background, shown shaded gray, is insignificant in the region of the signal. So, a signal of 10 events would be strong evidence for this model.

⁷The usage of these detection efficiencies, at least approximately, avoids the considerations of experimental signatures of the $t\bar{t}HH$ final states (number of jets etc.) and thereby bypasses the concerned combinatorial problems associated with the counting of the final state jets.

The detection efficiency of boosted top quarks and Higgs bosons have been under much investigation in the literature. Using jet substructure features the tagging efficiency of boosted top quarks with p_T in the 800 - 1000 GeV range is estimated around $\epsilon_{top} = 0.40$ - 0.45 [171]. For a boosted Higgs boson similar analyses yield an efficiency of $\epsilon_{h \rightarrow b\bar{b}} = 0.94$ for the $b\bar{b}$ decay mode [172] which has a branching ratio of about 60%.

As seen from the left panel of Fig. 5.4, for $\sqrt{s} = 13$ TeV with 300 fb^{-1} integrated luminosity the detection is unlikely. For the lowest $1/R$ that we consider, namely 600 GeV, one has around 30 events. Using the above-mentioned top quark and Higgs boson tagging efficiencies⁸ one is left with the signal of $((2/3)\epsilon_{top})^2(0.6\epsilon_{h \rightarrow b\bar{b}})^2 \times 30 \sim 1$ event only. For the high luminosity HL-LHC option ($\int \mathcal{L} dt = 3000 \text{ fb}^{-1}$) this will become a healthy 10-event signal. However, with $1/R = 800$ GeV the signal will fall to around 1 event. On the other hand, at a HE-LHC with $\sqrt{s} = 33$ TeV (right panel of Fig. 5.4) the signal is enhanced roughly by two orders of magnitude and could remain viable till $1/R = 1$ TeV with $\int \mathcal{L} dt = 3000 \text{ fb}^{-1}$. We have checked that with a 100 TeV hadron FCC even for 100 fb^{-1} integrated luminosity this reach would go up to $1/R = 2.5$ TeV for which we find 10 events.

5.4 Conclusion

In this chapter we have calculated the coupling of a $2n$ -level KK top-quark to a zero-mode top and a zero-mode Higgs boson in the universal extra-dimensional model. Such a coupling violates KK-number but respects KK-parity and is induced by loop diagrams. The dominant contribution comes from n -level quark and gluon mediation. We evaluate this coupling and show that it is independent of n .

We use this coupling to estimate the branching ratio of a second level KK-top quark to this mode which has the advantage of a large phase space. Considering the pair production of such second level top quarks at the LHC with $\sqrt{s} = 13$ TeV and 33 TeV we examine the prospects of the detection of both of them in this decay mode. Our results are encouraging for the higher energy run.

⁸We conservatively include only the $b\bar{b}$ decay mode of the Higgs.

Chapter 6

Summary and conclusions

The physics of electroweak symmetry breaking in the standard model has been consolidated by the discovery of Higgs boson. However, various other experimental observations give rise to a clamant need for going beyond the SM. Among other incarnations of new physics, the idea of the existence of extra spatial dimensions is a fascinating possibility in view of conceptual and phenomenological implications. In this thesis we consider a particular class of theories which is known as the universal extra dimensional model.

Here we have considered this model in its basic as well as in a non-minimal version. The basic form is actually a higher dimensional version of SM, where all the particles can propagate in the extra dimension, their Kaluza-Klein excitations have a simple mass formula, and the couplings of these excitations are similar to the ones of the SM particles. In the non-minimal avatar additional four-dimensional kinetic terms localized at the fixed points are incorporated. It has been investigated in this thesis how cosmological observations and results from LHC can shed light on this model.

In Chapter 1 we briefly reviewed the SM and theoretical as well as experimental motivations to go beyond this. In the later part of this chapter we introduced the basic features of extra dimensional models in the context of particle physics. The minimal and non-minimal version of the UED model have been discussed in Chapter 2. After this we describe the new works that constitute the thesis.

- Various astrophysical observations indirectly proved the existence of *dark matter* which none of the known particles of SM can account for. One of the nice features of the UED model is that it predicts a suitable dark matter candidate. In Chapter 3 we reviewed various observations that demand the existence of dark matter and also the standard methodology of calculating different observables related to dark matter. Later we examined how the dark matter candidate arising in the model

fares when subjected to the observational constraints, namely the relic density and direct detection constraints. It has been shown that while it can satisfy the relic density data, it requires more sensitive direct detection experiments to consolidate its candidature.

- The discovery of the Higgs boson at the LHC renews the enthusiasm in the field of particle physics which was otherwise long been wilted due to the non-observation of any new particle which was needed to understand the electroweak symmetry breaking. The data, obtained at LHC, that led to the discovery also serve the purpose of judging many new physics scenarios beyond SM. Chapter 4 concentrates on these aspects. We showed that the non-minimal version of UED can do a better job in terms of relaxing the constraint on the compactification radius that is put in the minimal version of the model from the Higgs data. However a detailed and rigorous collider study is imperative to assess the scenario in a thorough manner.
- In Chapter 5 we calculated the effective coupling of an even-numbered Kaluza-Klein top quark excitation to the zero mode top quark and a zero mode Higgs boson in the UED model. Although such couplings are KK-number violating but they are KK-parity conserving and are induced by loop diagrams. We used this coupling to estimate the branching ratio of a second level top quark to a zero mode top and the Higgs boson. Finally we examined the prospects of verifying the theory through the detection of the second level top quark decays through this mode at the LHC.

LHC is being prepared for the next phase run with a higher energy. So it is the right time to get prepared with the possible signals of alternative new physics scenarios. The exploration of physics at such an unprecedented high scale of energy can very well usher some major developments in the particle physics world. This thesis is just an humble effort to look for some of these aspects.

Bibliography

- [1] R. Streater and A. Wightman, *PCT, spin and statistics, and all that*. Princeton University Press, Princeton, USA, 1989.
- [2] Y. Nambu and G. Jona-Lasinio, *Dynamical Model of Elementary Particles Based on an Analogy with Superconductivity. 1.*, *Phys.Rev.* **122** (1961) 345–358.
- [3] Y. Nambu and G. Jona-Lasinio, *DYNAMICAL MODEL OF ELEMENTARY PARTICLES BASED ON AN ANALOGY WITH SUPERCONDUCTIVITY. II*, *Phys.Rev.* **124** (1961) 246–254.
- [4] J. Goldstone, *Field Theories with Superconductor Solutions*, *Nuovo Cim.* **19** (1961) 154–164.
- [5] J. Goldstone, A. Salam, and S. Weinberg, *Broken Symmetries*, *Phys.Rev.* **127** (1962) 965–970.
- [6] F. Englert and R. Brout, *Broken Symmetry and the Mass of Gauge Vector Mesons*, *Phys.Rev.Lett.* **13** (1964) 321–323.
- [7] P. W. Higgs, *Broken Symmetries and the Masses of Gauge Bosons*, *Phys.Rev.Lett.* **13** (1964) 508–509.
- [8] G. Guralnik, C. Hagen, and T. Kibble, *Global Conservation Laws and Massless Particles*, *Phys.Rev.Lett.* **13** (1964) 585–587.
- [9] P. W. Higgs, *Spontaneous Symmetry Breakdown without Massless Bosons*, *Phys.Rev.* **145** (1966) 1156–1163.
- [10] T. Kibble, *Symmetry breaking in nonAbelian gauge theories*, *Phys.Rev.* **155** (1967) 1554–1561.
- [11] S. Glashow, *Partial Symmetries of Weak Interactions*, *Nucl.Phys.* **22** (1961) 579–588.

BIBLIOGRAPHY

- [12] S. Weinberg, *A Model of Leptons*, *Phys.Rev.Lett.* **19** (1967) 1264–1266.
- [13] A. Salam, *Weak and Electromagnetic Interactions*, *Conf.Proc.* **C680519** (1968) 367–377.
- [14] G. 't Hooft, *Renormalizable Lagrangians for Massive Yang-Mills Fields*, *Nucl.Phys.* **B35** (1971) 167–188.
- [15] G. 't Hooft and M. Veltman, *Regularization and Renormalization of Gauge Fields*, *Nucl.Phys.* **B44** (1972) 189–213.
- [16] S. R. Coleman, *There are no Goldstone bosons in two-dimensions*, *Commun.Math.Phys.* **31** (1973) 259–264.
- [17] N. D. Mermin and H. Wagner, *Absence of ferromagnetism or antiferromagnetism in one- or two-dimensional isotropic heisenberg models*, *Phys. Rev. Lett.* **17** (Nov, 1966) 1133–1136.
- [18] P. C. Hohenberg, *Existence of long-range order in one and two dimensions*, *Phys. Rev.* **158** (Jun, 1967) 383–386.
- [19] J. Ellis and L. Álvarez-Gaumé, *Eyes on a prize particle*, *Nature Physics* **7** (2011) 2–3.
- [20] ATLAS Collaboration, G. Aad et al., *Observation of a new particle in the search for the Standard Model Higgs boson with the ATLAS detector at the LHC*, *Phys.Lett.* **B716** (2012) 1–29, [[arXiv:1207.7214](https://arxiv.org/abs/1207.7214)].
- [21] CMS Collaboration, S. Chatrchyan et al., *Observation of a new boson at a mass of 125 GeV with the CMS experiment at the LHC*, *Phys.Lett.* **B716** (2012) 30–61, [[arXiv:1207.7235](https://arxiv.org/abs/1207.7235)].
- [22] R. Mohapatra, S. Antusch, K. Babu, G. Barenboim, M.-C. Chen, et al., *Theory of neutrinos: A White paper*, *Rept.Prog.Phys.* **70** (2007) 1757–1867, [[hep-ph/0510213](https://arxiv.org/abs/hep-ph/0510213)].
- [23] K. Abazajian, M. Acero, S. Agarwalla, A. Aguilar-Arevalo, C. Albright, et al., *Light Sterile Neutrinos: A White Paper*, [arXiv:1204.5379](https://arxiv.org/abs/1204.5379).
- [24] G. Nordstrom, *On the possibility of unifying the electromagnetic and the gravitational fields*, *Phys.Z.* **15** (1914) 504–506, [[physics/0702221](https://arxiv.org/abs/physics/0702221)].
- [25] T. Kaluza, *On the Problem of Unity in Physics*, *Sitzungsber.Preuss.Akad.Wiss.Berlin (Math.Phys.)* **1921** (1921) 966–972.

- [26] O. Klein, *Quantum Theory and Five-Dimensional Theory of Relativity. (In German and English)*, *Z.Phys.* **37** (1926) 895–906.
- [27] E. Witten, *Search for a Realistic Kaluza-Klein Theory*, *Nucl.Phys.* **B186** (1981) 412.
- [28] I. Antoniadis, *A Possible new dimension at a few TeV*, *Phys.Lett.* **B246** (1990) 377–384.
- [29] N. Arkani-Hamed, S. Dimopoulos, and G. Dvali, *The Hierarchy problem and new dimensions at a millimeter*, *Phys.Lett.* **B429** (1998) 263–272, [[hep-ph/9803315](#)].
- [30] L. Randall and R. Sundrum, *A Large mass hierarchy from a small extra dimension*, *Phys.Rev.Lett.* **83** (1999) 3370–3373, [[hep-ph/9905221](#)].
- [31] L. Randall and R. Sundrum, *An Alternative to compactification*, *Phys.Rev.Lett.* **83** (1999) 4690–4693, [[hep-th/9906064](#)].
- [32] T. Appelquist, H.-C. Cheng, and B. A. Dobrescu, *Bounds on universal extra dimensions*, *Phys.Rev.* **D64** (2001) 035002, [[hep-ph/0012100](#)].
- [33] D. Bailin and A. Love, *KALUZA-KLEIN THEORIES*, *Rept.Prog.Phys.* **50** (1987) 1087–1170.
- [34] **Particle Data Group** Collaboration, K. A. Olive et al., *Review of Particle Physics (RPP)*, *Chin.Phys.* **C38** (2014) 090001.
- [35] V. Rubakov and M. Shaposhnikov, *Do We Live Inside a Domain Wall?*, *Phys.Lett.* **B125** (1983) 136–138.
- [36] V. Rubakov and M. Shaposhnikov, *Extra Space-Time Dimensions: Towards a Solution to the Cosmological Constant Problem*, *Phys.Lett.* **B125** (1983) 139.
- [37] R. Sundrum, *Tasi 2004 lectures: To the fifth dimension and back*, [hep-th/0508134](#).
- [38] T. Gherghetta, *TASI Lectures on a Holographic View of Beyond the Standard Model Physics*, [arXiv:1008.2570](#).
- [39] https://atlas.web.cern.ch/Atlas/GROUPS/PHYSICS/CombinedSummaryPlots/EXOTICS/ATLAS_Exotics_Summary/history.html.
- [40] https://twiki.cern.ch/twiki/bin/view/CMSPublic/PhysicsResultsEXO#CMS_EXO_Summary_of_Mass_Limits.

- [41] T. Appelquist, B. A. Dobrescu, E. Ponton, and H.-U. Yee, *Proton stability in six-dimensions*, *Phys.Rev.Lett.* **87** (2001) 181802, [[hep-ph/0107056](#)].
- [42] B. A. Dobrescu and E. Poppitz, *Number of fermion generations derived from anomaly cancellation*, *Phys.Rev.Lett.* **87** (2001) 031801, [[hep-ph/0102010](#)].
- [43] K. R. Dienes, E. Dudas, and T. Gherghetta, *Extra space-time dimensions and unification*, *Phys.Lett.* **B436** (1998) 55–65, [[hep-ph/9803466](#)].
- [44] K. R. Dienes, E. Dudas, and T. Gherghetta, *Grand unification at intermediate mass scales through extra dimensions*, *Nucl.Phys.* **B537** (1999) 47–108, [[hep-ph/9806292](#)].
- [45] A. Perez-Lorenzana and R. Mohapatra, *Effect of extra dimensions on gauge coupling unification*, *Nucl.Phys.* **B559** (1999) 255, [[hep-ph/9904504](#)].
- [46] G. Altarelli and F. Feruglio, *SU(5) grand unification in extra dimensions and proton decay*, *Phys.Lett.* **B511** (2001) 257–264, [[hep-ph/0102301](#)].
- [47] D. Hooper and S. Profumo, *Dark matter and collider phenomenology of universal extra dimensions*, *Phys.Rept.* **453** (2007) 29–115, [[hep-ph/0701197](#)].
- [48] H.-C. Cheng, K. T. Matchev, and M. Schmaltz, *Bosonic supersymmetry? Getting fooled at the CERN LHC*, *Phys.Rev.* **D66** (2002) 056006, [[hep-ph/0205314](#)].
- [49] J. M. Smillie and B. R. Webber, *Distinguishing spins in supersymmetric and universal extra dimension models at the large hadron collider*, *JHEP* **0510** (2005) 069, [[hep-ph/0507170](#)].
- [50] B. Dobrescu, *TASI 2008: Introduction to extra dimensions: ADD, UED, RS, and dual to TC, etc.*, .
- [51] R. S. Chivukula, D. A. Dicus, and H.-J. He, *Unitarity of compactified five-dimensional Yang-Mills theory*, *Phys.Lett.* **B525** (2002) 175–182, [[hep-ph/0111016](#)].
- [52] C. Csaki, C. Grojean, H. Murayama, L. Pilo, and J. Terning, *Gauge theories on an interval: Unitarity without a Higgs*, *Phys.Rev.* **D69** (2004) 055006, [[hep-ph/0305237](#)].
- [53] C. Schwinn, *Higgsless fermion masses and unitarity*, *Phys.Rev.* **D69** (2004) 116005, [[hep-ph/0402118](#)].

- [54] A. Datta, K. Kong, and K. T. Matchev, *Minimal Universal Extra Dimensions in CalcHEP/CompHEP*, *New J.Phys.* **12** (2010) 075017, [[arXiv:1002.4624](#)].
- [55] A. Datta, U. K. Dey, A. Raychaudhuri, and A. Shaw, *Boundary Localized Terms in Universal Extra-Dimensional Models through a Dark Matter perspective*, *Phys.Rev.* **D88** (2013) 016011, [[arXiv:1305.4507](#)].
- [56] U. K. Dey and T. S. Ray, *Constraining minimal and nonminimal universal extra dimension models with Higgs couplings*, *Phys.Rev.* **D88** (2013), no. 5 056016, [[arXiv:1305.1016](#)].
- [57] U. K. Dey and A. Raychaudhuri, *KK-number non-conserving decays: Signal of $n = 2$ excitations of Extra-Dimensional Models at the LHC*, [arXiv:1410.1463](#).
- [58] H.-C. Cheng, K. T. Matchev, and M. Schmaltz, *Radiative corrections to Kaluza-Klein masses*, *Phys.Rev.* **D66** (2002) 036005, [[hep-ph/0204342](#)].
- [59] H. Georgi, A. K. Grant, and G. Hailu, *Brane couplings from bulk loops*, *Phys.Lett.* **B506** (2001) 207–214, [[hep-ph/0012379](#)].
- [60] **Particle Data Group** Collaboration, J. Beringer et al., *Review of Particle Physics (RPP)*, *Phys.Rev.* **D86** (2012) 010001.
- [61] F. del Aguila and J. Santiago, *Low-energy constraints on orbifold models*, *Nucl.Phys.Proc.Suppl.* **116** (2003) 326–330, [[hep-ph/0212205](#)].
- [62] F. del Aguila, M. Perez-Victoria, and J. Santiago, *Bulk fields with general brane kinetic terms*, *JHEP* **0302** (2003) 051, [[hep-th/0302023](#)].
- [63] F. del Aguila, M. Perez-Victoria, and J. Santiago, *Some consequences of brane kinetic terms for bulk fermions*, [hep-ph/0305119](#).
- [64] F. del Aguila, M. Perez-Victoria, and J. Santiago, *Bulk fields with brane terms*, *Eur.Phys.J.* **C33** (2004) S773–S775, [[hep-ph/0310352](#)].
- [65] F. del Aguila, M. Perez-Victoria, and J. Santiago, *Physics of brane kinetic terms*, *Acta Phys.Polon.* **B34** (2003) 5511–5522, [[hep-ph/0310353](#)].
- [66] T. Flacke, A. Menon, and D. J. Phalen, *Non-minimal universal extra dimensions*, *Phys.Rev.* **D79** (2009) 056009, [[arXiv:0811.1598](#)].

- [67] A. Datta, K. Nishiwaki, and S. Niyogi, *Non-minimal Universal Extra Dimensions with Brane Local Terms: The Top Quark Sector*, *JHEP* **1401** (2014) 104, [[arXiv:1310.6994](#)].
- [68] M. S. Carena, T. M. Tait, and C. Wagner, *Branes and orbifolds are opaque*, *Acta Phys.Polon.* **B33** (2002) 2355, [[hep-ph/0207056](#)].
- [69] A. Datta, U. K. Dey, A. Shaw, and A. Raychaudhuri, *Universal Extra-Dimensional Models with Boundary Localized Kinetic Terms: Probing at the LHC*, *Phys.Rev.* **D87** (2013) 076002, [[arXiv:1205.4334](#)].
- [70] A. Datta, A. Raychaudhuri, and A. Shaw, *LHC limits on KK-parity non-conservation in the strong sector of universal extra-dimension models*, *Phys.Lett.* **B730** (2014) 42–49, [[arXiv:1310.2021](#)].
- [71] A. Shaw, *KK-parity non-conservation in UED confronts LHC data*, [arXiv:1405.3139](#).
- [72] A. Datta, K. Nishiwaki, and S. Niyogi, *Non-minimal Universal Extra Dimensions: The Strongly Interacting Sector at the Large Hadron Collider*, *JHEP* **1211** (2012) 154, [[arXiv:1206.3987](#)].
- [73] T. Flacke, K. Kong, and S. C. Park, *Phenomenology of Universal Extra Dimensions with Bulk-Masses and Brane-Localized Terms*, *JHEP* **1305** (2013) 111, [[arXiv:1303.0872](#)].
- [74] **Planck** Collaboration, P. Ade et al., *Planck 2013 results. XVI. Cosmological parameters*, [arXiv:1303.5076](#).
- [75] E. W. Kolb and M. S. Turner, *The Early Universe*, *Front.Phys.* **69** (1990) 1–547.
- [76] G. Jungman, M. Kamionkowski, and K. Griest, *Supersymmetric dark matter*, *Phys.Rept.* **267** (1996) 195–373, [[hep-ph/9506380](#)].
- [77] L. Bergstrom, *Nonbaryonic dark matter: Observational evidence and detection methods*, *Rept.Prog.Phys.* **63** (2000) 793, [[hep-ph/0002126](#)].
- [78] G. Bertone, D. Hooper, and J. Silk, *Particle dark matter: Evidence, candidates and constraints*, *Phys.Rept.* **405** (2005) 279–390, [[hep-ph/0404175](#)].
- [79] H. Murayama, *Physics Beyond the Standard Model and Dark Matter*, [arXiv:0704.2276](#).

- [80] G. Bertone, J. Silk, B. Moore, J. Diemand, J. Bullock, et al., *Particle Dark Matter: Observations, Models and Searches*, .
- [81] S. Profumo, *TASI 2012 Lectures on Astrophysical Probes of Dark Matter*, [arXiv:1301.0952](https://arxiv.org/abs/1301.0952).
- [82] F. Zwicky, *Die Rotverschiebung von extragalaktischen Nebeln*, *Helv.Phys.Acta* **6** (1933) 110–127.
- [83] R. Tully and J. Fisher, *A New method of determining distances to galaxies*, *Astron.Astrophys.* **54** (1977) 661–673.
- [84] M. Aaronson, J. Huchra, and J. Mould, *The infrared luminosity/H I velocity-width relation and its application to the distance scale*, *ApJ* **229** (Apr., 1979) 1–13.
- [85] J. A. Tyson, G. P. Kochanski, and I. P. Dell’Antonio, *Detailed mass map of CL0024+1654 from strong lensing*, *Astrophys.J.* **498** (1998) L107, [[astro-ph/9801193](https://arxiv.org/abs/astro-ph/9801193)].
- [86] R. Massey, J. Rhodes, R. Ellis, N. Scoville, A. Leauthaud, et al., *Dark matter maps reveal cosmic scaffolding*, *Nature* **445** (2007) 286, [[astro-ph/0701594](https://arxiv.org/abs/astro-ph/0701594)].
- [87] D. Clowe, M. Bradac, A. H. Gonzalez, M. Markevitch, S. W. Randall, et al., *A direct empirical proof of the existence of dark matter*, *Astrophys.J.* **648** (2006) L109–L113, [[astro-ph/0608407](https://arxiv.org/abs/astro-ph/0608407)].
- [88] G. Hinshaw, D. Larson, E. Komatsu, D. N. Spergel, C. L. Bennett, J. Dunkley, M. R. Nolta, M. Halpern, R. S. Hill, N. Odegard, L. Page, K. M. Smith, J. L. Weiland, B. Gold, N. Jarosik, A. Kogut, M. Limon, S. S. Meyer, G. S. Tucker, E. Wollack, and E. L. Wright, *Nine-year Wilkinson Microwave Anisotropy Probe (WMAP) Observations: Cosmological Parameter Results*, *ApJS* **208** (Oct., 2013) 19, [[arXiv:1212.5226](https://arxiv.org/abs/1212.5226)].
- [89] E. Otten and C. Weinheimer, *Neutrino mass limit from tritium beta decay*, *Rept.Prog.Phys.* **71** (2008) 086201, [[arXiv:0909.2104](https://arxiv.org/abs/0909.2104)].
- [90] S. Tremaine and J. Gunn, *Dynamical Role of Light Neutral Leptons in Cosmology*, *Phys.Rev.Lett.* **42** (1979) 407–410.
- [91] K. Griest, *Galactic Microlensing as a Method of Detecting Massive Compact Halo Objects*, *Astrophys.J.* **366** (1991) 412–421.

BIBLIOGRAPHY

- [92] B. J. Carr, *Baryonic dark matter*, *Ann.Rev.Astron.Astrophys.* **32** (1994) 531–590.
- [93] L. Bergstrom, *Dark Matter Candidates*, *New J.Phys.* **11** (2009) 105006, [[arXiv:0903.4849](#)].
- [94] R. Peccei and H. R. Quinn, *CP Conservation in the Presence of Instantons*, *Phys.Rev.Lett.* **38** (1977) 1440–1443.
- [95] M. S. Turner, *Windows on the Axion*, *Phys.Rept.* **197** (1990) 67–97.
- [96] G. G. Raffelt, *Astrophysical methods to constrain axions and other novel particle phenomena*, *Phys.Rept.* **198** (1990) 1–113.
- [97] L. Visinelli and P. Gondolo, *Dark Matter Axions Revisited*, *Phys.Rev.* **D80** (2009) 035024, [[arXiv:0903.4377](#)].
- [98] P. Sikivie, *Dark matter axions*, *Int.J.Mod.Phys.* **A25** (2010) 554–563, [[arXiv:0909.0949](#)].
- [99] M. Archidiacono, S. Hannestad, A. Mirizzi, G. Raffelt, and Y. Y. Wong, *Axion hot dark matter bounds after Planck*, *JCAP* **1310** (2013) 020, [[arXiv:1307.0615](#)].
- [100] K. S. Jeong, M. Kawasaki, and F. Takahashi, *Axions as Hot and Cold Dark Matter*, *JCAP* **1402** (2014) 046, [[arXiv:1310.1774](#)].
- [101] E. Di Valentino, E. Giusarma, M. Lattanzi, A. Melchiorri, and O. Mena, *Axion cold dark matter: status after Planck and BICEP2*, [arXiv:1405.1860](#).
- [102] S. Profumo, *Neutralino dark matter: where particle physics meets cosmology*. PhD thesis, UC, Santa Cruz & UC, Santa Cruz, Inst. Part. Phys., 2005.
- [103] L. Calibbi, J. M. Lindert, T. Ota, and Y. Takanishi, *Cornering light Neutralino Dark Matter at the LHC*, *JHEP* **1310** (2013) 132, [[arXiv:1307.4119](#)].
- [104] G. Bélanger, G. Drieu La Rochelle, B. Dumont, R. M. Godbole, S. Kraml, et al., *LHC constraints on light neutralino dark matter in the MSSM*, *Phys.Lett.* **B726** (2013) 773–780, [[arXiv:1308.3735](#)].
- [105] T. Han, Z. Liu, and S. Su, *Light Neutralino Dark Matter: Direct/Indirect Detection and Collider Searches*, [arXiv:1406.1181](#).

- [106] L. Lopez Honorez, E. Nezri, J. F. Oliver, and M. H. Tytgat, *The Inert Doublet Model: An Archetype for Dark Matter*, *JCAP* **0702** (2007) 028, [[hep-ph/0612275](#)].
- [107] A. Arhrib, Y.-L. S. Tsai, Q. Yuan, and T.-C. Yuan, *An Updated Analysis of Inert Higgs Doublet Model in light of the Recent Results from LUX, PLANCK, AMS-02 and LHC*, [arXiv:1310.0358](#).
- [108] G. Servant and T. M. Tait, *Is the lightest Kaluza-Klein particle a viable dark matter candidate?*, *Nucl.Phys.* **B650** (2003) 391–419, [[hep-ph/0206071](#)].
- [109] G. Servant and T. M. Tait, *Elastic scattering and direct detection of Kaluza-Klein dark matter*, *New J.Phys.* **4** (2002) 99, [[hep-ph/0209262](#)].
- [110] K. Kong and K. T. Matchev, *Precise calculation of the relic density of Kaluza-Klein dark matter in universal extra dimensions*, *JHEP* **0601** (2006) 038, [[hep-ph/0509119](#)].
- [111] M. Kakizaki, S. Matsumoto, Y. Sato, and M. Senami, *Relic abundance of LKP dark matter in UED model including effects of second KK resonances*, *Nucl.Phys.* **B735** (2006) 84–95, [[hep-ph/0508283](#)].
- [112] M. Kakizaki, S. Matsumoto, Y. Sato, and M. Senami, *Significant effects of second KK particles on LKP dark matter physics*, *Phys.Rev.* **D71** (2005) 123522, [[hep-ph/0502059](#)].
- [113] T. Flacke, D. Hooper, and J. March-Russell, *Improved bounds on universal extra dimensions and consequences for LKP dark matter*, *Phys.Rev.* **D73** (2006) 095002, [[hep-ph/0509352](#)].
- [114] F. Burnell and G. D. Kribs, *The Abundance of Kaluza-Klein dark matter with coannihilation*, *Phys.Rev.* **D73** (2006) 015001, [[hep-ph/0509118](#)].
- [115] T. Flacke and D. W. Maybury, *Constraints on UED KK-neutrino dark matter from magnetic dipole moments*, *Int.J.Mod.Phys.* **D16** (2007) 1593–1600, [[hep-ph/0601161](#)].
- [116] M. Kakizaki, S. Matsumoto, and M. Senami, *Relic abundance of dark matter in the minimal universal extra dimension model*, *Phys.Rev.* **D74** (2006) 023504, [[hep-ph/0605280](#)].

BIBLIOGRAPHY

- [117] S. Arrenberg, L. Baudis, K. Kong, K. T. Matchev, and J. Yoo, *Kaluza-Klein Dark Matter: Direct Detection vis-a-vis LHC*, *Phys.Rev.* **D78** (2008) 056002, [[arXiv:0805.4210](#)].
- [118] G. Belanger, M. Kakizaki, and A. Pukhov, *Dark matter in UED: The Role of the second KK level*, *JCAP* **1102** (2011) 009, [[arXiv:1012.2577](#)].
- [119] S. Arrenberg, L. Baudis, K. Kong, K. T. Matchev, and J. Yoo, *Kaluza-Klein Dark Matter: Direct Detection vis-a-vis LHC (2013 update)*, [arXiv:1307.6581](#).
- [120] T. Flacke, *Phenomenology of dark matter in non-minimal UED*, *AIP Conf.Proc.* **1200** (2010) 583–586.
- [121] J. D. Wells, *Annihilation cross-sections for relic densities in the low velocity limit*, [hep-ph/9404219](#).
- [122] M. Srednicki, R. Watkins, and K. A. Olive, *Calculations of Relic Densities in the Early Universe*, *Nucl.Phys.* **B310** (1988) 693.
- [123] K. Griest and D. Seckel, *Three exceptions in the calculation of relic abundances*, *Phys.Rev.* **D43** (1991) 3191–3203.
- [124] J. L. Feng, A. Rajaraman, and F. Takayama, *Graviton cosmology in universal extra dimensions*, *Phys.Rev.* **D68** (2003) 085018, [[hep-ph/0307375](#)].
- [125] S. Matsumoto, J. Sato, M. Senami, and M. Yamanaka, *Solving cosmological problem in universal extra dimension models by introducing Dirac neutrino*, *Phys.Lett.* **B647** (2007) 466–471, [[hep-ph/0607331](#)].
- [126] S. Matsumoto, J. Sato, M. Senami, and M. Yamanaka, *Relic abundance of dark matter in universal extra dimension models with right-handed neutrinos*, *Phys.Rev.* **D76** (2007) 043528, [[arXiv:0705.0934](#)].
- [127] S. Matsumoto, J. Sato, M. Yamanaka, and M. Senami, *Introducing neutrino mass into universal extra dimension models and solving cosmological problem*, *Int.J.Mod.Phys.* **E16** (2007) 1571–1582.
- [128] H. Melbeus, A. Merle, and T. Ohlsson, *Higgs Dark Matter in UEDs: A Good WIMP with Bad Detection Prospects*, *Phys.Lett.* **B715** (2012) 164–169, [[arXiv:1204.5186](#)].

-
- [129] J. Bonnevier, H. Melbeus, A. Merle, and T. Ohlsson, *Monoenergetic Gamma-Rays from Non-Minimal Kaluza-Klein Dark Matter Annihilations*, *Phys.Rev.* **D85** (2012) 043524, [[arXiv:1104.1430](https://arxiv.org/abs/1104.1430)].
- [130] **WMAP** Collaboration, J. Dunkley et al., *Five-Year Wilkinson Microwave Anisotropy Probe (WMAP) Observations: Likelihoods and Parameters from the WMAP data*, *Astrophys.J.Suppl.* **180** (2009) 306–329, [[arXiv:0803.0586](https://arxiv.org/abs/0803.0586)].
- [131] http://www.mpi-hd.mpg.de/lin/research_DM.en.html.
- [132] C. Munoz, *Dark matter detection in the light of recent experimental results*, *Int.J.Mod.Phys.* **A19** (2004) 3093–3170, [[hep-ph/0309346](https://arxiv.org/abs/hep-ph/0309346)].
- [133] P. Salati, *Indirect and direct dark matter detection*, *PoS CARGESE2007* (2007) 009.
- [134] M. W. Goodman and E. Witten, *Detectability of Certain Dark Matter Candidates*, *Phys.Rev.* **D31** (1985) 3059.
- [135] CDMS II, Z. Ahmed, D. S. Akerib, S. Arrenberg, C. N. Bailey, D. Balakishiyeva, L. Baudis, D. A. Bauer, P. L. Brink, T. Bruch, R. Bunker, B. Cabrera, D. O. Caldwell, J. Cooley, P. Cushman, M. Daal, F. DeJongh, M. R. Dragowsky, L. Duong, S. Fallows, E. Figueroa-Feliciano, J. Filippini, M. Fritts, S. R. Golwala, D. R. Grant, J. Hall, R. Hennings-Yeomans, S. A. Hertel, D. Holmgren, L. Hsu, M. E. Huber, O. Kamaev, M. Kiveni, M. Kos, S. W. Lemmon, R. Mahapatra, V. Mandic, K. A. McCarthy, N. Mirabolfathi, D. Moore, H. Nelson, R. W. Ogburn, A. Phipps, M. Pyle, X. Qiu, E. Ramberg, W. Rau, A. Reissetter, T. Saab, B. Sadoulet, J. Sander, R. W. Schnee, D. N. Seitz, B. Serfass, K. M. Sundqvist, M. Tarka, P. Wikus, S. Yellin, J. Yoo, B. A. Young, and J. Zhang, *Dark Matter Search Results from the CDMS II Experiment*, *Science* **327** (Mar., 2010) 1619–, [[arXiv:0912.3592](https://arxiv.org/abs/0912.3592)].
- [136] EDELWEISS, E. Armengaud, C. Augier, A. Benoît, L. Bergé, J. Blümer, A. Broniatowski, V. Brudanin, B. Censier, G. Chardin, M. Chapellier, F. Charlieux, P. Coulter, G. A. Cox, X. Defay, M. de Jesus, Y. Dolgorouki, J. Domange, L. Dumoulin, K. Eitel, D. Filosofov, N. Fourches, J. Gascon, G. Gerbier, J. Gironnet, M. Gros, S. Henry, S. Hervé, A. Juillard, H. Kluck, V. Kozlov, H. Kraus, V. A. Kudryavtsev, P. Loaiza, S. Marnieros, X.-F. Navick, C. Nones, E. Olivieri, P. Pari, L. Pattavina, B. Paul, M. Robinson, S. Rozov, V. Sanglard, B. Schmidt, S. Scorza, S. Semikh, A. S. Torrento-Coello, L. Vagneron, M.-A. Verdier, R. J. Walker, and

- E. Yakushev, *Final results of the EDELWEISS-II WIMP search using a 4-kg array of cryogenic germanium detectors with interleaved electrodes*, *Physics Letters B* **702** (Aug., 2011) 329–335, [[arXiv:1103.4070](#)].
- [137] G. Angloher, M. Bauer, I. Bavykina, A. Bento, C. Bucci, C. Ciemniak, G. Deuter, F. von Feilitzsch, D. Hauff, P. Huff, C. Isaila, J. Jochum, M. Kiefer, M. Kimmerle, J.-C. Lanfranchi, F. Petricca, S. Pfister, W. Potzel, F. Pröbst, F. Reindl, S. Roth, K. Rottler, C. Sailer, K. Schäffner, J. Schmalzer, S. Scholl, W. Seidel, M. v. Sivers, L. Stodolsky, C. Strandhagen, R. Strauß, A. Tanzke, I. Usherov, S. Wawoczny, M. Willers, and A. Zöller, *Results from 730 kg days of the CRESST-II Dark Matter search*, *European Physical Journal C* **72** (Apr., 2012) 1971, [[arXiv:1109.0702](#)].
- [138] DAMA Collaboration, R. Bernabei et al., *First results from DAMA/LIBRA and the combined results with DAMA/NaI*, *Eur.Phys.J.* **C56** (2008) 333–355, [[arXiv:0804.2741](#)].
- [139] E. Aprile, E. Baltz, A. Curioni, K.-L. Giboni, C. Hailey, et al., *XENON: A 1 Tonne liquid xenon experiment for a sensitive dark matter search*, [astro-ph/0207670](#).
- [140] E. Aprile, M. Alfonsi, K. Arisaka, F. Arneodo, C. Balan, L. Baudis, B. Bauermeister, A. Behrens, P. Beltrame, K. Bokeloh, E. Brown, G. Bruno, R. Budnik, J. M. R. Cardoso, W.-T. Chen, B. Choi, D. Cline, A. P. Colijn, H. Contreras, J. P. Cussonneau, M. P. Decowski, E. Duchovni, S. Fattori, A. D. Ferella, W. Fulgione, F. Gao, M. Garbini, C. Ghag, K.-L. Giboni, L. W. Goetzke, C. Grignon, E. Gross, W. Hampel, F. Kaether, A. Kish, J. Lamblin, H. Landsman, R. F. Lang, M. Le Calloch, C. Levy, K. E. Lim, Q. Lin, S. Lindemann, M. Lindner, J. A. M. Lopes, K. Lung, T. Marrodán Undagoitia, F. V. Massoli, A. J. Melgarejo Fernandez, Y. Meng, A. Molinario, E. Nativ, K. Ni, U. Oberlack, S. E. A. Orrigo, E. Pantic, R. Persiani, G. Plante, N. Priel, A. Rizzo, S. Rosendahl, J. M. F. dos Santos, G. Sartorelli, J. Schreiner, M. Schumann, L. Scotto Lavina, P. R. Scovell, M. Selvi, P. Shagin, H. Simgen, A. Teymourian, D. Thers, O. Vitells, H. Wang, M. Weber, and C. Weinheimer, *Dark Matter Results from 225 Live Days of XENON100 Data*, *Physical Review Letters* **109** (Nov., 2012) 181301, [[arXiv:1207.5988](#)].
- [141] LUX Collaboration, D. Akerib et al., *First results from the LUX dark matter experiment at the Sanford Underground Research Facility*, *Phys.Rev.Lett.* **112** (2014) 091303, [[arXiv:1310.8214](#)].

- [142] H.-C. Cheng, J. L. Feng, and K. T. Matchev, *Kaluza-Klein dark matter*, *Phys.Rev.Lett.* **89** (2002) 211301, [[hep-ph/0207125](#)].
- [143] **EDELWEISS** Collaboration, A. Benoit et al., *First results of the EDELWEISS WIMP search using a 320-g heat-and-ionization Ge detector*, *Phys.Lett.* **B513** (2001) 15–22, [[astro-ph/0106094](#)].
- [144] **CDMS** Collaboration, D. Abrams et al., *Exclusion limits on the WIMP nucleon cross-section from the cryogenic dark matter search*, *Phys.Rev.* **D66** (2002) 122003, [[astro-ph/0203500](#)].
- [145] T. Flacke, A. Menon, D. Hooper, and K. Freese, *Kaluza-Klein Dark Matter And Neutrinos From Annihilation In The Sun*, [arXiv:0908.0899](#).
- [146] **XENON100** Collaboration, E. Aprile et al., *Limits on spin-dependent WIMP-nucleon cross sections from 225 live days of XENON100 data*, *Phys.Rev.Lett.* **111** (2013), no. 2 021301, [[arXiv:1301.6620](#)].
- [147] **ATLAS** Collaboration, G. Aad et al., *Evidence for the spin-0 nature of the Higgs boson using ATLAS data*, *Phys.Lett.* **B726** (2013) 120–144, [[arXiv:1307.1432](#)].
- [148] **ATLAS** Collaboration, *Measurements of the properties of the Higgs-like boson in the four lepton decay channel with the ATLAS detector using 25 fb⁻¹ of proton-proton collision data*, .
- [149] A. Freitas and P. Schwaller, *Higgs CP Properties From Early LHC Data*, *Phys.Rev.* **D87** (2013), no. 5 055014, [[arXiv:1211.1980](#)].
- [150] A. Djouadi, R. Godbole, B. Mellado, and K. Mohan, *Probing the spin-parity of the Higgs boson via jet kinematics in vector boson fusion*, *Phys.Lett.* **B723** (2013) 307–313, [[arXiv:1301.4965](#)].
- [151] A. Djouadi and G. Moreau, *The couplings of the Higgs boson and its CP properties from fits of the signal strengths and their ratios at the 7+8 TeV LHC*, *Eur.Phys.J.* **C73** (2013) 2512, [[arXiv:1303.6591](#)].
- [152] M. R. Buckley and D. Hooper, *Are There Hints of Light Stops in Recent Higgs Search Results?*, *Phys.Rev.* **D86** (2012) 075008, [[arXiv:1207.1445](#)].

- [153] A. Djouadi, *The Anatomy of electro-weak symmetry breaking. I: The Higgs boson in the standard model*, *Phys.Rept.* **457** (2008) 1–216, [[hep-ph/0503172](#)].
- [154] G. Cacciapaglia, A. Deandrea, and J. Llodra-Perez, *Higgs \rightarrow Gamma Gamma beyond the Standard Model*, *JHEP* **0906** (2009) 054, [[arXiv:0901.0927](#)].
- [155] M. Spira, A. Djouadi, D. Graudenz, and P. Zerwas, *Higgs boson production at the LHC*, *Nucl.Phys.* **B453** (1995) 17–82, [[hep-ph/9504378](#)].
- [156] J. Ellis and T. You, *Updated Global Analysis of Higgs Couplings*, *JHEP* **1306** (2013) 103, [[arXiv:1303.3879](#)].
- [157] A. Datta and S. Raychaudhuri, *Vacuum Stability Constraints and LHC Searches for a Model with a Universal Extra Dimension*, *Phys.Rev.* **D87** (2013), no. 3 035018, [[arXiv:1207.0476](#)].
- [158] G. Belanger, A. Belyaev, M. Brown, M. Kakizaki, and A. Pukhov, *Testing Minimal Universal Extra Dimensions Using Higgs Boson Searches at the LHC*, *Phys.Rev.* **D87** (2013) 016008, [[arXiv:1207.0798](#)].
- [159] T. Kakuda, K. Nishiwaki, K.-y. Oda, and R. Watanabe, *Universal extra dimensions after Higgs discovery*, *Phys.Rev.* **D88** (2013) 035007, [[arXiv:1305.1686](#)].
- [160] T. Kakuda, K. Nishiwaki, K.-y. Oda, and R. Watanabe, *Constraint on Universal Extra Dimensions from scalar boson searches*, [arXiv:1305.1874](#).
- [161] A. Datta, A. Patra, and S. Raychaudhuri, *Higgs Boson Decay Constraints on a Model with a Universal Extra Dimension*, *Phys.Rev.* **D89** (2014) 093008, [[arXiv:1311.0926](#)].
- [162] F. J. Petriello, *Kaluza-Klein effects on Higgs physics in universal extra dimensions*, *JHEP* **0205** (2002) 003, [[hep-ph/0204067](#)].
- [163] A. Datta and S. K. Rai, *Identifying the contributions of universal extra dimensions in the Higgs sector at linear $e^+ e^-$ colliders*, *Int.J.Mod.Phys.* **A23** (2008) 519–528, [[hep-ph/0509277](#)].
- [164] P. Bandyopadhyay, B. Bhattacharjee, and A. Datta, *Search for Higgs bosons of the Universal Extra Dimensions at the Large Hadron Collider*, *JHEP* **1003** (2010) 048, [[arXiv:0909.3108](#)].

- [165] A. Belyaev, M. Brown, J. Moreno, and C. Papineau, *Discovering Minimal Universal Extra Dimensions (MUED) at the LHC*, *JHEP* **1306** (2013) 080, [[arXiv:1212.4858](#)].
- [166] L. Edelhäuser, T. Flacke, and M. Krämer, *Constraints on models with universal extra dimensions from dilepton searches at the LHC*, *JHEP* **1308** (2013) 091, [[arXiv:1302.6076](#)].
- [167] M. Blennow, H. Melbeus, T. Ohlsson, and H. Zhang, *RG running in a minimal UED model in light of recent LHC Higgs mass bounds*, *Phys.Lett.* **B712** (2012) 419–424, [[arXiv:1112.5339](#)].
- [168] **D0** Collaboration, V. M. Abazov et al., *Precision measurement of the top-quark mass in lepton+jets final states*, *Phys.Rev.Lett.* **113** (2014) 032002, [[arXiv:1405.1756](#)].
- [169] G. Passarino and M. Veltman, *One Loop Corrections for $e^+ e^-$ Annihilation Into $\mu^+ \mu^-$ in the Weinberg Model*, *Nucl.Phys.* **B160** (1979) 151.
- [170] J. Pumplin, D. Stump, J. Huston, H. Lai, P. M. Nadolsky, et al., *New generation of parton distributions with uncertainties from global QCD analysis*, *JHEP* **0207** (2002) 012, [[hep-ph/0201195](#)].
- [171] D. E. Kaplan, K. Rehermann, M. D. Schwartz, and B. Tweedie, *Top Tagging: A Method for Identifying Boosted Hadronically Decaying Top Quarks*, *Phys.Rev.Lett.* **101** (2008) 142001, [[arXiv:0806.0848](#)].
- [172] M. Backović, T. Flacke, J. H. Kim, and S. J. Lee, *Boosted Event Topologies from TeV Scale Light Quark Composite Partners*, [arXiv:1410.8131](#).